



Insight perspective on the synthesis and morphological role of the noble and non-noble metal-based electrocatalyst in fuel cell application

Kirti Mishra ^a, Nishu Devi ^b, Samarjeet Singh Siwal ^{a,*}, Vijay Kumar Thakur ^{c,d,e,***}

^a Department of Chemistry, M.M. Engineering College, Maharishi Markandeshwar (Deemed to be University), Mullana-Ambala, Haryana 133207, India

^b Mechanics and Energy Laboratory, Department of Civil and Environmental Engineering, Northwestern University, 2145 Sheridan Road, Evanston, IL 60208, USA

^c Biorefining and Advanced Materials Research Center, 'Scotland's Rural College (SRUC), Kings Buildings, West Mains Road, Edinburgh EH9 3JG, UK

^d School of Engineering, University of Petroleum & Energy Studies (UPES), Dehradun 248007, Uttarakhand, India

^e Centre for Research & Development, Chandigarh University, Mohali 140413, Punjab, India



ARTICLE INFO

Keywords:

Direct fuel cell
Morphology
Noble metal catalyst
Electrodeposition
Electrode material
Alcohol oxidation

ABSTRACT

In the modern era, we all depend on energy for everything. However, we have limited traditional energy sources like coal, petroleum etc. Various alternative energy sources have been developed to fulfill the energy requirements from time to time. Despite this, we are in continuous need of energy sources that are of low cost and cause less environmental pollution. To overwhelm prospective energy concerns, when the world is exploring ways for net carbon zero or negative carbon emissive energy techniques FCs are predicted as one of the clean energy origins with low operating temperatures and high energy modifications. Nevertheless, a superior and steady catalyst for the electrodes is essential for the electrochemical reactions in FCs to work efficiently. Noble and non-noble metal electrocatalysts are extensively utilized as catalysts for the transformation of energy within fuel cells (FCs). For many years many pieces of research have been done to enhance the performance of FC technology. The literature review shows the role of various metal/ polymer-based nanomaterials as anode catalysts to robust fuel cell performance by the electro-oxidation of alcohols. Here, we have demonstrated the different morphology of the stimulus (such as nanowires and nanospheres, nanotubes, nanodendrites, nanofibers

Abbreviations: DAFC, Direct alcohol fuel cell; FC, Fuel cell; NF, Nanofibres; NASA, National Aeronautics & Space Administration; PEMs, Proton exchange membrane; DFCs, Direct fuel cells; DEFCs, Direct ethanol fuel cells; YSZ, Yttria-stabilized Zirconia; AEM, Anion exchange membrane; DMFCs, Direct methanol fuel cells; MeOH, Methanol; EtOH, Ethanol; FTIR, Fourier transfer infra-red spectroscopy; CV, Cyclic voltammetry; NPs, Nanoparticles; PEDOT, Poly(3,4-ethylenedioxy thiophene); NWs, Nanowires; NSs, Nanospheres; LSV, Linear sweep voltammetry; ORR, Oxygen reduction reaction; OER, Oxygen evolution reaction; HR-TEM, High resolution transmission electron microscopy; 1D, One dimensional; CA, Chronoamperometry; MORs, Methanol oxidation reactions; ECSA, Electrochemical surface area; CNTs, Carbon nanotubes; CVD, Chemical vapour deposition; GCE, Glassy carbon electrode; MWCNTs, Multiwalled carbon nanotubes; EOR, Ethanol oxidation reaction; XRD, X-ray diffraction; NDs, Nanodendrites; CD, Current density; GDE, Galvanostatic electrodeposition; rGO, Reduced graphene oxide; GF, Graphite felt; CCM, Catalyst coated membrane; PED, Potentiostatic electrodeposition; GDE, Gas diffusion electrode; SEM, Scanning electron microscope; CC, Carbon cloth; EIS, Electrochemical impedance spectroscopy; R_{CT} , Charge transfer resistance; ES, Electrospinning; PPy, Polypyrrole; PVR, Polyvinyl pyrrolidone; PAN, Polyacrylonitrile; CNFs, Carbon nano frames; PVA, Poly vinyl alcohol; DNP, Dinitro phenol; DPV, Differential pulse voltammetry; FESEM, Field emission scanning electron microscope; XPS, X-ray photoelectron spectroscopy; GN, Graphene nanosheets; HOR, Hydrogen oxidation reaction; DFC, Direct fuel cell; D_{step} , Step density; THH, Tetra hexa hedral; NCs, Nano chains; DBFC, Direct borohydride fuel cell; EDX, Energy dispersive X-ray analysis; TGA, Thermogravimetric analysis; ICPMS, Inductively coupled plasma mass spectroscopy; PANI, Polyaniline; NTs, Nanotubes; GS, Graphene sheets; CNNF, Carbon nitride nanoflakes; MOF, Metal organic framework; ZIFs, Zeolites-based imidazolate frameworks; BTC, Benzene tricarboxylic acid; GO, Graphene oxide; NMR, Nuclear magnetic resonance; CPE, Carbon paste electrode; KB, Ketjen black; NPC, Nitrogen doped porous carbon; NCS, Nitrogen doped carbon nanosheets; CP, Conductive polymers; MN, Metal nanoparticles; NGE, Nitrogen mixed graphene; IPCF, in-situ Polymerization and composite formation; CSA, Camphor sulphonic acid; PPCA, Poly(pyrrole co-aniline); HN, Hollow nanospheres; MFCs, Microbial fuel cells; CHP, Combined heat and power; APU, Auxiliary power unit; SOFC, Solid oxide fuel cell; LPG, Liquified petroleum gas; ZEBRA, Zeolite battery research in Africa; FCEVs, Fuel cell electronic vehicles; PHEFCB, Plugin hybrid-electric hydrogen fuel cell bus; UAV, Uncrewed aerial vehicles; PAFC, Phosphoric acid fuel cell; NMRIs, Naval materials research laboratory; PGM, Platinum group metal; MT, Mass transport; DRT, Distribution of relaxation times; HT, High temperature; PNPs, Porous nanospheres; TM, Transition metal; LIBs, Lithium-ion batteries; AEMFCs, Anion exchange membrane fuel cells; CST, Controlled surface tension; PHNCs, Porous hollow nanocatalysts; DC, Direct-current; PC, Pulse-current.

* Corresponding author.

** Corresponding author at: Biorefining and Advanced Materials Research Center, 'Scotland's Rural College (SRUC), Kings Buildings, West Mains Road, Edinburgh EH9 3JG, UK.

E-mail addresses: samarjeet6j1@gmail.com (S.S. Siwal), Vijay.Thakur@sruc.ac.uk (V.K. Thakur).

<https://doi.org/10.1016/j.apcatb.2023.122820>

Received 18 December 2022; Received in revised form 3 April 2023; Accepted 26 April 2023

Available online 27 April 2023

0926-3373/© 2023 The Author(s). Published by Elsevier B.V. This is an open access article under the CC BY license (<http://creativecommons.org/licenses/by/4.0/>).

and nanosheets) and fabrication methods (such as electrodeposition, electrospinning, wet chemical, chemical vapor deposition, solvothermal, reduction, microwave-assisted polyol synthesis method) in detail. Further, the role of different noble and non-noble metal catalysts in FC application in FC technology and the relationship between morphology, synthesis and composition of catalysts have been discussed. Finally, the advantages of the fuel cell, current challenges, and prospects in this field, with concluding remarks, have been presented at the end.

1. Introduction

Recently, with the thriving population expansion and ongoing severe environmental issues, the consumption of conventional fossil energy and the significant need for clean energy is growing. Moderate growth of fuel cells with good portability and low pollution is an acceptable way to crack this issue. Alcohol-based fuel is ideal for energy transportation within direct alcohol fuel cells (DAFCs) owing to their straightforward availability, low poisonous nature, and increased energy density [1,2]. The present era is the era of energy, as every human being depends on energy. The traditional energy sources are fossil fuels, i.e., coal and petroleum. The global demands for fossil fuels have increased tremendously; and humans face the depletion of coal, oil, natural gas, etc. Using these fuels leads to environmental issues like ozone layer depletion, acid rain and global warming (which is because of greenhouse gases present in atmosphere), and air quality also deteriorates [3]. It is required to develop some renewable energy resources which are less costly, environmentally friendly and have high calorific value to overcome the above-discussed issues. The best suitable option for this is FC technology. An FC is a tool that changes the chemical energy of redox reactions into electrical energy. FC is a clean energy source that decreases greenhouse gas emissions and inhibits air pollution with high energy efficiency [4]. It also harnesses the power of hydrogen. The catalyst is used at the anode to enhance the oxidation of fuel. Noble metals (Ru, Rh, Pt, Pd, Au & Ag) are used primarily as catalysts [5,6] because of their chemical inertness and higher stability toward heat. In this study, we discussed some electrode catalysts based on noble and non-noble metals for the electrooxidation of alcohols in FCs. The study reveals that these catalysts enhance FC's efficiency [7,8].

Noble metals, for example, platinum (Pt) and palladium (Pd) are significantly necessary and suitable catalysts within FCs, but growing the catalyst effectiveness and cost deduction of stimuli is a considerable hurdle. The electrocatalytic performance would improve by tuning the dimensions, arrangement, and morphology [9–12]. Current investigation endeavors have been concentrated upon:

1. The accumulation of reasonable transition or d-block metals to reduce the price and enhance the electronic consequence of Pt,
2. Adjusting the outer surfaces with higher index aspects, ultrathin borders and 3D surface accessibility,
3. Nanofibres (NFs) architecture that delivers a three-dimensional (3D) surface having higher catalytically active surface area and extensive use of noble metals,
4. Composition exclusion of Pt upon the boundaries and junctions of NFs increases the usage of Pt.
5. Similarly, simulating the advanced nano catalyst's superior performance and resilience is essential.

Here, in this report, we have tried to compile all the information, such as the different morphology of the stimulus (such as nanowires and nanospheres, nanotubes, nanodendrites, nanofibers and nanosheets) and fabrication methods (such as electrodeposition, electrospinning, wet chemical, chemical vapor deposition, solvothermal, reduction, microwave-assisted polyol synthesis method) in detail. As per the literature survey, this is the first report describing the synthesis and morphological role of the noble and non-noble metal-based electrocatalyst in fuel cell application. A few key points are;

1. Morphology of catalyst/electrode in subsections,
2. Method of fabrication (electrodeposition in detail),
3. Polymer-based catalysts are discussed in detail.

Further, the role of different noble and non-noble metal catalysts in FC application in FC technology and the relationship between morphology, synthesis and composition of catalysts have been discussed. Finally, the advantages of the fuel cell, current challenges, and prospects in this field, with concluding remarks, have been presented at the end.

2. Background of fuel cell

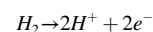
First, in 1839, Sir William Grove, also acknowledged as the Forefather of FC Technology, revealed that water electrolysis can also produce electricity. After that, in 1889, researchers Langer and Mond [13] laid the foundation of the FC by using air and coal gas. Later, at the start of the 1900 s, some extra work was done to improve FC technology, which internally changed the carbon in electricity. However, the internal ignition engine's growth temporarily inhibits this innovative technology's growth. After this, FC technology was expanded by Francis in 1932 by using an H₂-O₂ cell in which affordable electrodes of nickel and electrolytes is alkaline electrolytes were used as an alternative in place of the high-cost catalysts that Mond and Langer proposed. Later on, the construction of a small current engine was started by the National Aeronautics and Space Administration (NASA) [14] for space programmes. NASA also provided funds to the researchers of the FC technology. FCs are now a promising technique in the space program after providing electricity to many space missions. Some big companies further support the research in the field of FCs for the development of automobiles. To replace traditional energy sources, FC Techniques have been wanted for coming times, from micro-level FCs used in portable mobiles to higher-efficiency FCs for standard car contests [15].

2.1. General construction and working principle of fuel cell

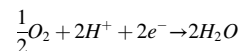
An FC has three main components:

- an anode (known as a fuel electrode)
- a cathode (known as an oxidant electrode)
- an electrolyte sandwiched in between the cathode & anode

The electrodes are composed of porous substances and decorated through a layer of catalyst, mainly Pt. In FC, Hydrogen gas (H₂) passes through an anode, and electrochemical reactions occur. Oxidation of H₂ occurs at the anode to give hydronium ions (H⁺) and e⁻, as shown in the given equation:



The H⁺ ions move using electrolytes; on the other hand, e⁻s move from the exterior circuit towards the cathode. The H⁺ ion and e⁻'s react with the oxygen at the cathode, which is provided from outside to give water, as shown in the given reaction:



The overall reaction of FC shows the production of water, heat and electrical work, which is shown in the following equation:



The by-products of heat and water are removed from time to time for the efficient working of FC and to maintain its temperature for electricity production. When the fuel cell works with catalysts, it follows a 6-electron mechanism [16]. In this process, the analyte adsorbs over the surface of catalysts for further processing. The mechanism of the method shown in reactions as:

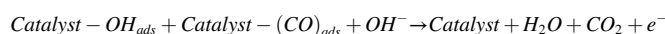
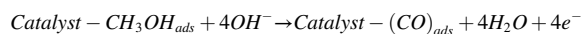
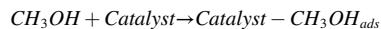


Fig. 1 shows the schematic representation of the fuel cell.

The main principal features with applications of FCs are given below in Fig. 2.

2.2. Efficiency of fuel cell

FCs do not store energy inside but give power directly from fuel to the target place. FC requires space inside them to keep the fuel for combustion in the presence of oxygen to produce energy. FCs have shown much better performance compared to traditionally used batteries. They are small in size, rechargeable, durable etc. Most of the energy we obtain from coal, petroleum, natural gas, etc., is less efficient and pollution-causing. On the other hand, FCs are eco-friendly in nature [18].

Further, FC is used for both portable as well as stationary devices. Due to the large energy consumption in the modern era, fossil fuels are unsuitable. Furthermore, fossil fuel combustion causes some lethal environmental problems. At this time, we require some alternative energy sources. Considering this, many researchers work day and night in the field of renewable energy sources with fewer environmental hazards [19]. FC has more importance and is used in producing on-site energy, mobile equipment and transportation based on electricity because of its higher energy efficiency and eco-friendly nature. Despite these features, the commercialization of FC is not accessible due to its higher cost and less durability [20]. The liquid oxidising agent currently substitutes the gaseous H₂ because the former has more mass, high voltage, better warehouse handling, and easy work ability [21–23]. Various materials are incorporated from time to time inside the FC to maintain FC's working potential and effectiveness. These introduced materials are

oxidizing agents, used electrolyte pH and the electrode catalyst used on the anode by modifying their surfaces. The proton exchange membranes (PEMs) always decide the design, nature, or type of FC. Due to its excellent performance with H₂, the PEM FCs are more popular among all [24]. The value and amount of present hydrogen are away from explanation in the future. However, by polluting the H₂, its preparation is always harshly affected. FCs always utilize those materials which provide energy for burning. The ratio of produced electrical energy to the heat obtained (its enthalpy of formation or ΔH_f) by fuel burning gives the efficiency of FCs. We can also say that the quantity of power obtained from fuel burning defines FC's efficiency (around 70%) [25].

2.3. Different types of fuel cells

FC is an energy-converting device. Various kinds of FC are based on the type of electrolyte present. This shows the chemical properties of the type of FC. The type of electrochemical reaction in the operation process also explains its kind. There are various FCs made for a specific purpose. Every FC has its quality, advantages and boundaries, which define the potential of the FC. Based on this, the applicability of the FC is decided. Researchers have done further work in this field, which invents the newer FC. Each type of fuel cell contains a specific kind of electrolyte, its working temperature, redox reactions, applications, merits and demerits [26,27]. In recent years, the most relevant for energy production by fuel combustion is direct alcohol fuel cells (DAFCs) due to their being environmentally friendly and efficient. Many scientists are working continuously on the DAFCs technology. First of all, we had paid attention to where a DAFC is transformed, and DAFC is the crucial centre of the researchers in the current time. All of this, a range of DAFCs, direct ethanol fuel cells (DEFCs), which work in the essential medium, are the main attractive concern due to their more profit [28].

In DMFCs, MeOH fuel at the FC anode is immediately transformed into electrical energy. In contrast, DMFCs and other kinds of FCs (like the normal hydrogen-powered cells) depend on an external system that produces hydrogen; the system primarily does not respond. Direct methanol fuel cells (DMFCs) are not used at large scale because of their poor activity compared to H₂/air systems. Various kinds of FCs are described in Table 1 below:

Here, Fig. 3 shows the various type of fuel cells and their working conditions.

It has been investigated that the main reason behind the inadequate performance of DMFCs is the lack of competent electrocatalysts for the electrooxidation of methanol. While research on the catalytic performance of various electrocatalyst for the oxidation of methanol (MeOH) shows that the Pt-based electrocatalyst exhibit outstanding performance and superior stability [42,43]. Recently, many researchers have investigated a substitute energy resource, i.e., DEFCs. Though significant results have been predicted from DEFCs, a few advances still require to be done to boost their probability in upcoming utilization [44]. Compared to MeOH, ethanol (EtOH) is environment friendly, and simple production methods produce high yields, i.e., from farming outcomes or biological mass. This is the individual most reliable cause of why DEFCs have currently paid much concentration. Still, this growing technique needs some improvements before the DEFCs commercialization due to its few limitations. Many scientists are making many improvements from time to time to accelerate the performance of DEFCs.

These improvements contribute much to the energy-based applications, i.e., enhanced their working potential. Regarding the presence of electrolyte membranes in FCs, DEFCs are divided into two types: acidic-membrane DEFCs and basic-membrane DEFCs [45]. Lin et al. have described the function of water during the electrocatalytic oxidation of MeOH on electrodes that are Pt-modified directly on a Nafion film & after that, they stimulate the MeOH through a gaseous state [46]. On behalf of this report, they concluded that surrounding enveloping and incorporation of methyl alcohol towards the outer side of the electrode influence the consequences of MeOH oxidation. Gootzen et al. [47] have

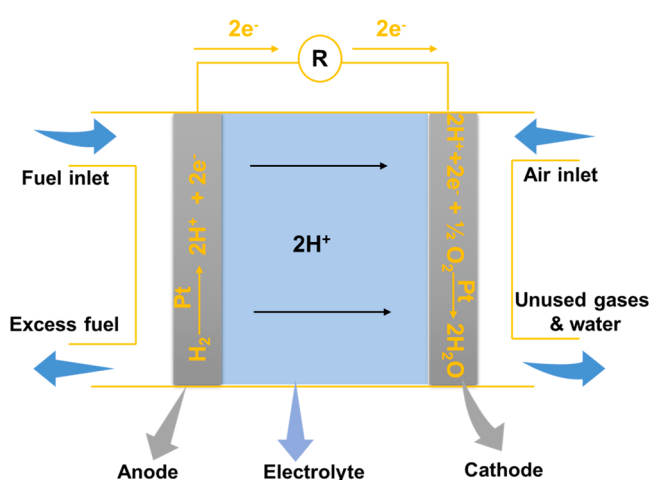


Fig. 1. Schematic representation of fuel cell.

Principals
Features
Applications

Principal of Operation	Features
Electrochemical Energy Conversion	✓ High and Consistent Efficiency ✓ Reduced/Eliminated Harmful Emissions ✓ High Energy Density ✓ Prompt Load-Following ✓ Reduced/Eliminated Noise
Fewer Energy Transformations	✓ High and Consistent Efficiency ✓ Reduced/Eliminated Harmful Emissions ✓ Prompt Load-Following
Runs as Long as Fuel is Supplied	✓ Long Operational Cycles ✓ High Energy Density
Expansion by Adding Cells to a Stack and/or Stacks to a System	✓ Modularity ✓ High Integrability with Renewable Sources
Runs Best on Pure Hydrogen	✓ Reduced/Eliminated Harmful Emissions ✓ High Integrability with Renewable Sources
Static Operation with No Dynamic Parts	✓ Modularity ✓ Reduced/Eliminated Noise
Fuel Reformation Fueling Option	✓ Reduced/Eliminated Harmful Emissions ✓ Long Operational Cycles ✓ Fuel Flexibility
Direct Alcohol Fueling Option	✓ Long Operational Cycles ✓ Prompt Load-Following ✓ Fuel Flexibility

Feature	Application Areas
High and Consistent Efficiency	✓ Propulsion Systems ✓ Light Traction Vehicles ✓ Auxiliary Power Units ✓ Distributed Generation
Reduced/Eliminated Harmful Emissions	✓ Propulsion Systems ✓ Light Traction Vehicles ✓ Auxiliary Power Units ✓ Distributed Generation
Long Operational Cycles	✓ Portable Applications ✓ Propulsion Systems ✓ Light Traction Vehicles ✓ Emergency Back-Up
High Energy Density	✓ Portable Applications ✓ Propulsion Systems ✓ Light Traction Vehicles ✓ Emergency Back-Up
Prompt Load-Following	✓ Propulsion Systems ✓ Light Traction Vehicles ✓ Auxiliary Power Units ✓ Distributed Generation
Modularity	✓ Portable Applications ✓ Auxiliary Power Units ✓ Distributed Generation
Reduced/Eliminated Noise	✓ Propulsion Systems ✓ Light Traction Vehicles ✓ Auxiliary Power Units ✓ Distributed Generation
Fuel Flexibility	✓ Portable Applications ✓ Distributed Generation ✓ Emergency Back-Up
High Integrability with Renewable Sources	✓ Propulsion Systems ✓ Distributed Generation

Fig. 2. The basic outline of the fuel cell's principal features and applications. Reproduced with permission from [17]. Copyright 2014 Elsevier.

examined the adsorption that cannot reverse a variety of three carbon-based alcohols, C_2H_6 and n-butyl alcohol, on Platonized (Pt) by using techniques like Fourier transform infrared spectroscopy (FTIR) & electrochemical mass spectrometry in an acidic electrolyte ($HClO_4$). With C_2H_6 and propan-2-ol at the C_1 position, a minimal amount of O_2 was associated. It was followed by the production of CO via decarbonylation, as concluded by the earlier explained study. At the Pt electrodes, the oxidation of C_4 alcohols was examined by Hai and Gang [48] by using in situ FTIR & cyclic voltammetry (CV). They gave a double route method for the electrocatalytic oxidation of butyl alcohol in a homogeneous mixture of perchloric acid.

Lamy et al. [22] studied the process of reaction & catalytic performance of the materials used to make anode based on the electro-oxidation of numerous alcohols having a lower molecular mass that includes EtOH, n-propyl alcohol, and ethane-1,2-diol. Researchers showed the obtained outcome using the different exemplars of a specific cell. It is mainly for ethyl alcohol's electrooxidation, where a PEM is used as an electrolyte. Patra and Munichandraiah [49] did their work on Pt nanoparticles (Pt-NPs) that were decorated with a polymer sheet that is conductive in nature, namely poly(3,4-ethylene dioxythiophene) (PEDOT). This shows a higher catalytic activity for the electrocatalytic oxidation of MeOH. These researchers also investigate the consequence of electrolyte concentration, Pt weight, & the quantity of PEDOT on movement that are mass-specific. The elevated catalytic activity of

electrochemical oxidation of MeOH on Pt-based catalysts to acquire the dimensions of catalyst strips should be nanometric with a comparable form in a protective matrix. The protective form of the dispersed Pt-NPs has an important role in the fabrication of the electrode catalyst. Carbon-based stuff also plays a vital role in transferring the particles of catalyst [50–52]. The carbon-based support provides electrical communication among the isolated subdivisions.

Solla-Gullon et al. [53] examined the morphology of the Pt NP surface. The reactivity of these NPs for MeOH and HCOOH electrooxidation equated the activity with solitary crystal-based electrodes that possess basal arrangement. The outcomes showed the significance of the facade development/arrangement of well-known Pt-NPs and their role in the electrooxidation of MeOH and HCOOH. The electrocatalytic activity of NPs is controlled by using its surface morphology, particularly the positions of (111) symmetry. The surface texture of electrodes provides a significant function in the activity of both oxidation methods. Some conclusions allowed the chance to fabricate novel and suitable electrocatalytic materials with elegant structure-disciplined Pt NPs initially described with discrete Pt-crystal electrodes. Based on further research, various noble metal-based anode catalysts were synthesized, positively promoting FC technology.

Table 1

Various type of fuel cells.

Types of FC	Electrolyte Used	Anode catalyst	Cathode catalyst	Working temperature (°C)	Interconnecting materials	Fuel Used	Charge carrier	Efficiency (%)	System output	Pollutants	Merits	Demerits	Applications	Ref.	
Proton Exchange membrane FC	Perfluoro sulfonic acid	-	-	60–80	-	-	-	60:35% for transportation and stationary	<1–100 kW	-	<ul style="list-style-type: none"> The decay & organization-based difficulties are overcome by using a solid electrolyte. Lower temperature Quick start-up Extremely supportive for the majority of applications. Higher power density Small size Quick starting because its lower the working temperature Outstanding energetic reaction 	<ul style="list-style-type: none"> Expensive catalyst Lower temperature, warmth releasing 	Convenient power, supplement Power, broaden group, transportation of motor vehicle	[29]	
Low temperature proton exchange membrane FC	Solid Nafion	Platinum supported on carbon	Platinum supported on carbon	60–80	Graphite	Hydrogen	H ⁺	40–60	-	Carbon monoxide (CO), Hydrogen sulfide (H ₂ S)	<ul style="list-style-type: none"> Complex water and thermal management Low-grade heat High sensitivity to contaminants Expensive catalyst 	-	-	[17]	
High temperature proton exchange membrane FC	Solid composite Nafion -Polybenzimidazole doped in phosphoric acid	Platinum-Ruthenium supported on carbon	Platinum-Ruthenium supported on carbon	110–180	Graphite	Hydrogen	H ⁺	50–60	-	Carbon Monoxide (CO)	<ul style="list-style-type: none"> Simple water management Simple thermal management Enhanced reaction speed Higher-grade heat Higher endurance to pollutants. 	<ul style="list-style-type: none"> Accelerated stack degradation Humidification issues Expensive catalyst 	-	-	[17]
Alkaline FC	KOH solution in water absorbed in a matrix	Nickel	Silver supported on carbon	90–100	Metallic wires	Hydrogen	OH ⁻	60%	10–100 kW	Carbon dioxide (CO ₂)	<ul style="list-style-type: none"> Negatively charged electrode perform better in basic medium. Can be applied over a range of catalyst. 	<ul style="list-style-type: none"> Susceptible to CO₂ in Air and fuel Electrolyte management 	Armed forces, Space	[30]	
Direct formic acid FC	Solid Nafion	Palladium or platinum	platinum supported on carbon	30–60	-	Liquid formic acid (HCOOH)	H ⁺	30–50	-	Carbon monoxide (CO)	<ul style="list-style-type: none"> Better speed for oxidation at anode Higher potential to utilize fuel Restricted fuel crossover Facile passage and storage of fuel Elevated power density During oxidation reaction at anode, no need of water Small size and simple structure 	<ul style="list-style-type: none"> Fuel toxicity Components Corrosion issues Low fuel gravimetric and volume measuring Expensive cost Lower working temperature 	-	-	[31]
Enzymatic FC	Membrane-less-Ion exchange membrane	Biocatalyst supported on carbon	Biocatalyst supported on carbon	20–40	-	Organic matters (e.g., glucose)	H ⁺	30	-	Foreign physical and/or chemical exposure to	<ul style="list-style-type: none"> Capacity for miniaturization 	<ul style="list-style-type: none"> Quick breakdown of enzyme-based catalyst while working 	-	[32]	

(continued on next page)

Table 1 (continued)

Types of FC	Electrolyte Used	Anode catalyst	Cathode catalyst	Working temperature (°C)	Interconnecting materials	Fuel Used	Charge carrier	Efficiency (%)	System output	Pollutants	Merits	Demerits	Applications	Ref.		
6	Molten carbonate FC	Liquid solution of Li, Na and/or Na CO_3^{2-} absorbed in a matrix	Nickel Chromium (NiCr)	Litigated nickel oxide (NiO)	600–700 °C	Stainless steel	Methane	CO_3^{2-}	50%	300 kW ⁻³ MW (300 kW module)	Sulphides, Halides	<ul style="list-style-type: none"> • Simple arrangement • Much feedback time 	<ul style="list-style-type: none"> • Higher susceptibility to enzyme toxicity • Electron transfer mechanism to FC electrodes from the labile point of the biological catalysts is not easy • Immobilizing the enzymes is problematic • Lower power density • Minute columbic product • Lower flexibility for fuel • Inflexible working conditions 	on outside environment	Electric utility, Distributed Generation	[33]
	Direct carbon FC	Solid yttria-stabilized zirconia (YSZ), Melted carbonate and made up of hydroxide	Graphite or carbon	Strontium-doped lanthanum manganite (LSM)	600–1000	-	Carbon in solid form (e.g., coal, coke, biomass)	O_2	70–90	-	Residue, S	<ul style="list-style-type: none"> • Highly efficient • Workable on many fuels • Operated on many catalyst 	<ul style="list-style-type: none"> • At higher temperature cell component decay occurs and leads to corrosion • Takes much time for starting • Power density is less. 	<ul style="list-style-type: none"> • Carbon dioxide (CO_2) emissions • Rapid material corrosion and degradation • Durability issues • Sensitivity to fuel impurities • Low power density 	-	[34]
	Microbial FC	Microbes	Biocatalyst supported on carbon	Platinum supported on carbon	Ambient Temperature	-	Any organic materials (e.g., glucose, acetate, Polluted water)	H^+	50%	-	Bacterial contamination of cathode	<ul style="list-style-type: none"> • Highly efficient toward electricity • Greater measurable power density • Flexible to fuel Not emit any harmful gas like SO_x NO_x and particulate matter • Simple arrangement • More ability for the capture of carbon. 	<ul style="list-style-type: none"> • e-transport mechanisms from the metabolism in the microorganisms to the FC oxidation electrode is problematic • Relatively less power density by utilization of few 	Bio energy process	[25]	

(continued on next page)

Table 1 (continued)

Types of FC	Electrolyte Used	Anode catalyst	Cathode catalyst	Working temperature (°C)	Interconnecting materials	Fuel Used	Charge carrier	Efficiency (%)	System output	Pollutants	Merits	Demerits	Applications	Ref.	
Phosphoric acid FC	Liquid H_3PO_4 acid absorbed in a matrix	Platinum supported on carbon	Platinum supported on carbon	150–200 °C	Graphite	Hydrogen	H^+	40%	400 kW (100 kW module)	Carbon monoxide (CO), Siloxane, Hydrogen sulfide (H_2S)	<ul style="list-style-type: none"> Ability to regenerate enzymes. Combined heat and power works at higher temperatures. Highly tolerated for impurities present in fuel. 	<ul style="list-style-type: none"> Extremely less energy density Columbic product is very less. Inflexible operation situations. 	energies relative to microorganisms' responses.	Distributed generation	[35]
Solid oxide FC	YSZ	Ni-YSZ composite	Strontium-doped lanthanum manganite	800–1000	Ceramics	Methane	O_2^-	55–65	1 kW-2 MW	Sulfides	<ul style="list-style-type: none"> High electrical efficiencies High-grade heat. High endurance towards pollutants. Chance of inner reforming. Issues regarding electrolytes that are eliminated. Work on various fuel. Use cheap catalyst. Small size Easy system The volumetric power density of the fuel is high. Facile storage and transfer fuel. Easy heat managing for liquid CH_3OH systems. 	<ul style="list-style-type: none"> Slow start-up time Low power density Strict material requirements High thermal stresses Sealing issues Durability issues High manufacturing price. 	Supplementary Power, Electric usefulness, Spread age group	[36]	
Direct methanol FC	Solid Nafion	Platinum-Ruthenium supported on carbon	Platinum supported on carbon	Ambient-110	Graphite	Liquid methanol-water solution	H^+	35–60	-	Carbon monoxide (CO)	<ul style="list-style-type: none"> Bad anode kinetics results into less potential & voltage of cell. Lower energy density. Absence of capable catalysts for direct oxidation of CH_3OH. Water and fuel cross the membrane. Difficult administration of H_2O. Expensive. Carbon dioxide (CO_2) removal system Fuel toxicity Energy density is low. Highly sensitive towards CO. 	-	-	[37]	
Direct ethanol FC	Solid Nafion, basic medium, Acidic-basic medium	Platinum-Ruthenium supported on carbon	Platinum supported on carbon	Ambient-120	Graphite	Liquid ethanol-water solution	H^+	20–40	-	Carbon monoxide (CO)	<ul style="list-style-type: none"> Compact size Environmentally-suitable fuel. 	<ul style="list-style-type: none"> Extremely less energy density Columbic product is very less. Inflexible operation situations. 	Distributed generation	[38]	

(continued on next page)

Table 1 (continued)

Types of FC	Electrolyte Used	Anode catalyst	Cathode catalyst	Working temperature (°C)	Interconnecting materials	Fuel Used	Charge carrier	Efficiency (%)	System output	Pollutants	Merits	Demerits	Applications	Ref.
Direct borohydride FC	Solid Nafion, AEM	Au, Ag, Ni, or Pt supported on carbon	Platinum supported on carbon	20–85	Graphite	Sodium borohydride (NaBH ₄)	Na ⁺	40–50	-		<ul style="list-style-type: none"> • Higher volumetric power density of fuel. • Comparatively less fuel poisoning. • Greater gravimetric power density • Storage and delivery of fuel is easy. • Facile management of heat. • Small size. • Used maximum fuel. • Higher fuel gravimetric H₂ amount • Non-emission of CO₂ • Less poisonous and works eco-friendly. 	<ul style="list-style-type: none"> • Because of bad anode kinetics voltage and efficiency of cell is less. • Absence of capable catalyst • Expensive • Membrane of cell is permeable to fuel & H₂O • Fuel crossover • High cost • Low power density • Lack of analytical modelling techniques due to unknown borohydride oxidation reaction mechanisms • Expensive catalyst • Chemical instability of membrane and catalyst • Inefficient cathodic reduction reaction 	-	[39]
Direct ethylene glycol FC	Solid Nafion, Anion exchange membrane (AEM)	Platinum supported on carbon	Platinum supported on carbon	Ambient–130	Graphite	Liquid ethylene glycol	H ⁺	20–40	-	Carbon monoxide (CO)	<ul style="list-style-type: none"> • Small size. • Higher volumetric fuel power density. • Convert into vapour at higher temperature leads to higher boiling point. • Transfer and storage of fuel is easy. • Heat produced is easy to handle. • Facile H₂O management • Presence of distribution network. 	<ul style="list-style-type: none"> • Less energy density • Absence of capable electrode catalyst. • Lower fuel gravimetric power density • Less durable. • Expensive • Allows crossover of fuel. 	-	[40]

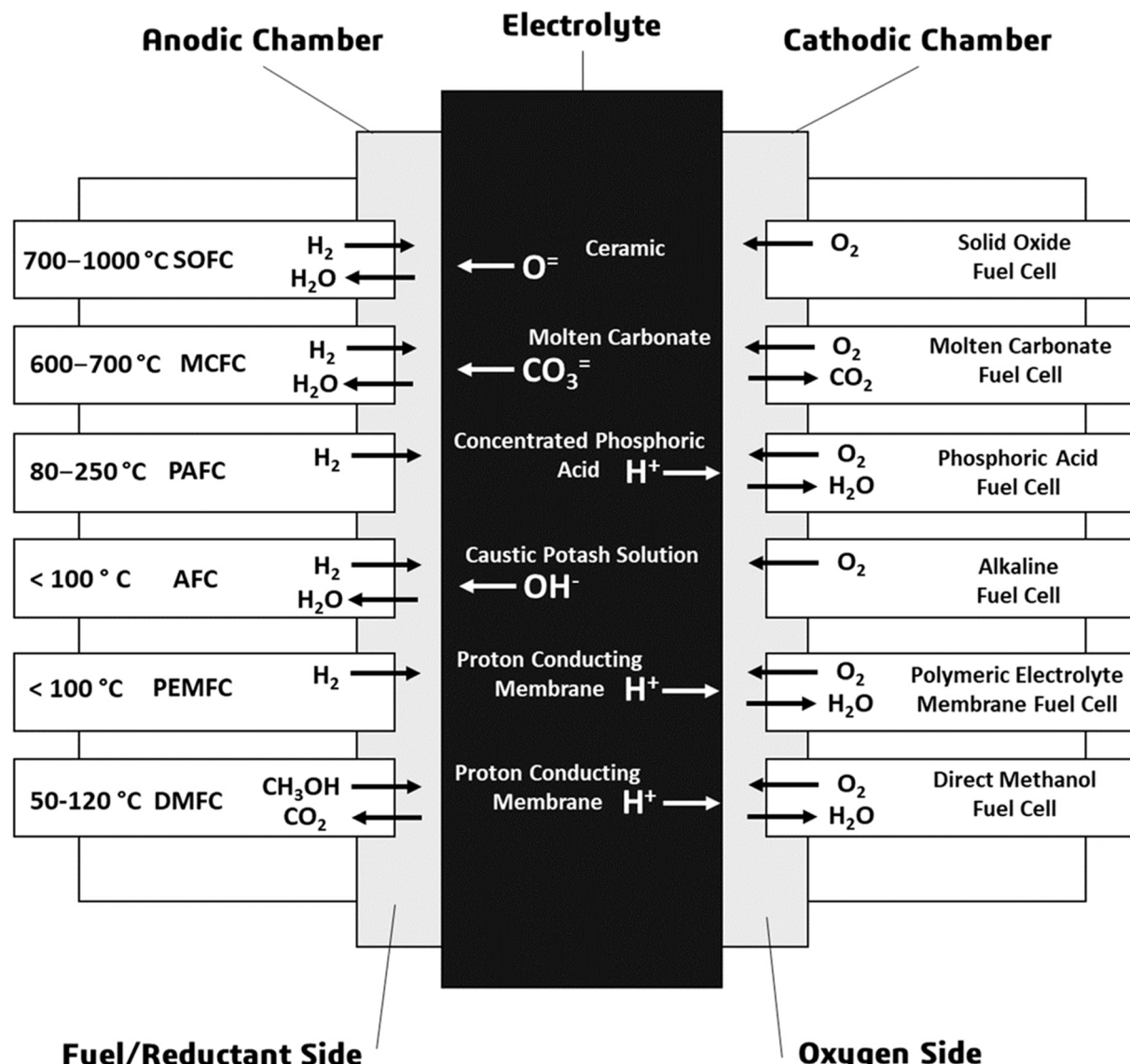


Fig. 3. Various type of fuel cells and their working conditions. Reproduced with permission from [41]. Copyright 2021 MDPI.

2.4. Applications of fuel cell

Fuel cell technology proved perfect a long time ago. Only three crucial classes of fuel cell technology are used viably and effectively, i.e., portable, stationary and transportation. The working temperature of fuel cells determines by their respective electrolyte, which further provides information regarding fuel cells' efficiency, startup time and dynamic behavior. Fig. 4 displays the applications of fuel cells in various fields.

2.4.1. Stationary applications

For this application, the system should have high efficiency and less start-up time; the dynamic behavior is the secondary consideration. This application requires large combined heat and power (CHP), residential CHP and prime power, and uninterrupted power supply. The present generations are focused on the growth of heat, cooling, and energy [54]. FCs can produce electricity instantly by using fuel, with significant activity. For immobile applications, they modify the system that supports the combustion and produces electricity in which energy failure occurs at the hot engine with the electric dynamo. They are useful in residential, industrial, backup, and off-grid power applications [55]. Steam improvement can produce hydrogen in fewer amounts by using natural

gas for household FCs applications. For 0.5¹ kW systems, a small fuel processor developed by Osaka gas was based on the H₃PO₄ FC technology. The section where fuel is processed consists of a desulfurized water gas shift section, steam reformer, and an oxidation reactor which support a single stage of the reaction and can produce reformate with a CO amount of less than 1 ppm. And has a concentration of H₂ of about 75% (dry basis). The high amount of hydrogen production is a chief benefit of steam reforming. This fuel processor is also fabricated by Tokyo gas, Nuvera etc., for many other gases like natural gas, propane etc. [56].

The mobile broadcasting trade is an illustration of a field that requires support and off-grid energy, with approximately 70 lacs sites worldwide, surging each year by 100,000. FC can give many authentic and secure operations applicable to these applications, providing flexibility to inconsiderate atmospheric situations other than batteries without influencing its activity in a harsh atmosphere and without any cooling equipment. Current investigation criteria follow the chance of mixing green H₂, 20% by volume, with natural gas pipelines. Recent studies show that using these techniques, 5% of CO₂ emission is reduced in household activities, which can be between 32 and 58 kg of CO₂. By considering the 100% era of hydrogen, CHPs based on FCs will become

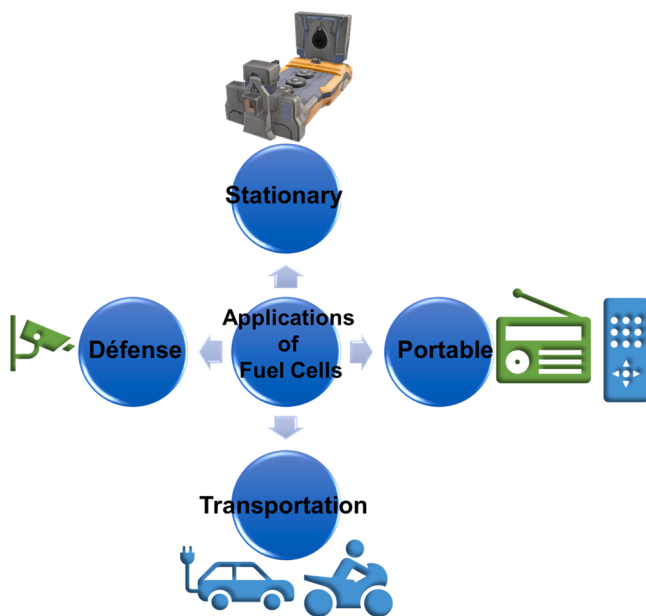


Fig. 4. Applications of fuel cells in various fields.

the most powerful and practical application in the coming years. This is economically good. When the price of hydrogen decreases in about 2030, nearly 1.9 USD/kg, it becomes 2700 USD per family. Hydrogen-fired combined-cycle gas turbines are tried in Italy and Japan, which work on hydrogen power to give heat and electricity [41].

2.4.2. Portable applications

A standard description is that transportable FCs include the type of FCs devices that moved, together with auxiliary power units (APU) of subordinate power. For this, the primary consideration is the lesser starting time and higher load-following dynamics, even low temperature. These portable devices range in energy necessity from 25 W to 5 kW. These types of FC utilizations are mainly not motivated by energy capacity but somewhat by a decrease in sound and emissions and an improvement in appliance operational time. Army utilizations are a unique area of portable FCs-based applications [57]. The portable fields mainly cover 4 C applications, i.e., computers, cameras, cordless phones, and cordless tools. Mobiles, phones and notebooks with power ranges of ~5 W and 75 W for their current supplies depend on H₂-PEFCs and DMFCs.

Toshiba has expanded trials for notebooks, Hitachi, NEC, Panasonic, Sanyo, Samsung and LG (50–250 cm³, 10–75 W, mainly driven direct by MeOH) [58]. Due to the incredible advancement in Li⁺-based batteries (e.g., Panasonic NCR18650B, 266 Wh kg⁻¹, 691 Wh L⁻¹), using FCs commercially in portable computing devices is not easy. However, external chargers for lower current required electronic appliances like cell phones, computers, tablets etc., are presently on sale. Transferable liquid propane gas-fuelled micro-tubular SOFC (eZelleron) having starting time of 0.3 kW/kg is also under improvement. Due to lower costs, Li-ion-based batteries are more in use. A Li-ion battery has a 38 W-h USB charger weighing 272 g and costs about \$50 [59]. The notable characteristics of a handy or micro-FC are just a little object. The lower function temperature concerning the PEM FC is an essential advantage for a portable motive. It is the exclusive FC competent in working at an environmental temperature. In comparison to hydrogen FCs, parallel DMFC is also used.

Now a day FC system is continuously developing and needs much improvement both in the case of price and technology. Some researchers reported a most competent and highly-active tubular segmented-in-series yttria-stabilized zirconia electrolyte-based direct carbon-solid

oxide FC, i.e., DC-SOFC stack [60]. The yttria-stabilized zirconia electrolyte supports are prepared by dip-coating. The two biochar, i.e., pure walnut shell and Fe-loaded, are utilized as fuels. The individual cell can attain the highest CD of 147 mW/cm² at 800 °C, which further increases up to 205 mW cm⁻² when the Fe_xO_m catalyst is added to the biochar fuel. After that, two cells of DC-SOFC working with Fe-containing walnut shell char are constructed and examined. It shows excellent activity, with an open circuit voltage of 1.98 V, the highest volumetric CD of 505 mW cm⁻³ at 800 °C and an output power of 1.11 W. It shows the higher capacity for growing into a battery that exhibits higher performance for portable or distributed applications [61].

2.4.3. Transportation applications

The main advantages of FC-based conveyance are that it comprises zero harmful environmental release and much better well-to-wheel effectiveness than internal combustion engines or battery vehicles. While comparing battery-based electric vehicles with FC-based cars found that the latter is much superior with high range and less refilling time [62,63]. Now a day, PEFCs are used widely due to their lower starting time & the much more emotional load appeal in vehicle driving systems. Compressed hydrogen with a pressure of 350 and 700 bar is used as fuel due to fewer filling stations. On-board handing out liquid fuels like methanol, gasoline, LPG, or diesel to give H₂ is considered impractical. Transport utilizations generally focus on buses, cars, and goods carrying conveyance. Some work is also done on small channels (golf cars, airport carts, wheelchairs etc.), cycles, ships, bikes, aeroplanes, locomotives & trams.

PEFC techniques based on hydrogen and oxygen have effectively been used in underwater military ships, allowing silently slowed cruising for up to 21 days without coming onto water surfaces. An example from 2006 is the ZEBRA battery-SOFC hybrid (ZEBRA was expanded for 'Zeolite Battery Research in Africa' after the project made it). The ZEBRA battery works at a high temperature of about 300 °C; before the rapid growth of the Li-ion battery, it was one of the chief candidates for battery electric vehicles. The intermediate power and energy would supply by the ZEBRA battery, with the SOFC giving a comparatively steady flow of power to charge the battery. SOFCs are at a period of growth where they have been introduced into test vehicles in a range of applications, an enormous development given that at the beginning of this century, there was no concern that SOFCs could be used for transport purposes. However, they are still short of full industrial adoption [64]. Fig. 5 shows the transportation applications of SOFCs.

FC electric vehicles (FCEVs) are the outcomes of immense investigation powered by the growth in reliable transport applications. Electric cars such as the Toyota Mirani and the Hyundai Tucson encourage the option of the substitution of FCs in the power production of systems. Due to the cost of competing with fossil fuel cars [65]. The dynamic behaviour of the hydrogen-based FC was tested in the road transport system using a mainly premeditated FC set-up. To improve the combustion process, a thermoelectric generator fitted outside with a novel NH₃-H₂ internal combustion engine, which leads to the hand-on generation of H₂. The developed system's work efficiency and energy efficiency are 28.94% and 31.1%, respectively. To enhance overall performance and combustion, this system provides sufficient H₂. The technology used in the bidirectional plugin hybrid electric hydrogen FC bus (PHEFCB) is shown pictorially in Fig. 6 [66].

Intelligent Energy UK developed an FC power based on the uncrewed aerial vehicle (UAV) in 2018. FC's performance improved daily in relation to weight competence, rapid refuelling and productivity. The system based on FC is appropriate in aviation as it is the source of clean power because it works with hydrogen and ambient air. It is also possible to use it in another modules and UAVs. It was fruitful with all the aeronautics regulations and presented a low-cost solution to clean power production [67].

Marine transportation includes boats, canoes and ships. FC

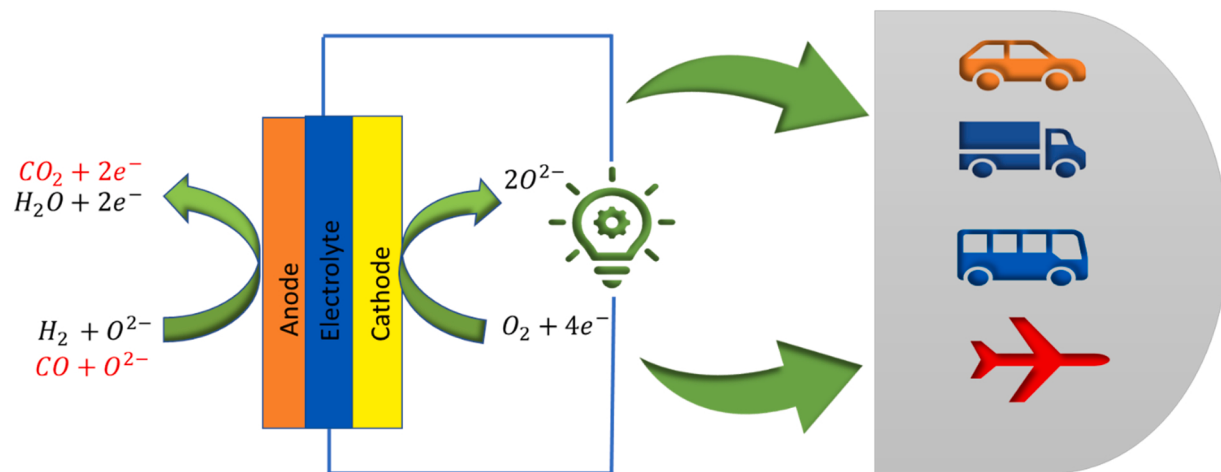


Fig. 5. Shows the transportation applications of SOFCs.

technology provides lower emission, low noise, higher specific power and high marine and underwater transport efficiency. 5.5 kW of power supplied by FC as told by scholars during flying in air like the cathode. While working on pure O₂, the energy production was enhanced up to 8.1 kW by 81% and whenever a mixed system of FC in combination with battery was used. In which FC provided 4.83 kW and the batteries provided 18.53 kW, the highest yield of 23.37 kW was obtained [68]. The constant supply and lower emission of H₂-based FCs also benefit the warship and merchant ships for electric propulsion. Troya et al. [69] revealed H₂-FC to warships and merchant ships for electric propulsion.

2.4.4. Defence applications

Defense teams look ahead to themselves-competence in all circumstances and localities. The essential properties of military applications are simplicity, a higher level of autonomy, durability, and ruggedness. Appliances should have defect-finding and auto-security techniques. Air force bases in backward locations required guaranteed electricity for battery charging, auxiliary power for supervision & uninterrupted energy for communicating devices. Aerial vehicles without human beings have existed in space for a long time and need a tremendous power supply. The naval force also required an extended supply of power for uncrewed submarine and air self-regulating driving systems for underwater vehicles which are non-nuclear. The army is not only limited to previously decided areas. The newly allocated spaces may either have been destroyed or have no power supply.

Based on this tough environment and to make them user-friendly, the power of army necessities can be grouped into the power of soldiers (portable high-density power source), APU (land vehicles of soldiers and tanks used by the army in war), distributed energy producing plants, autonomous systems, etc. [70]. Higher temperature PEFC has MeOH as reformist prefers 25–55 W framework. Transportable specimen JENNY 600 S manufactured by M/s. SFC Energy can straightforwardly give energy to electrical appliances or boost chargeable batteries. The fuel container has CH₃OH and has a capability of 400 Wh in everyone. As a result of the harsh examination by the US army, ultra-cells can leave behind various types of improved CH₃OH FCs. In the case of APU, the system should be designed to provide higher levels of consistency under adverse environmental conditions like temperature, humidity, dust, shock and vibrations. During these processes, the emission of smoke, sound, harmful chemicals, light etc., should not occur. A phosphoric acid FC, i.e., PAFC-based 10 kW generator car, was manufactured by Naval Materials Research Laboratory, India (NMRL) that utilizes a unified CH₃OH improving in situ generations of H₂. Repairing field equipment's use of this type of power source can have many advantages. These power sources are helpful in relief operations during a disaster

and in remote areas to provide emergency medical services [71]. As projected by M/s Fuel Cell energy, mixing direct FC through turbine cycles and utilizing the FC consequence heat also increase its efficiency. This is also utilized in ships that are used in war. Others also industrialized FC-based air-independent propulsion systems for the submarine.

2.5. Advantages of direct fuel cell

FC is an energy transformation gadget that can be utilized in many power techniques and are comprehensive for further growth. During methanol oxidation, FC gives six electrons and protons for every atom. Due to its incredible energy density, methanol is used as a fuel in FCs applications [72]. By using a feeble suspension of methyl alcohol in water as fuel, the DMFC operates at lower and mean temperatures, which enhance up to 150 °C. The kinetics of FC improved by using extraordinary temperatures. In this way, the methanol crossover decreases by supplying a gas phase.

On the other hand, vaporizations are not allowed [73]. Alkaline alcohol FCs exhibit considerable progress while PEMFCs examined it: (i) acidic electrolytes are the better alternative for the ongoing redox couple reactions, namely oxidation of alcohols and reduction of oxygen in alkaline medium and show better advancements [74,75], (ii) in essential confirmation, scanty-Pt or also without Pt catalyst placed over Au [76] & Pd [77,78] through the anode, Ag [79] & perovskite-style oxides [80] in the cathode might be used together with brilliant electrocatalytic potential so it can enhance the commercialization opportunity of DAFC (iii) in alkaline FC, accumulation of hydroxyl on the cathode to the anode by electro-osmosis leads to the passing of the fuel crossover. It is considered that the FCs as integrated transportable devices, particularly the DMFCs, have huge potential. Some were established to supply current cell phones, digital cameras and laptops. DMFC's widespread in portable appliances because of their high potential and lower pollution-causing nature.

Compared to previously used batteries, DMFCs have some great merits like a continuous supply of power, higher-power density and extended life. Besides this, there are some hurdles to the industrialization of DMFCs. Good fuel quality and feed situations are also required to obtain the necessary activity and potential in DMFCs. Parallel to the case of different types of FC, the central aspect of the efficient performance of FC is the electrode catalyst used on the anode for the oxidation of fuel. That is why this review article primarily concentrated on the anode catalysts of DMFCs and on some factors that lead to the commercialization of DMFCs.

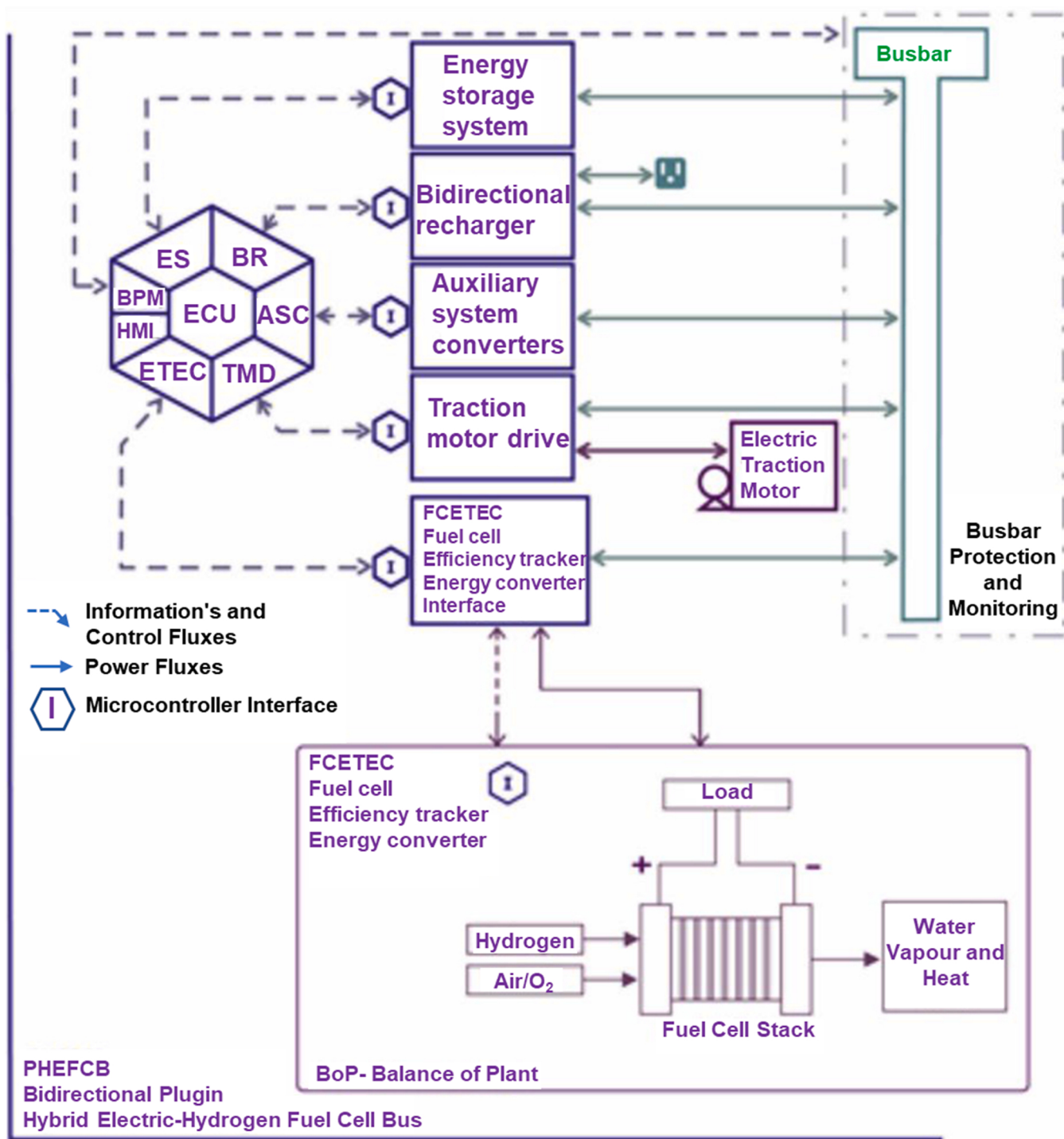


Fig. 6. Pictorial presentation of the total technology of the bidirectional PHEFCB.
Reproduced with permission from [66]. Copyright 2017 Elsevier.

3. Effect of morphology on electrocatalytic performance

Recent methods of catalysis synthesis show that the nanoscale mesoporous structure of a nanoscale catalyst leads to durability and enhances its electrochemical performance to a greater extent. The morphology of the catalyst significantly affects the catalytic performance of the materials.

PEMFCs have been broadly studied over the previous years [81,82]. They promise to evolve a neat, compact power origin for static and mobile utilization. The cell's performance is additionally affected by the

catalytic performance of the cathode catalyst, where the oxygen reduction reaction (ORR) appears. To enhance its speed, Pt electrocatalysts (e.g. carbon-based Pt NPs, the advanced PEMFC cathode electrocatalyst) are usually substituted by Pt-alloys, seeking to improve the ORR inherent performance via the strain-ligand and/or coarsening results to decrease thereby the quantity of the costly Pt within a fuel cell [83–85]. Pt alloy with a 3D transition metal, Ni or Co, has significantly improved. For instance, the Pt₃Co particles show a Pt-enriched exterior coating with a decreased interatomic space, which results in the incorporation of the Pt electronic network and, therefore, a reduced binding

force of the oxygen intermediate upon the catalytic consistency. Similarly, the non-noble portion of the catalyst drains out during the process, forming a coarse catalyst texture. All these improve the cell's response rate and activity [86].

This typical factor is anticipated to be far less of a restriction when managing platinum group metal (PGM) electrocatalysts [87], as the NPs, varying from 2 to 3 nm for pure-Pt and Pt-alloys to numerous layers of nm for intricate nanostructures (e.g. Pt-doped hollow NPs [88], nano-frames [89], octahedra [90]) are far less possible to dock/nucleate within the least porosities and are therefore readily obtainable for the reaction, indicating a lower carrier resistance. Nevertheless, the catalyst coating morphology reconstructs a part in mass transport (MT) and ORR. Thus it conclusively affects the activity of the cell [91].

MT also contains the carrier of protons to the reaction zones. Therefore, the reaction zones must be in touch with phosphoric acid to donate to cell activity. Excellent wetting of the carbon doped could have the least porosities, no flooding, and a thin layer over the entire carbon substrate to optimize MT to the functional areas. The proton conduction within the cathode is observable within the distribution of relaxation times (DRT) scope of a high temperature (HT)-PEMFC [92]. Therefore, various wetting behaviour within catalysts with variable pore dimensions may be marked by employing DRT. Various Pt-based catalysts with their advancement in morphology are shown in Fig. 7. Some of them are discussed in the sections below.

3.1. Nanowires and nanospheres

By using the hydrothermal method, Yang et al. [93] synthesize CeO_2 nanowires (NWs) and nanospheres (NSs). The electrocatalytic performance of fabricated materials was checked using CV and linear sweeping voltammetry (LSV). It was found that both materials show similar performance for oxygen reduction reaction (ORR) [94]. However, NSs perform better than NWs for oxygen evolution reactions (OER) because of their higher surface area. The higher surface area of CeO_2 was proved by X-ray photoelectron spectroscopy, Raman spectroscopy and high-resolution transmission electron microscopy (HR-TEM). The self-supported one-dimensional (1D) morphology has more durability and benefits in all the known shapes of Pt. Other mesoporous structures enhance the electrochemically active surface area and provide extra catalytic active sites on its concave surface. Cuiling et al. [95] fabricated Pt NWs that are self-supported and had 1D mesoporous morphology using a micelle assembly approach. For this purpose, polycarbonate membrane channels were used. The results obtained from CV and

chronoamperometry demonstrated (as shown in Fig. 8 (a-c) below) that 1D mesoporous Pt nanowires (red curve) show better stability, superior catalytic performance for MeOH oxidation reactions (MORs), while in comparison to Pt black catalyst (black curve). The sample's reduction/oxidation cycles cyclic measurements were observed at a potential range of 0.6–1.0 V in H_2SO_4 (0.5 M). In Fig. 8(d, e), CV curves are obtained after several periods. In comparison to Pt black catalyst ($19.7 \text{ m}^2\text{g}^{-1}$), the initial electrochemical surface area (ECSA) of 1D mesoporous nanowires ($40.2 \text{ m}^2\text{g}^{-1}$) is high. In the case of 1D mesoporous NWs, the loss of ECSA is less than 10%, while in the case of Pt black, it is 12%, as shown in Fig. 8(f).

Jiang et al. fabricated mono-dispersed and mesoporous NSs of Pt by using a surfactant-assisted reduction approach. These mesoporous Pt NSs showed higher electrochemical active surface area (97%) than Pt-black, dendritic Pt NPs and Pt carbon-20% after calcination for 3 h at 250 °C either 350 °C. This is due to the restricted accumulation of the particles of mesoporous Pt NSs over higher temperatures [96,97]. On moving towards the NSs, it was found that porous nanospheres have a much large surface area and structural properties. Due to this, they are prevalent in the field of electrocatalysis. Considering this, Wang et al. [98] fabricated PdPtAg-based porous nanospheres (PdPtAg PNSs) using a one-pot cetyltrimethylammonium chloride-assisted approach at room temperature. The catalyst is highly porous in nature.

The fabrication approach is shown in Fig. 9(a). The fabricated PdPtAg PNSs have a unique morphology, more charge transfer ability, suitable composition, high tolerance toward CO poisoning, and enhanced electrocatalytic activity. PdPtAg PNSs catalysts are highly durable with high mass activity toward glycerol oxidation reaction ($3.06 \text{ A/mg}_{\text{metal}}$) and ethylene glycol oxidation reaction ($5.00 \text{ A/mg}_{\text{metal}}$) that are much higher than commercially available Pd/C catalysts. The result shows that by improving the morphology of the catalyst, the electrocatalytic performance also improved.

The morphology configurations of the synthesized material PdPtAg PNSs were determined via TEM and HRTEM investigation. As shown within Fig. 9(b, c), the as-synthesized PdPtAg PNSs were expected of 3D nanosphere networks with an average size of around 50 nm. A high-resolution TEM (HRTEM) photo was employed to investigate the lattice distance of PdPtAg PNSs of 0.227 nm (Fig. 9(d)), which established the presence of the (1 1 1) plane of the PdPtAg PNSs. The PdPtAg PNSs also defined 3D nanospheres within the HADDF-STEM picture (Fig. 9(e)). The Pd/Pt/Ag composition ratio in PdPtAg PNSs was near 62/18.4/19.6, defined by EDS (Fig. 9(f)). The cross-sectional compositional line shape study (Fig. 9(g)) and elemental mapping (Fig. 9(h)) revealed the

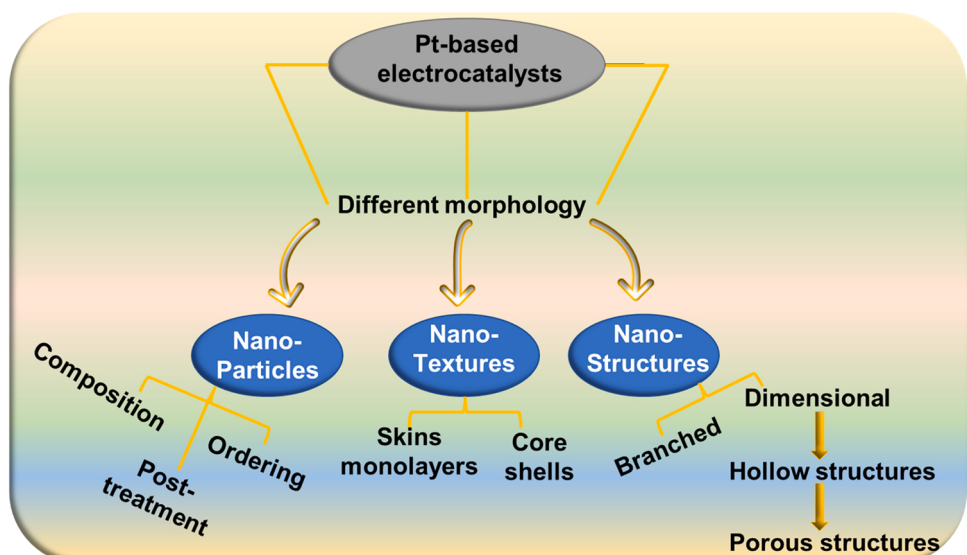


Fig. 7. Graphical display of advancement in Pt-based catalyst for PEM FC applications.

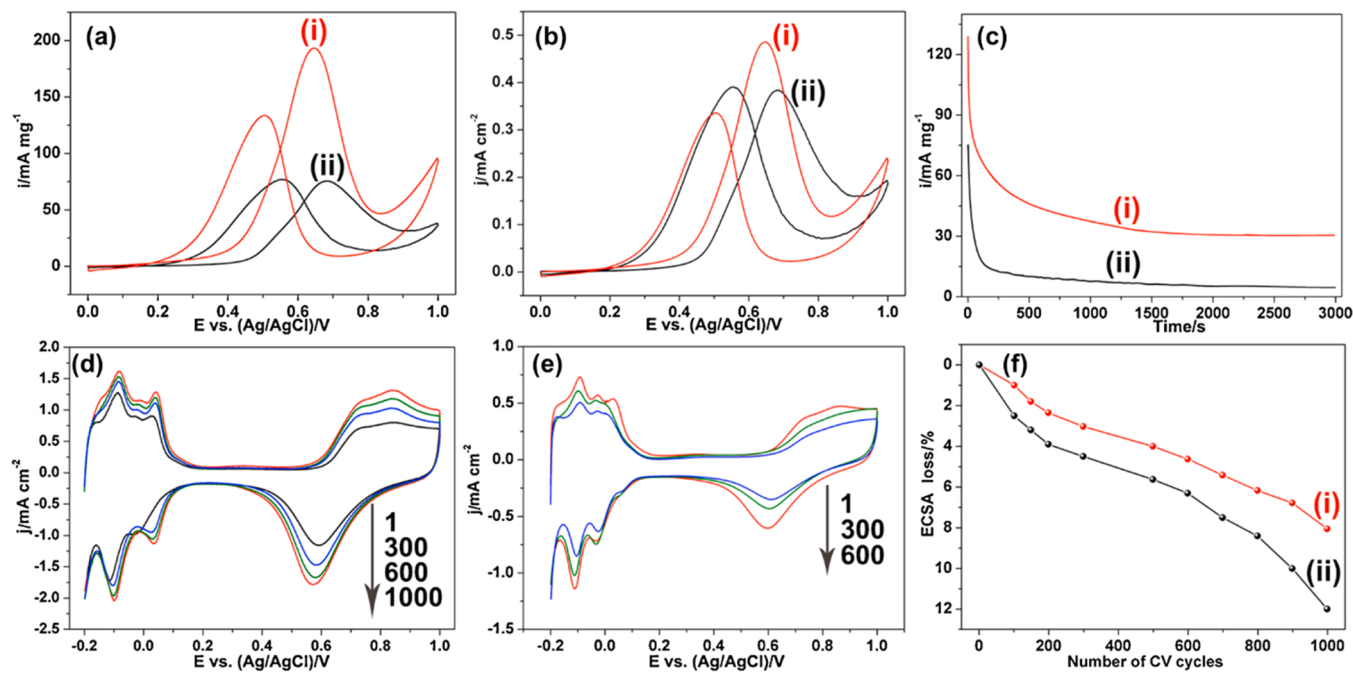


Fig. 8. (a, b) CV in H_2SO_4 (0.5 M) with MeOH (0.5 M), with the $i = 50 \text{ mV s}^{-1}$ scan rate and (c) CA curve (at constant 0.6 V potential) of the 1D mesoporous NWs (I, red curve) and the commercially present Pt black catalyst (II, black curve) for oxidation of MeOH . The currents were normalized by the (a, c) Pt mass amount and (b) Pt ECSA. (d, e) electrochemical durability comparison after 300, 600 & 1000 cycles in 1D mesoporous NWs (d) & Pt black catalyst (e), (f) loss in the ECSA shown with an increase in CV cycles of 1D mesoporous NWs (I) & Pt black (II).

Reproduced with permission from [95]. Copyright 2015 Elsevier.

homogeneous dispersal of Pd, Pt and Ag within the PNSs.

Gao et al. [99] fabricated PtNi-based ultrafine NWs, ultrashort NWs and sinuous NWs by taking suitable amounts of citric acid, glucose and ascorbic acid. Out of these three types of electrocatalyst PtNi sinuous NWs shows superior electrocatalytic performance compared to other fabricated materials and commercially available Pt/C catalyst. They are used in ethylene glycol oxidation reaction with mass activity 4.5 (4889.5 mA/mg) times and specific activity 4.3 times (8.6 mA/cm^2) higher than Pt/C on the other hand, in the case of glycerol oxidation reaction its mass and specific activity is 4.3 (4250 mA/mg) and 3.9 times (7.3 mA/cm^2) higher than Pt/C electrocatalyst. They are highly stable and used in DAFC applications with improved electrocatalytic activity. To enhance the electrocatalytic performance of Pt toward the ORR, the incorporation of 3d transition metal (TM) is also done, but it also affects the catalyst's durability. To overcome this situation, an ultrathin alloy NWs of PtGa was fabricated that deals with the unconventional *p-d* hybridization interactions. The as-prepared catalyst $\text{Pt}_{4.31}\text{Ga}$ NWs/C catalyst performs better, i.e., 12.1 times higher specific activity and 10.5 times higher mass activity than commercially available Pt/C catalyst. The tolerance toward CO and long-term stability of the catalyst was also enhanced by adding Ga for ORR. After 30000 cycles, the mass activity decreases to 15.8% for $\text{Pt}_{4.31}\text{Ga}$ NWs/C while decreasing by 79.6% for Pt/C catalyst [100].

3.2. Nanotubes

Carbon-based materials are the emerging supporting material for the Pt-based catalyst in different applications. These catalysts work very well in alkaline medium but have some limitations in acidic media. To overcome this problem, Chen et al. [101] doped carbon nanotubes (CNTs) with nitrogen using a single-step chemical vapour deposition (CVD) approach. For this purpose, ferrocene or iron (II) phthalocyanine is used as a catalyst and pyridine are used as a precursor for carbon and nitrogen. Nitrogen-doped CNTs are synthesized with the catalyst of various morphology. The surface defect has an essential role in the

electrocatalytic activity, i.e., by increasing the deficiency of surface in nitrogen-doped CNTs, ECSA increases; as a result, the electrocatalytic performance also increases.

Further, in this manner, a comparable outcome was obtained by Zhang et al. [102], who arranged homogeneous & stable CNT layer sheets on glassy carbon electrodes (GCE) using a layer-by-layer approach. The electrostatic attraction occurs between shortened & negatively charged multi-walled CNTs (MWCNTs) with positively charged poly(diallyl dimethylammonium chloride) for this assembly. The fabricated material exhibits better stability and uniformity, adsorbed from tiny MWCNT bundles either single tube on the substrate and outstanding electrocatalytic performance in the alkaline medium for ORR. These properties are due to the higher surface area and good conductivity of MWCNTs [103–105]. Zhang et al. [106] revealed that toward the ethanol oxidation reaction (EOR), the catalytic performance of Pd-NPs was enhanced by the presence of inner tubes of CNTs. Further, Pd-NPs supported on CNTs with 3–7 walls exhibit more electrocatalytic performance than multi-walled and single-walled CNTs.

Last few years, much attention has been paid to the Kirkendall effect for the formation of nanotubes. In this effect, the motion of the interface takes place between two metals due to the difference in their rate of diffusibility. Based on this, CdS nanotubes are fabricated using the Kirkendall effect, in which, Cd-NWs are fabricated by electrochemical step-edge decoration on a graphite electrode. Further, high-temperature sulphidation of Cd NWs gives CdS nanotubes. In this process, when Cd NWs come in contact with the graphite surface result in the partial restriction in the diffusion of sulphur and produce hemicylindrical CdS nanotubes.

Some reports also informed the formation of nanotubes by Kirkendall-induced hollowing route due to ejection and diffusion rates of vacancies. It was also responsible for the uniform thickness of nanotubes' walls, i.e., when the rate of ejection of vacancies is higher than its rate of diffusion, nanotubes with uniform wall thickness were obtained [107].

Further, control over the diameter and density of nanotubes is also

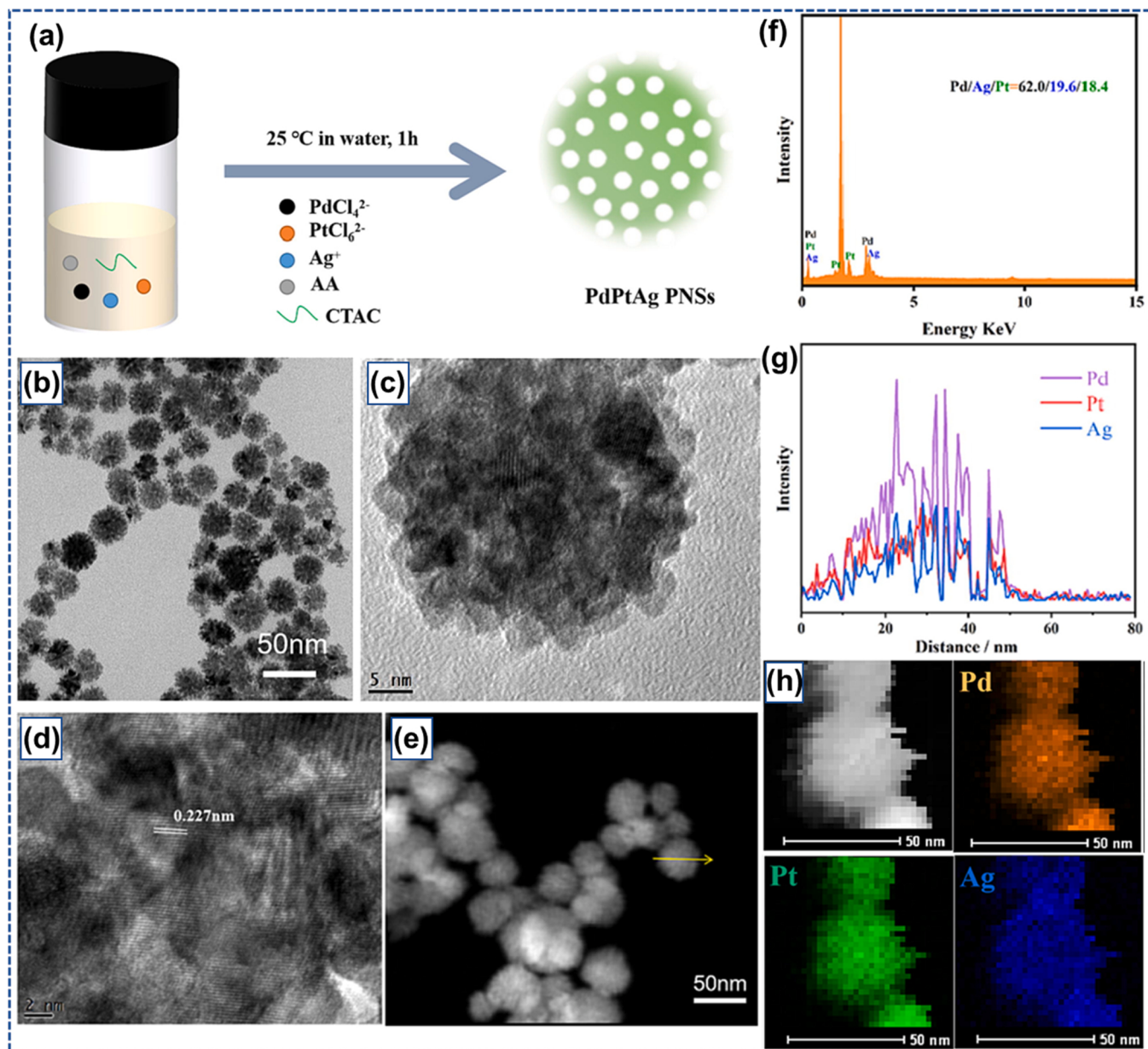


Fig. 9. (a) Graphic representation of fabrication of PdPtAg porous nanospheres. (b) TEM picture of PdPtAg PNSs, (c, d) HRTEM photos, (e) HADDF-STEM picture, (f) SEM-EDS study, (g) EDX line-scan shape (the yellow zone within Fig. 9e), and (h) STEM-EDS mapping photos of PdPtAg PNSs. Reproduced with permission from [98]. Copyright 2023 Elsevier.

necessary. This can be done by managing the formation of a catalyst. The process of catalyst formation is modified by using the Ostwald ripening mechanism. In this process, the small particles of liquid and solid solution are deposited over the large particles to give a more thermodynamically stable structure in which surface to area ratio is decreased. To control the diameter and density of single-walled nanotube forests, the Ostwald ripening approach is applied in which catalyst formation is altered with exposure to H₂. Diameter and thickness are inversely proportional to each other. Investigation shows that by using Ostwald ripening, the surface energy of the catalyst is enhanced by exposure to H₂ and the diffusion coefficient of the Fe catalyst was also controlled by growth temperature to produce single-walled nanotubes [108].

Nowadays, the energy storage problem is a big issue, and lithium-ion batteries (LIB) are more competent in solving this. But the graphite-based anode is the major problem for LIB. This problem is solved by using one-dimensional nanotubes with large surface areas and routes for the continuous transport of electrons. In research using a selective

dissolution-regrowth mechanism, amorphous FeOOH hierarchical nanotubes are fabricated from FeVO₄ NWs. These nanotubes are used in LIB and enhance their performance [109].

Beltrán-Gastélum et al. [110] fabricated Pt-Au/ MWCNT using a reverse microemulsion approach. To know the electrocatalytic performance of as prepared material toward ORR, it is compared to Pt/C, which is available commercially. The homogeneous distribution of Pt-Au on MWCNT is properly shown by the Pt-Au/MWCNT electrode catalyst micrographs. Due to this, a multi-dimensional network-like arrangement has also been produced that help in the transfer of electrons/protons and in this manner, active sites are also increasing, as shown in Fig. 10(a, b). The commercially available Pt/C NPs more and less magnification, shown in Fig. 10(c, d) over the Vulcan carbon with a brilliant deposition of Pt over the support of carbon. Homogeneous distribution of particles is observed at lower magnifications, and no overlapping of particles is observed at higher. Spectroscopic and microscopic techniques were also used to characterize these materials.

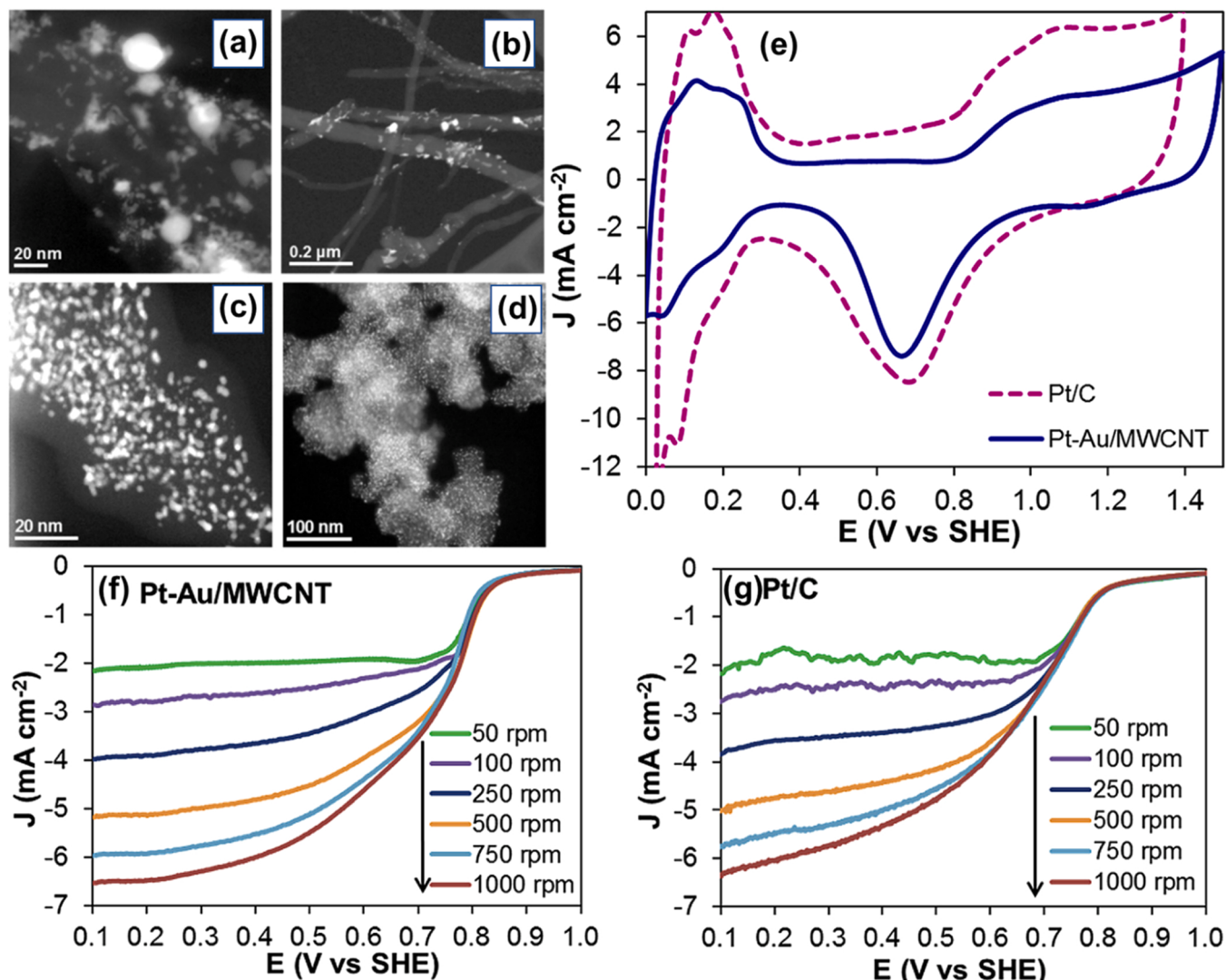


Fig. 10. TEM images of (a, b) Pt-Au/MWCNT and (c, d) Pt/C commercial. (e) Pt-Au/MWCNT and commercially available Pt/C electrocatalyst's CVs in 0.5 M H₂SO₄ at a scan rate of 100 mV s⁻¹. By using various rotation speeds, Linear voltammograms are noted in H₂SO₄ saturated with O₂ at a scan rate of 5 mV s⁻¹ for (f) Pt-Au/MWCNT, (g) Pt/C at a scan rate of 5 mV s⁻¹.

Reproduced with permission from [110]. Copyright 2016 Elsevier.

The result shows that the kinetic current density (CD) of Pt-Au/MWCNT is more than Pt/C at 0.7 V, as shown by a CV shown in Fig. 10(e) below. The power density of Pt-Au/MWCNT was 625 mW cm⁻², and for Pt/C, it is 355 mW/cm². LSV was used to measure the electrocatalytic performance of the catalyst toward ORR using the rotating disk electrode method. The voltammogram of Pt-Au/MWCNT is shown in Fig. 10(f), and Pt/C is demonstrated in Fig. 10(g). The onset potential for ORR has been found at 0.8 V vs SHE for both materials.

An anode catalyst is fabricated using the reduction method for FC applications. The catalyst comprises three materials: MWCNT, CeO₂ and Pt or Pd metal. The fabricated catalyst was tested using X-ray diffraction (XRD), TEM, Raman spectroscopy, CV, CA, and carbon monoxide stripping voltammetry. The result shows that 1Pt1Pd-CeO₂/CNT electrocatalyst has a superior electrochemically active surface area, better stability and advanced oxidation activity for HCOOH, EtOH and MeOH in comparison to commercially available Pt/C catalysts. This is due to the alteration of the surface electronic structures [111].

3.3. Nano dendrites

Due to its higher electrochemically active surface area, low-density bimetallic nano dendrites (NDs) are used in diverse catalytic applications. On behalf of this, PtRu NDs are fabricated by Ru & Pt co-reduction as a precursor in oleylamine with dihydrogen. The PtRu NDs show excellent catalytic performance and better stability compared to nanocrystals of PtRu and Pt, which are fabricated in the same pathways for MORs [112]. Modifying tiny particles' structure and morphology is very easy and efficient to boost the electro-oxidation performance. Considering that Pham and Huynh fabricated bi-metal-based Pt₃Cu NDs having multi-branched arrangement on W-shaped nano support of TiO₂. The above-discussed material was fabricated using a microwave-assisted approach in which ascorbic acid acted as a reductant. The synthesized catalyst exhibited excellent activity toward C-supported NPs (E-TEK) for MOR having negative onset potential, higher current density, good tolerance to CO and better stability. These characteristics are due to dendritic morphology and the electronic effect and synergic of material, Pt₃Cu, and mesoporous W-shaped TiO₂ nano-support. NDs have more excellent active sites as compared to spherical nanocrystals. The

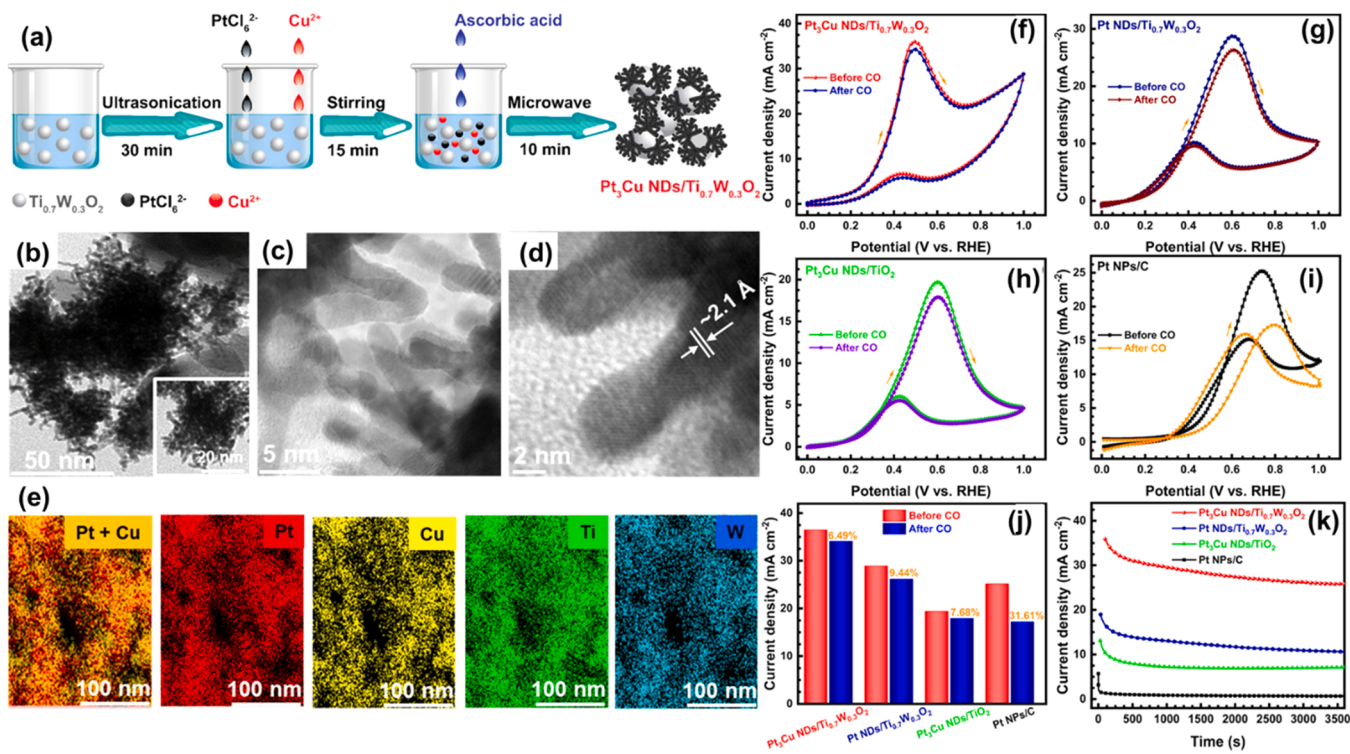


Fig. 11. (a) Schematic representation of the W-shaped TiO_2 -supported bimetallic Pt_3Cu NPs electrocatalyst. (b, c & d) TEM & HR-TEM images; and (e) elemental mapping of Pt_3Cu NPs electrocatalyst decorated on W-shaped TiO_2 -support. (f-i) CV of as-prepared catalyst and (j) anodic peak CD comparison of various electrocatalysts before and after CO removal at a scan rate of 25 mV s^{-1} . (k) CA curves of the catalyst at a constant potential of $0.5 \text{ V}_{\text{RHE}}$ in N_2 -purged KOH (1.0 M) + MeOH (1.0 M) for 3600 s.

Reproduced with permission from [113]. Copyright 2021 American Chemical Society.

diagrammatic presentation of the complete procedure showed in Fig. 11 (a) below. TEM images displayed the bimetal-based Pt_3Cu nanoalloy dendritic-like shape in Fig. 11(b, c). The high-resolution TEM image (Fig. 11(d)), near 0.21 nm , shows the interplanar spacing related to pre-performed works. Moreover, during the MOR test, CO was expelled to check the electrocatalyst tolerance possibility toward CO. Fig. 11(f-i) displayed the CV curves of nanocatalysts in MeOH alkaline medium before and after removal of CO. By the adsorption of CO at the surface of the electrocatalyst, the CD for all the electrocatalysts decreases. This all happens when the supply of CO is cut off. Due to this, the current density of catalysts decreases to 6.49% in Pt_3Cu NPs/ $\text{Ti}_{0.7}\text{W}_{0.3}\text{O}_2$, 9.44% in Pt NPs/ $\text{Ti}_{0.7}\text{W}_{0.3}\text{O}_2$, and 7.68% in Pt_3Cu NPs/ TiO_2 catalyst. Further, a significant decrease in the current density of 31.61% was found in the case of the C-supported Pt (NPs) electrocatalyst (Fig. 11(j)). The result indicates that oxidation of adsorbed CO is accessible in the case of a prepared catalyst compared to a C-supported Pt (NPs) catalyst. For all the fabricated electrocatalysts, in the starting, a fast decrease is observed in polarization current as shown by CA curves Fig. 11(k); this results from the aggregation of adsorbed particles due to MeOH incomplete oxidation [113].

Sun et al. [114] synthesized several PdPb NPs, similar to sea urchins, as high-efficiency electrocatalysts for ethane-1,2-diol and glycerol oxidation reactions. Out of them, Pd_3Pb NPs show superior electrocatalytic behaviour and durability compared to other commercially available Pt/C. This behaviour is due to its morphology, which provides a large electrochemically active surface area. Later, chlorine-free Rhodium-NPs (Rh-NPs) are fabricated using a one-step wet chemical synthesis method that proceeds in single-step for the alkaline DMFCs. In suitable conditions, Rh-NPs show an increase in electroactivity up to 3.17-fold with increased stability for MOR due to irregular-shaped Rh-nanocrystals. These ND shapes not only give huge surface area & rich edge atoms that have higher electroactivity but, on the other hand,

also prevent the aggregation of NPs. In this way, both, i.e., KOH and MeOH concentration, affect the electroactivity of Rh-NPs [115].

3.4. Nanofibers

Fibres with a diameter between 1 nm and $1 \mu\text{m}$ are known as nanofiber (NFs). These NFs can be produced from various polymers. Due to this, they have different utilities with different physical properties. NFs can be classified into multiple classes, i.e., (1) based on raw materials (organic, inorganic and carbon & composite fibres), (2) based on structure (nanoporous, hollow, nanoporous and core-shell fibres). Using different approaches like electrospinning, phase separation, self-assembly and template synthesis. For the fabrication of NFs polymers like keratin, silk fibroin, collagen, gelatin, poly(lactic-co-glycolic acid), cellulose, poly(lactic acid), poly(ethylene-co-vinyl acetate) as well as polysaccharides like chitosan, alginate etc. NFs are lightweight with high surface-to-volume ratios and small diameters with adjustable pore structures. Due to this, they are used in various applications [116].

Hsin et al. [117] investigated a novel poly(vinylpyrrolidone) (PVP) modification approach in a solution of water that are useful in the incorporation of high-density and homogeneous surface functional group on various carbon-based nanomaterials. Using PVP and conventional acid-oxidation approaches, they modified the surface of herringbone graphitic carbon NFs, multiwalled carbon nanotubes (MWCNTs) from arc discharge & from chemical vapour deposition (CVD) and commercially available carbon black Vulcan XC-72R. Further, NPs of Pt with size 1.8 nm were homogeneously deposited over the surface of the PVP-modified carbon nanomaterials, i.e., Pt-PVP-carbon nanocomposite and their performance for direct methanol oxidation. In addition, PtRu-PVP-graphitic carbon NFs are also fabricated by them. The electrical conductivity was tested for these materials, and it was found that MWCNTs arc shows much electrical conductivity of 31 S/cm as

compared to graphitic carbon NFs (14.2 S/cm), Vulcan XC-72R black (7.6 S/cm) and MWCNTs CVD (13.6 S/cm). Generally, surface modification decreases electrical conductivity, but PVP modification leads to higher conductivity than acid-oxidized nanomaterials.

Alvi et al. [118] fabricated Pd-Ce bimetal-based carbon NFs using an electrospinning approach and used it as an electrode catalyst for detecting MeOH FCs. The Pd-Ce decorated carbon NFs also used to prepare an anode for DMFCs. They show higher electrocatalytic performance toward methanol oxidation. DMFCs work like next-generation power sources in portable devices. But the main problem associated with the DMFCs is membrane electrode assembly (MEA), which can be solved by applying flexible electronic gadgets. Considering this, researchers fabricated flexible titanium carbide/carbon NFs (TiC/CNFs) film using an electrospinning approach used as a gas diffusion layer (GDL) and microporous layer in a dual role. Using TiC/CNFs increases the power density of flexible DMFCs up to 20.2 mWcm^{-2} compared to previously used carbon cloth which is 18.1 mWcm^{-2} [119].

Further, a new electrode catalyst was fabricated based on polypyrrole-CNF (Ppy-CNF) materials supported on Pt NPs that enhance the stability of Pt/CNF/GDL electrocatalyst in DMFC by using the solution dispersion method. In which 0.4 mg/cm^2 loading of Pt done with 20 wt% Ppy-CNF. The particle size of Pt/PPy-CNF is 3.69 nm, Pt/CNF is 6.51 nm, and Pt/C it is 2.91 nm. The fabricated Pt/PPy-CNF/GDL electrode shows a comparable electrochemical active surface area, MOR performance and high durability (in the presence of MeOH) compared to the Pt/CNF /GDL and Pt/C/GDL. A rather significant decrease in the peak potential of MeOH electro-oxidation from 0.69 V for Pt/C/GDL to 0.76 V for Pt/PPy-CNF/GDL electrode shows an enhancement in the performance for MOR is obtained by using the PPy-CNF in place of C. The equivalent electrochemical active surface area values for the electrodes Pt/PPy-CNF/GDL is $108.69 \text{ m}^2/\text{g}$, Pt/CNF/GDL is $53.93 \text{ m}^2/\text{g}$, and Pt/C/GDL is $17.98 \text{ m}^2/\text{g}$ [120].

3.5. Nanosheets

The two-dimensional (2D) nano arrangement with 1–100 nm thickness is known as nanosheets (NSs). The most commonly used nanosheet is graphene, the thinnest nanosheet, i.e., 0.34 nm. Like graphene NSs may be single-layer, or it may be a multilayer. Nanomaterials are of various shapes, like zero-dimensional NPs, one-dimensional NWs, and 2D NSs. Currently, noble metal-based 2D NSs took much attention because of their different and versatile properties, like higher surface area, huge uncovered unsaturated atoms etc., that increases the catalytic performance of these NSs [121]. Due to their superior properties, NSs-based Pd is used as an efficient electrode catalyst for the oxidation

of monobasic and polyhydric alcohols. Pd-based NSs are generally fabricated by a nonuniversal approach and involve surfactants. This result in a surface covered with residue that extremely damages electrocatalytic characteristics. To improve this, a universal one-pot method consists of no surfactant.

Pd-M-based NSs with tremella-like morphology are fabricated using this method with the ultrathin 2D NSs, where M= Pb, Ga, Ag, Au, Pt, Cu, etc. The fabrication method is shown in Fig. 12. The Pd-M NSs show 3D structures with a clean surface that overcome the problems related to 2D NSs. The NSs of Pd-Ag, Pd-Pb and Pd-Au, having tremella-like morphology, exhibited superior performance toward ethanol oxidation reaction and ethylene glycol oxidation reaction and enhanced tolerance toward CO poisoning with good electronic effect. The as-prepared NSs, i.e., Pd₇Pb, Pd₇Ag NSs and Pd₇Au NSs, show 7.2, 8.2 and 5.3 times higher for EOR and 5.7, 7.3 and 4.4, times higher for EGOR mass activity as compared to commercially available Pd/C catalysts. The as-prepared Pd-M NSs also exhibited excellent electrocatalytic stability [122].

Zhao et al. [123] fabricated PdAuBiTe-based 2D ultrathin NSs using a novel visible-light-induced template method. The fabricated catalyst shows a higher mass activity of 2.48 A mgPd^{-1} toward ORR, 27.5 times higher than industrial Pd/C and 17.7 times higher than commercial Pt/C. No reduction in ORR performance was observed after 10000 cycles with high tolerance toward methanol and CO poisoning. The NSs of PdAuBiTe act as cathode catalysts in DMFCs with high power density and durability. Due to their remarkable surface morphology and electronic characteristics, the ultrathin 2D NSs enhanced the electrochemical activity of fuel cell oxidation reaction and hence get much attention nowadays.

The ultrathin 2D morphology of NSs provides an ultra-high specific surface area that permits the maximum fraction of visible surface atoms to work as active sites and is hence helpful in advancing the kinetics of electrocatalytic reactions. This ultrathin property of NSs also decreases the diffusion path and leads to the fast interfacial transport of electrons throughout the electrocatalytic performances. It is concluded in various studies that the more defective structure of 2D NSs that are reduced to atomic scale does not affect its physicochemical and electronic behaviour. Due to this, they highly enhanced the performance of the MOR. It is considering various defect engineering done in NSs to enhance the active site number and reactivity with the electrical conductivity of different materials. One defect engineering uses oxygen vacancies, making NSs more suitable for electrochemical applications [124].

Further, in this way, Yang et al. [125] fabricated ultrathin NSs of NiO crystals which is rich in oxygen vacancies. This material plays a very significant role in enhancing the MOR process. Theoretical results also indicate that introducing oxygen vacancies increases NiO crystal's

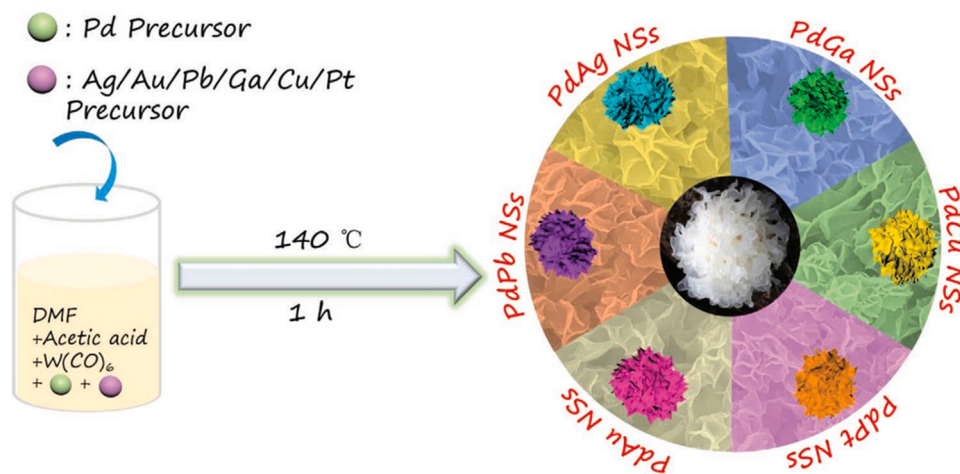


Fig. 12. Schematic representation of 3D tremella-like Pd-M NSs fabrication (M= Ag, Pb, Au, Cu, Ga and Pt). Reproduced with permission from [122]. Copyright 2020 John Wiley and Sons.

electrical conductivity and reduces MeOH molecules' adsorption energy over the active surface. Both these processes are much favorable to robust electrocatalytic MOR activity.

4. Catalyst synthesis for fuel cell applications

Polymer electrolyte membrane FC is a most excellent energy-converting device. FC's efficiency effectively increases using an electrode catalyst, mainly at the working electrode. The overpotential of FC reactions is also altered by altering the arrangement and composition of the electrode catalyst [126]. Other supporting materials also affect the electrochemical reactions and the electronic conductivities of FCs [127]. Much attention was paid to synthesizing cathode catalysts due to the higher overpotential of ORR compared to hydrogen oxidation reaction (HOR). In the initiation of FC, catalysts are only made from Pt to enhance the effectiveness of FC. However, the cost of Pt is so high also has some chances of catalyst poisoning. To solve these problems, Pt is alloyed with other materials like metals, polymers, carbon supporting materials etc. [128]. NPs of metals on carbon-based supports have more significant surface areas and retain tremendously large electrochemically active surface areas [129].

Various carbons materials like CNT, graphene, & CNFs, including carbon blacks, act as supporting substances to increase the catalyst activity and longevity of NPs [130–132]. Moreover, some metal-based oxides are also used because of their metal-support solid connections and are more corrosion-resistant. And it acts as support materials in place of freshly used carbon-based substances [133,134]. In place of Pt, now Pd-based electrocatalysts paid much consideration for alcohol-based FCs due to its less price and more tolerance to the poisoning of CO, which is liberated during electrooxidation of alcohols. It also noticed that pure Pd is not much competition for FCs as a catalyst.

On behalf of the above facts, various Pd-based bi-metallic and tri-metallic electrode catalysts were fabricated from time to time by many researchers to robust the FC activity by decorating it on GCE. Highly dispersed Pd-nanostructures use a substitute approach with measured size and structure on supporting materials with an enormous specific surface area to robust the catalytic performance and effectiveness. The nano size of metal particles has more tendencies for oxidation to stabilize nanomaterial, which has successful alternatives with incorporating polymer matrices that work as a supporting material and stabilizer for the NPs. Numerous bi-metallic-based catalysts like Pd-Co [135], AuNPs carbon-nitride (AuNPs-CN) [136], Pd poly diaminonaphthalene (Pd-pDAN) [137], Pd poly [4-thiophene-3-yl] aniline (Pd-pTA) [138] etc. are produced to robust electrooxidation of the MeOH in the presence of alkali like KOH in DMFC's applications.

4.1. Noble metal-based catalyst

Noble metal NPs broadly employed as electrode catalysts in the oxidation of alcohol and ORR in FCs and different heterogeneous catalytic reactions. However, inadequate support of noble metals throws objections to decreasing the amount of its application to scientists that work on materials. Processing of both (non-noble and noble metals) that consist of different parts and a mainly homogeneous mixture of metals is initiated. Due to their novel assembly and combinations, it would be an active protocol, which improves their catalytic performance and toxic endurance [139]. Concerning the selection of noble metals, comparatively low-priced Pd has been proposed as a suitable substitute for Pt. The price of Pt-based catalysts is the main drawback of using FC techniques, as the catalyst only estimates the acquisition cost of 54% of the total stack cost [140].

On the other hand, in an acidic medium, some FC shows less catalytic performance with Pd compared to Pt [141]. It stimulates the call for the investigation to discover an advanced, less expensive electrode catalyst based on Pd for the mechanical implementation of direct fuel cells (DFC). It is observed that the electrocatalytic behavior of Pd can be

enhanced by including an oxygen-loving metal within the electrode structure. It can improve the binary arrangements of electronic and structural characteristics [142] and decrease the expense. Pd can reduce protons and commodities and release H₂ that could extract adsorbed CO produced while electrocatalytic oxidation of alcohols [143].

Yu et al. [144] resourcefully filled or connected this research gap by synthesising an efficient nanocatalyst based on nanocrystals with endlessly tunable surface morphology. Fig. 13(a) displayed the fabricated Pd nanocrystals SEM and TEM images having different surface morphology. This Pd nanocrystal-based catalyst has high-index facets and acts as a perfect electrocatalyst for studies in structure-reactivity at the nanoscale. Electrooxidation of small organic particles related to fuel cells like HCOOH, MeOH, EtOH, C₃H₇OH and ethane-1,2-diol with its voltammograms is shown in Fig. 13(b). The sensitivity of surface structure was found to be different for electrocatalytic reactions up to a large extent. For the multi-carbon alcohols, the catalytic activity increases with step density (d_{step}) enhancement. Furthermore, a little change was observed for MeOH, and an HCOOH decrease in catalytic activity was observed with an increase in d_{step} , as shown in Fig. 13(c). The peak CD and d_{step} were normalized to estimate surface structure sensitivity quantitatively; did the normalization up to the obtained value on the lesser stepped tetrahedreal (THH) (1030) Pd nanocrystals. As shown in Fig. 13(d), the normalized activity was directly related to the normalized d_{step} , giving slopes for the electrooxidation of EtOH (2.93), n-propanol (1.99), ethylene glycol (1.35), MeOH (0.10), and HCOOH (−0.62).

For the FC utilizations, the bi-metal-based homogeneous mixture of Pd with an initial transition metal, for example, Pd-Co [145], Pd-Cu [146], Pd-Ni [147], Pd-Ag [148], etc. They showed tremendous catalytic performance compared with a single metal-based Pd catalyst and decreased the expense positively. It is also known that the catalytic activity of materials is also affected by the polymers due to a decrease in metal atom's surface area. To overcome the present obstacles, the preparation of catalysts, like Pd-doped catalysts distributed on a variety of solid supports (carbon-based) can enhance the properties and stabilities of the NPs over the surface of the as-prepared materials [149].

4.1.1. Pt-based catalysts

At first, Pt-metal was used as a catalyst for the electrooxidation of alcohols in FC applications to enhance efficiency. Scientists showed that hydrogen and alcohol (with low molecular weight) are used as fuel. At the same time, carbon-based Pt is usually utilized as an anode and cathode electro-catalyst at lower-temperature FCs [150]. The metals of the Pt-group can act as great electrode catalysts for MeOH or ethanol oxidation processes for DAFCs [151]. The catalytic behavior of Pt-based nanocatalysts depends on the pattern, diameter, and exposed surface part. Various pieces of research have been done from time to time to provide a suitable equilibrium between Pt and the metal, starting with superior complete identification [152–155]. Diverse structures of Pt-based electrode catalysts like nanoplates, nanowires, and nanotubes, and three-dimensionally arranged macroporous structures have been investigated [156–158]. Here in this section, we reviewed the morphology and synthesis method of Pt-based catalysts that could alter the FC performance.

In support of that, the effect of the orientation of NPs in the matrix was studied by Antoniassi et al. [159] where they fabricated Pt-SnO₂/C electrode catalyst carrying cubic-shaped Pt-NPs via facet (100) orientations for DEFC. The electrochemical effects for DEFC that Pt-SnO₂/C electrode catalyst supporting Pt-NPs by preferential (100) directions provide an improved achievement for EOR. Wang et al. [151] prepared planned nano-sized cathodes that were constructed on suitable vertically arranged Pt-nanotubes used in DMFC through a method involving sacrificial template outline and in-situ galvanic replacement.

Incorporating foreign metal is the most suitable approach to improve catalytic accomplishment, including performance and durability. It also decreases the consumption of Pt-metal. Bi-functional and electronic

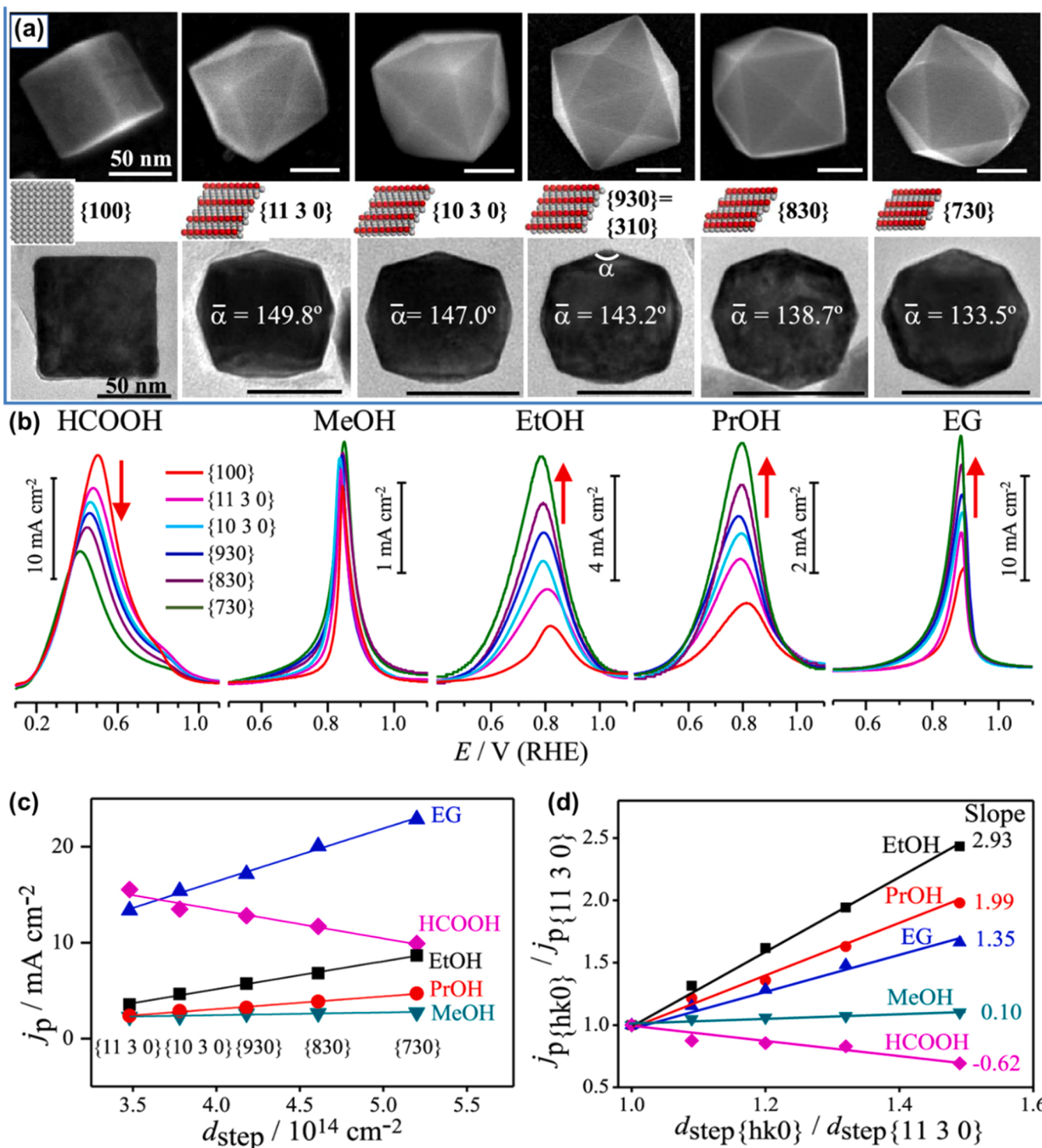


Fig. 13. (a) Pd nanocrystals SEM and TEM pictures, fabricated using electrochemical square-wave potential approach having diverse upper limit potential (E_U) in 0.1 M $HClO_4$ & 0.1 mM $PdCl_2$, 50 nm for bare scale. At E_U value 0.950 V, the Pd nanocubes are obtained; THH Pd nanocrystals having facets, (1030), (930), (830), (730) on E_U value 1.000 V, 1.010 V, 1020 V, 1.030 V & 1.040 V respectively. These facets of atomic models are also shown. (b) HCOOH (formic acid), MeOH (methyl alcohol), EtOH (ethyl alcohol), EG (ethylene glycol), PrOH (n-propanol) LSV on Pd nanocrystals at a scan rate of 0.05 $V s^{-1}$. The solution contained 0.1 M $NaOH$ or 0.1 M HCOOH with 0.1 M $HClO_4$ + MeOH/EtOH/EG/PrOH. (c) The peak CD depends on step site density. (d) Normalized peak CD vs normalized density of step sites, the reference value of THH (1030). Slopes reflect the reaction's sensitivity toward the structure of the surface.

Reproduced with permission from [144]. Copyright 2019 American Chemical Society.

consequences (ligand effect) are suggested for improved bi-metallic or tri-metal-based electrocatalytic activity [160]. Researchers have testified the PtNi alloy corrosion electrochemistry at the time of catalyst-based ORR, as given in Fig. 14(a). Fig. 14(b) displays the

ultrathin layer of obtained nanocage of PtNi, which consists of Pt_3Ni alloys and is covered by Pt skin. The half-wave potential diagram of PtNi hollow material compared with commercially available Pt/C catalyst is displayed in Fig. 14(c) that the PtNi nano chains exhibit an increase of

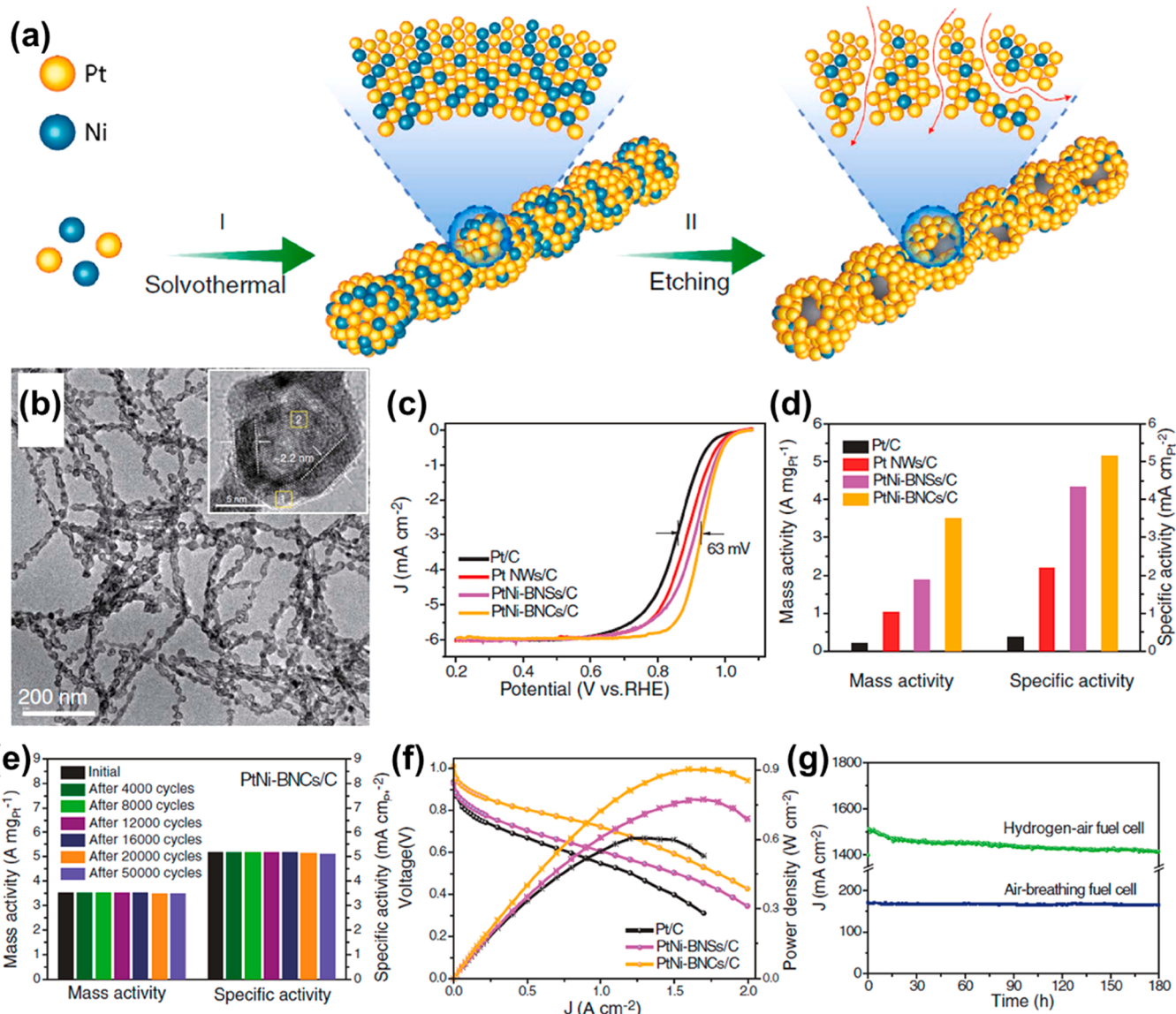


Fig. 14. Bunched PtNi hollow nanocage (a) Diagrammatic representation of fabrication, (b) TEM pictures, (c) polarization curves for ORR, (d) mass activity and surface activity at the potential of 0.9 V vs RHE, & (e) accelerated durability test for 50,000 cycles. (f) polarization plots of H₂-air FC. (g) Durability test of air-breathing FC & H₂-air FC at a potential 0.6 V.

Reproduced with permission from [161]. Copyright 2021 American Chemical Society.

63 mV on applying ORR. The mass and surface activity of the above-discussed catalyst is demonstrated in Fig. 14(d); the result shows that its mass activity is 17 times and surface activity is 14 times higher in comparison to commercial Pt/C catalyst. The PtNi hollow nanocage catalyst is highly durable and shows insignificant decay after proceeding with 50,000 potential cycles, as shown in Fig. 14(e). The PtNi nanocage also shows excellent activity toward FC applications, as shown in Fig. 14(f); when it was tested for H₂-air FC exhibited a CD of 1.5 A /cm² at a potential of 0.6 V and a peak power density of 920 mW/cm². Fig. 14(g) shows the PtNi hollow nanocage stability test for an H₂-air FC at a fixed voltage of 0.6 V for 180 h. The catalyst offers superior electrochemical activity and durability toward ORR [161].

Based on a successive reduction approach, an electrode catalyst, Pt_{shell}-Au_{core}/C was synthesized with a measured shell width. Different methods like XRD, UV-vis and some electrochemical procedures have recommended the development of core-shell arrangement. The electrocatalytic performance was examined by using MeOH electro-oxidation process as research. Core-shell catalysts with a whole and a

thin shell of Pt on Au exhibit superior catalytic performance compared to Pt/C as an outcome of advanced Pt use. Further, to know the advanced use of Pt in core-shell-like morphology compared to commercial Pt/C catalyst, the ECSA of Pt-based electrode catalyst is displayed by CV in Fig. 15(a), which is known by adding hydrogen desorption region. A specific surface area is obtained by dividing the ECSA by the weight of Pt. Fig. 15(b) the electrocatalytic behaviour of PtAu/C, which was investigated in H₂SO₄ (0.5 M) and MeOH (1 M) at 25 °C. As the ratio of Pt/Au increases, the specific catalytic performance of Pt retards, as shown by the peak current [162].

Regarding bi-functional effects, as in the MOR on Pt metal, the different metal is engaged for a breakdown of H₂O at a lesser potential value, which enhances the CO oxidation and increases the stability. Concerning the electronic factor, other metals can modify the electron-based characteristics of Pt and decrease the CO adsorption energy, promoting CO oxidation at lesser potentials. e.g., Ataee-Esfahani et al. [163] synthesized with space inside mesoporous Pt-Ru alloy materials, which shows more CO tolerance for MOR. Their research showed that

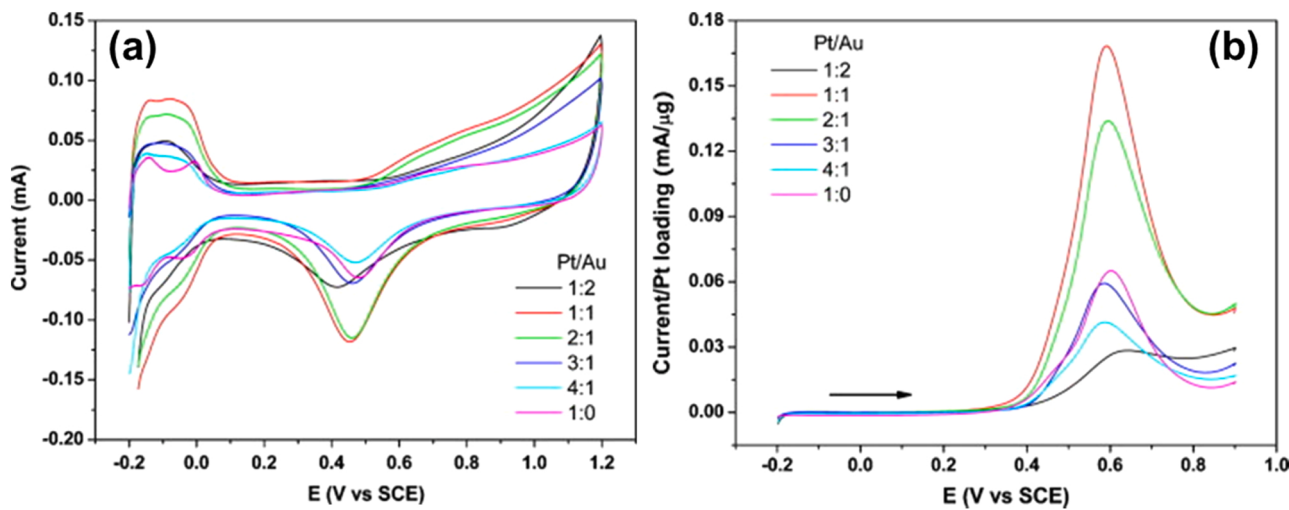


Fig. 15. (a) At a scan rate of 50 $mV s^{-1}$, CV of 20% Au-Pt/C and 20% Au/C with diverse mole ratios in N_2 purged 0.5 M H_2SO_4 . (b) Anodic scan of Pt/C and PtAu/C having diverse mole ratios at 10 mV^{-1} in CH_3OH (1 M) + H_2SO_4 (0.5 M). Reproduced with permission from [162]. Copyright 2008 Elsevier.

this advantage emerges from a dual point of view, a down-moved centre of the d -band (electronic factor). It adsorbed O_2 -retaining species on Ru atoms (bi-functional factor). The homogeneous mixture of Pt with different support metals, like V [164], Cr [165], Co [166], Ti [167], Pb [168], Hg [169], Cu [170], and Ni [171], & of some noble metals, like Pd [172,173], Ru [174], Au [175], and Ag [176], had been established to show considerably superior electrocatalytic durability and improved performance for the ORR in PEMFCs as compared to Pt.

A development to various organizational alterations that are produced by mixing homogeneously, like geometrical aspects (reduced bond length of Pt-Pt) [177], most oxidizing alloying substances solvation [178], alteration in surface texture [179], or electronic aspects (enlarged Pt d -band electrochemical empty space of the Pt skin film, which initiates from the interior alloy) [180,181]. Superior catalytic characteristics and durability can be obtained by using metal NPs on conductive or semi-conductive d -block metal oxides, like TiO_2 , CeO_2 , WO_3 , and NbO_2 , which robustly act together with right-side d -block elements, i.e., late transition metals [182–184]. The alternative support materials possess lower surface area but higher stability compared to some standard carbon support in an electrochemical atmosphere, leading to higher durability on Pt NPs. For example, Popov's group [185] verified that it could enhance the durability of Pt-NPs against Pt solvation by using NbO_2 as support material for ORR after 30,000 cycles.

Cao and co-workers [160] synthesized mesoporous TiO_2 base material for Pt NPs, which possess great FC activity & more excellent durability, even at a higher (+ve) potentials value of 1.2 V. Some researchers fabricated self-supported 1D nanorods of Pt having different lengths starting from 0.6 to 3.2 nm, as shown in Fig. 16(a, b) SEM pictures of the surface with its cross-section. The 1D Pt nanorods had more density of mesopores with a size of 6–8 nm, and the wall thickness was 2–3 nm. The mesoporous Pt nanorods are highly stable in nature. Their stability is explained on the basis that they lost 25% and 31% of the electrochemically active surface area after 1000 and 2000 cycles, respectively. The SEM pictures of 1D FePt (Fig. 16(c)) and CoPt (Fig. 16(d)) NWs are presented. The organic-phase decomposition of their precursors fabricates the FePt and CoPt nanowires. The FePt NWs become more active and durable after treatment with acetic acid toward ORR. The SEM images of PtNiP 1D porous nanotubes and broken nanotubes are shown in Figs. 16(e) and 16(f), respectively. These PtNiP nanotubes have enhanced electrochemical activity and long durability toward MOR. Besides these 1D catalysts, some 2D nanomaterials also originated as an excellent and durable catalyst for FC applications.

The 2D nanosheets of Pt were synthesized using an in-situ chemical

vapor reaction. The SEM picture of Pt nanosheets is displayed in Fig. 16(i). These nanosheets are highly active toward ORR because of the absence of carbon and surfactant. Fig. 16(j, k) shows nanosheet's CV and polarization curve, respectively. The loss in electrochemical active surface area is observed when the durability test is done for 30000 cycles.

Further, the dimensions of 3D materials are much higher than others, the Fig. 16(g) FESEM and Fig. 16(h) TEM pictures of 3D ultrathin Pt NWs. These 3D networks are interconnected and responsible for the large porosity and surface area. The 3D Pt nanowires are more stable toward ORR, MOR and formic acid oxidation reactions.

A mesoporous carbon CMK-3 can be prepared by slightly changing the synthesis mechanism, which has a well-defined structure decorated with Pt-NPs and Pt-Ru. Depending upon the concentration of Pt-precursor that was used before carbonization. The sequences of mesoporous carbon within the small amount will be impaired or weakened. A greater concentration of Pt precursor will lead to a bigger particle size and high order. A better activity was observed on the gas diffusion electrode made from fabricated materials than the commercially available catalyst. The electrochemical properties of redox reactions are due to the available larger surface area of the synthesized catalyst, which is obtained by uniform mesoporous of a nanometer in size. The synthesized Pt-Ru/CMK-3 * shows somewhat lesser activity than a commercially accessible Pt-Ru/C catalyst for MOR. However, some uneven performance displayed by the polarization curve in the mass-transfer region is possibly conveyed in the long mesopores [186].

A sequence of Ni/C & Ni-Pt/C catalysts was fabricated and tested by XRD, TEM, CV, chronopotentiometry and FC test. Further, they are applied in direct borohydride FC (DBFC) as the anode catalysts. The particle dimensions of $Ni_{37}-Pt_3/C$ (mass ratio, Pt: Ni = 3:37) catalysts were decreased by adding the extreme-low quantity of Pt. Electrochemical studies revealed that the $Ni_{37}-Pt_3/C$ catalysts' electro-catalytic performance and steadiness further showed enhanced activity compared to the Ni/C catalyst. DBFC is working on $Ni_{37}-Pt_3/C$ catalyst at the anode exhibited the highest power density of $221.0 mWcm^{-2}$ at $60^\circ C$; on the other hand, under a similar situation, the highest power density was $150.6 mWcm^{-2}$ for Ni/C. Moreover, during the active condition of DBFC, hydrogen evolution actions and polarization curves were examined [39].

While the comparative study of $PtCo_3$ and $PtCu_3$ NPs for the formation of alloy and electrochemical performance in ORR, it was established that the highest annealing temperature was 650, 800 and 900 $^\circ C$ up to 7 h for the Pt-Co system. This experiment reveals that the ORR

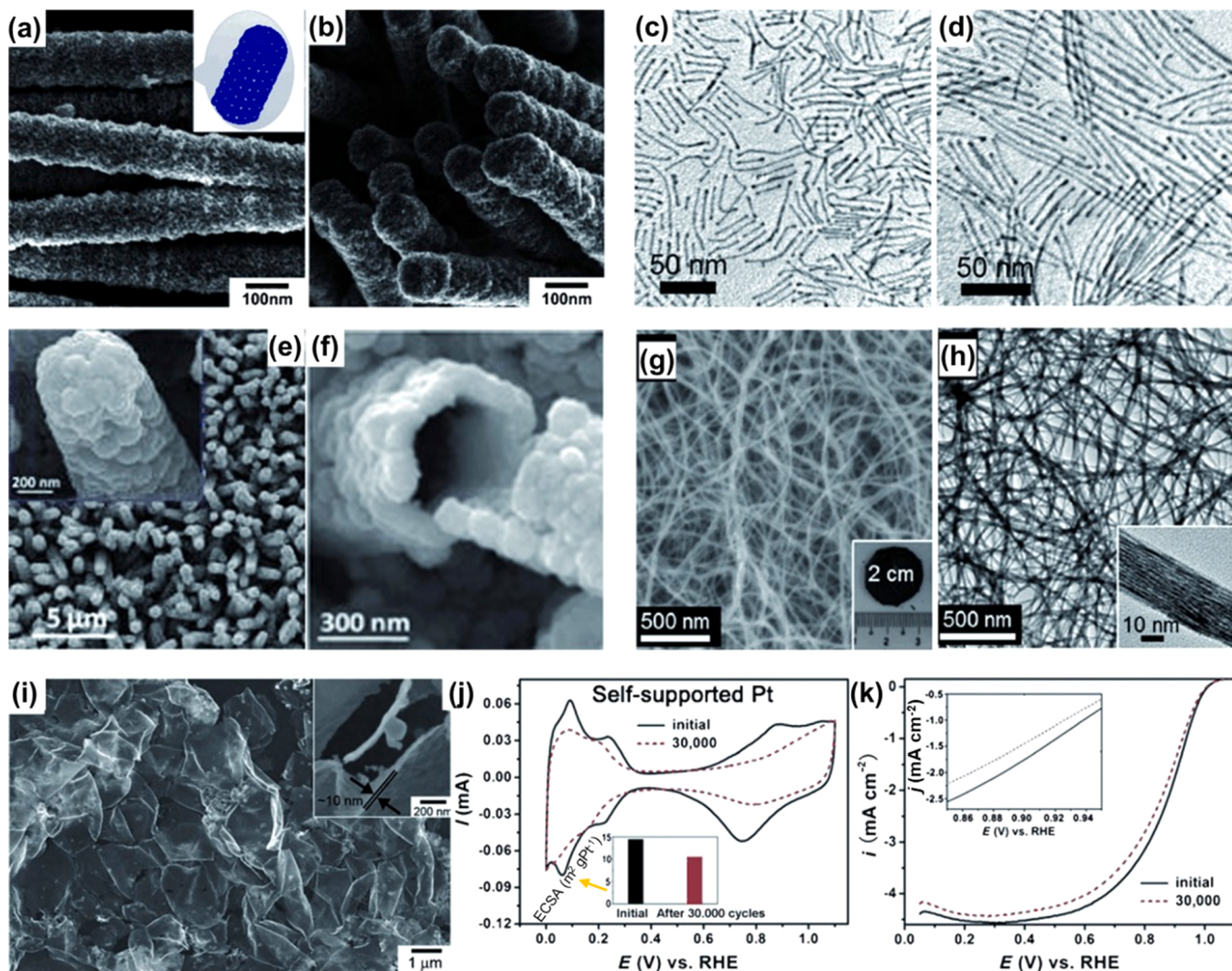


Fig. 16. (a) SEM picture of the surface (the geometrical model in inset) (b) SEM picture of a cross-section of 1D mesoporous Pt nanorods having length: 3.2 μm . (c) 1D FePt TEM images (d) CoPt nanowires TEM image. (e) 1D porous PtNiP hollow nanotubes SEM image, (f) SEM image of 1D porous PtNiP broken nanotube. (g) FESEM (inset shows a picture of Pt NW membrane having a length of 2 cm, and (h) TEM pictures of 3D ultrathin Pt NW clusters. (i) 2D Pt nanosheet SEM image (thickness of sheet shown in inset). (j) CV of nanosheets and (k) nanosheets polarization curves shown before and after 30 000 potential cycles.

Reproduced with permission from [160]. Copyright 2013 John Wiley and Sons.

Table 2
Pt and Pt-based materials/ C-based composite for MeOH oxidation reaction.

Electrocatalyst	Electrolyte used	Type of catalyst	Molarity of methanol (M)	Current density mA/cm ²	Peak potential mV (RHE) (V)	Stability (seconds)	Ref.
Pt ₅ Ru ₄ Ni	H ₂ SO ₄ (1 M)	Anodic	1	1.9	0.5	-	[190]
Pt/CoSe ₂	H ₂ SO ₄ (0.5 M)	Cathodic	0.5	-0.65	0.3	-	[191]
Pt-Ru (1:25)/C	H ₂ SO ₄ (0.5 M)	Anodic	1	3541.0	0.89 (NHE)	4500 s	[192]
Pt-Sn /C-PANI	H ₂ SO ₄ (0.5 M)	Anodic	1	-	1.63	-	[193]
PtCo /MWCNTs	H ₂ SO ₄ (0.5 M)	Anodic	0.5	42.4	1.70	7000 s	[194]
Pt-Co (9:1)/rGO	H ₂ SO ₄ (1 M)	Anodic	2	40.0	1.81	1000 s	[195]
Pt-Zn/CNT	H ₂ SO ₄ (0.5 M)	Anodic	1	-	1.71	600 cycles	[196]
Pt/p-Ni	NaOH (1 M)	Anodic	0.5	98.9	0.78	-	[197]
Pt/IrO ₂ /CNT	H ₂ SO ₄ (0.5 M)	Anodic	1	61.7	1.66	1800 s	[198]
Pt-Cu/rGO	H ₂ SO ₄ (0.5 M)	Anodic	1	45.9	1.78	7200 s	[199]
Pt-Fe /Graphene	H ₂ SO ₄ (0.5 M)	Anodic	1	3.6	1.73	3500 s	[200]
Pt/S-CNTs	H ₂ SO ₄ (0.5 M)	Anodic	1	862.8	1.78	500 cycles	[201]
Pt/CeO ₂ / Graphene	H ₂ SO ₄ (0.5 M)	Anodic	1	14.0	1.69	7200 s	[202]
Pt _{10-x} Fe _x /CNTs	H ₂ SO ₄ (0.5 M)	Anodic	1	38.0	1.65	3000 s	[203]
Pt-Ru/Graphene	H ₂ SO ₄ (0.5 M)	Anodic	1	16.5	1.70	-	[204]
Pt-Fe/C300	HClO ₄ (1.0 M)	Cathodic	1	382	0.3	-	[205]
Pt-Nd FeO ₃	H ₂ SO ₄ (0.5 M)	Anodic	1.68	1112.7	1.982	100 cycles	[206]

performances, specifically related to the surface area and mass of Pt-Cu and Pt-Co alloys after voltammetric activation, show significant advances compared to pure Pt/C [187]. Various bi-metal NPs based graphene nanoplatelets supported electrode catalysts, i.e., PtNi/GNPs, PtCu/GNPs, and PtFe/GNPs, were synthesised using the supercritical CO₂ technique. The synthesized catalyst was characterized using various methods like XRD, energy dispersive X-ray analysis (EDX), TEM, Thermogravimetric analysis (TGA), Raman spectroscopy and inductivity coupled plasma mass spectroscopy (ICP-MS). To check the catalytic performance of bi-metal-based catalysts, three-cell CV was used. PtNi/GNPs catalyst exhibits outstanding catalytic performance for HOR & ORR. A polarization curve was displayed to know the upgradation in the cell's performance, which shows that the PtNi/GNPs catalyst showed the best activity (907.5 mA/cm², 0.54 mW/cm² @ 0.6 V) when it was utilized as an anode electrode. To reduce the cost of the catalyst, the loading of Pt is done in small amounts by incorporating other TM with Pt for the anion exchange membrane fuel cells (AEMFCs). Considering Adabi et al. [188], using the controlled surface tension method (CST), fabricated four Pt and PtRu electrocatalysts and tested for ORR and HOR reactions in AEMFCs. The small multi-atom cluster with high density is allowed by CST. The loading of Pt decreased by a factor of 14 but showed performance like commercially available catalysts. AEMFCs are also decorated with ultra-low Pt loading, i.e., 0.05 mg_{PGM} cm⁻² and PtRu anodes were attached with Fe-N-C cathode to get the specific power of 25 W/mg_{PGM} (40 W/mg_{Pt}). This way, low-cost and efficient catalysts were synthesized for FC technology [189]. Table 2 summarizes some of the Pt-based catalysts for MeOH oxidation below.

4.1.2. Pd-based catalysts

Pt is the most excellent electrocatalyst and is broadly used to oxidize methanol. Pt is susceptible to poisoning by intermediate reactions, mainly CO, while doing electrochemical activities. Further, higher cost and less abundance are limitations to its practical uses. Additionally, work has been completed to synthesize a substance having less Pt amount or free from Pt to solve this problem. It found that in place of Pt, Pd-based nanomaterials are used as an alternative to the electro-oxidation of MeOH and are available in bulk [207].

To advance Pd-based catalysts, in 2012, Ju et al. [208] used the surface reductive deposition method in an acidic medium. They fabricated a novel electrode catalyst, Pd-Ni/TiO₂ nanotubes (NTs), by using Ni and Pd as precursors. The electrochemical test shows that Ni-Pt/TiO₂NTs remain an excellent material for methanol electro-oxidation. While titania NTs used to possess pores to perform as superior subsistence for the uniform scattering of Pd-Ni NPs & improve the presence of active positions at the Pd-Ni/TiO₂ boundary for easy oxidation of CO &, hence, enhancing the electrocatalytic performance for electro-oxidation of methanol.

Also, Hosseini et al. [209], in the year 2012, fabricated a pore-based Pd/TiO₂/Ti electrode catalyst having an excellent catalytic characteristic which follows a 2-step route (a) Anodizing of Titania, with (b) Electroplating of Pd. The layers of TiO₂ contain discrete tubes having a diameter of 70–90 nm, and the surface of the tubes is decorated with Pd-NPs; this is revealed by examination of the morphology and crystal structure of the synthesized electrode-catalyst. The CD response of Pd/TiO₂/Ti was superior compared to the Pd-based electrode. CD value increases with the enhancement of temperature and scan rate. In addition, at higher concentrations of MeOH, a decline in resistance and lesser resistance of charge transfer was observed in the activation range.

At suitable conditions, Mandal et al. [210] fabricated two metal-based Pd-Cu NPs by using the simple, soft chemical technique in an alkaline environment with the suitable constitution, dimensions, and grander electrocatalytic performance for MeOH electrooxidation. As the quantity of Cu increases, the electrocatalytic behavior of Pd-Cu-based alloy until the Pd-Cu ratio up to 3:1 also increases. After that, deterioration is detected. Multiple-scan CV and CA examinations proved prepared materials' long-term stability and electrocatalytic performance.

The Pd-Cu-based alloy having less Pd amount stimulates its actual utilization as a catalyst for the anode in the essential atmosphere in DMFC. The electrocatalyst, namely Pd-2-Ni and Pd-4-Ni, was fabricated using an easy galvanic replacement method in which deposition of Pd was done on Ni-foam. For this purpose, the two different precursors of Pd-used. The Pd-4-Ni exhibits better electrocatalytic performance as compared to Pd-2-Ni as well as Pt/C samples. In Pd-4-Ni, the introduction of Ni gives oxygen-loaded variety for the oxidation-based elimination of CO at a lesser potential.

On the other hand, the 3D pore-based structure of Ni-foam (a) helps in the easy transfer of products, substrates, reagents and reaction intermediates, and (b) is helpful in homogeneous distribution and presence of electroactive Pd particles. The obtained CD, Tafel slope, and durability are ~130 mV/dec, 12.7 mA/cm², and 5000 sec in primary condition. Fig. 17(a) shows the fabrication of Pd-2-Ni by [PdCl₄]²⁻ precursor and Pd-4-Ni by [PdCl₆]²⁻ with equivalent Ni at a high potential of 0.964 V vs SHE. The SEM images of Ni-foam (Fig. 17(b)), Pd-2-Ni (Fig. 17(c)), and Pd-4-Ni (Fig. 17(d)) are displayed to represent the surface morphology of the catalyst. Fig. 17(e) shows the steady CVs in deoxidized NaOH solution (1 M) of Pd/C, Pd-2-Ni and Pd-4-Ni. Both the catalyst Pd-2-Ni and Pd-4-Ni offer an excellent cathodic signal at –0.35 V for electrochemical reduction of Pd oxide, similar to the Pd/C catalyst. Fig. 17(f) CVs of Pd/C, Pd-2-Ni and Pd-4-Ni catalysts show the electrochemical performance of these catalysts for MOR at a scan rate of 5 mV s⁻¹ in MeOH (1 M) and NaOH (1 M). Pd-4-Ni catalyst shows the highest peak CD in all three materials at 180.8 mA/mg. Fig. 17(g) displayed the CA diagrams of Pd/C, Pd-2-Ni and Pd-4-Ni at 0.1 V, which shows the accelerated electrochemical performance of Pd-4-Ni toward MOR. The CA investigation was done in Ar-saturated NaOH (1.0 M) and MeOH (1.0 M). Fig. 17(h) represents the Tafel slope of all three catalyst-based electrodes. The slope obtained for three catalysts in the region between 130 and 210 mV/dec shows the reaction going similarly for MOR in the case of three catalysts [211].

In 2016, Cao et al. [212] effectively fabricated the tri-metal-based Pd/CuO/TiO₂ NPs using dealloying and facile deposition methods. The tolerance power of Pd toward CO was improved by homogeneously dispersed Titania NPs having functional groups that contain 'O'. Besides this, their activity toward methanol oxidation also increases in the basic medium due to better interaction among continuous assemblies. That enhances liquid distribution and network-like arrangements, having uncovered active positions. The prepared substance had a superior electrochemically active surface area. It exhibited lower Tafel plots and higher CD compared to Pd/C and Pd/CuO.

Further, information of the preparation of Mn-Ti-O-OH based Pd electrode catalyst, i.e. (Pd@MTOH) in 2016 was given by using a hydrothermal method followed by an in-situ reduction procedure. Various examination methods confirmed the formation of Pd-NPs with multi-valent MTOH [213]. The fine particles of CeO₂ doped with Co having a diameter of 3.6 nm were used to electro-oxidize MeOH in an alkaline environment. It also possesses anti-poisoning activity and acts as a Pd promoter. The synthesized Pd/Co-CeO₂ hybrid shows better electrocatalytic performance than pure Pd and Pd/CeO₂ toward MOR, having 4 times better performance compared to the Pt-Ru catalyst [214].

Enhanced nano-carbon support of Ti_{0.5}Cr_{0.5}N for a conductive Pd-Ag alloy was fabricated using the solid-solid phase segregation method to efficiently, i.e., acidic and basic. Compared to Pd, the bi-metal-based Pd-Ag/alloy exhibit better catalytic activity and greater stability for the MeOH electro-oxidation reaction and HCOOH oxidation in ternary nitride base materials. The fabricated electrode catalyst has a CD of 844 mA/mg on a maximum potential value of 0.87 V. It keeps the highest amount of this CD for 3600 s [215]. Some more Pd-based catalysts have been summarized in Table 3.

4.1.3. Role of bimetallic carbon-based composites as a catalyst

Support materials are used to make advancements in the characteristics of pure substances. They improve the conductivity and stability

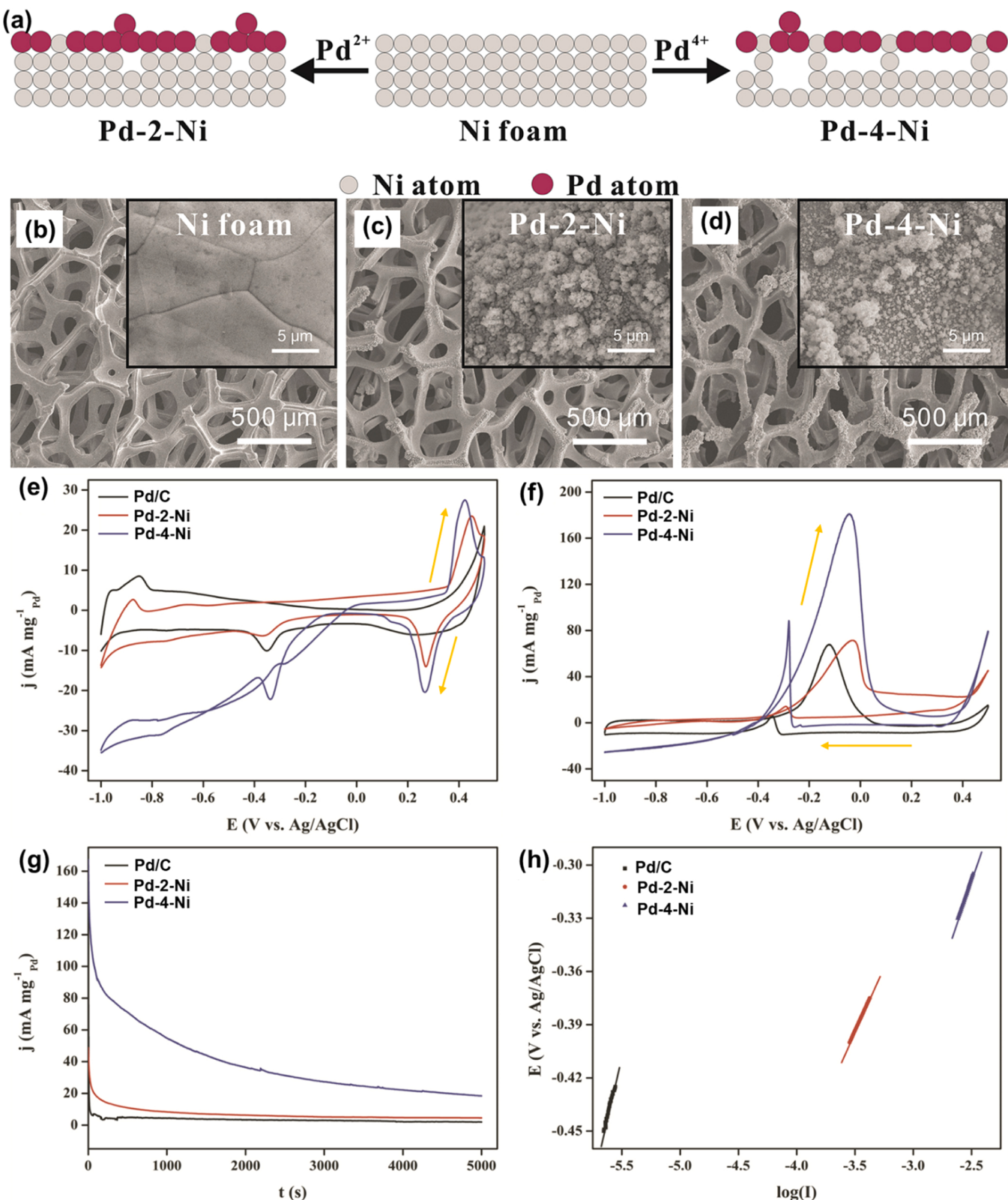


Fig. 17. (a) Graphical representation of the synthesis of Pd-2-Ni and Pd-4-Ni with diverse organisation and covering of Pd deposition automatically develops on Ni foam using a ordinary galvanic replacement method. (b) pre-treated Ni foam (c)) the fabricated Pd-2-Ni (d) Pd-4-Ni, SEM pictures. (e) constant CVs of the commercially available Pd/C and the fabricated Pd-2-Ni and Pd-4-Ni in NaOH (1.0 M) saturated with Ar at 5 mV s⁻¹ scan rate; (f) CVs of electrooxidation of MeOH of the commercially available Pd/C and fabricated Pd-2-Ni and Pd-4-Ni in Ar-saturated NaOH (1.0 M) with MeOH (1.0 M) noted at a scan rate of 5 mV s⁻¹; (g) CA plots of Pd/C, Pd-2-Ni and Pd-4-Ni in Ar-saturated NaOH (1.0 M) with MeOH (1.0 M) at -0.1 V; (h) Tafel slopes of the Pd/C, Pd-2-Ni and Pd-4-Ni in Ar-saturated NaOH (1.0 M) with MeOH (1.0 M) over a scan rate of 1 mV s⁻¹.

Reproduced with permission from [211]. Copyright 2015 Elsevier.

Table 3

Pd-based materials/C-based composite for MeOH oxidation reaction.

Electrocatalyst	Electrolyte used	Type of catalyst	Molarity of methanol (M)	Current density mA/cm ²	Peak potential mV (RHE) (V)	Stability (seconds)	Ref.
Pd-4-Ni	NaOH (1 M)	Anodic	1	12.7	0.94	5000 s	[211]
Pd/TiO ₂ /Ti	KOH (1 M)	Anodic	0.5	~9.6	~ 0.85	500 s	[212]
Pd/Co-CeO ₂	KOH (1 M)	Anodic	0.5	176.6	1.02	10 800 s	[214]
Pd-NPs/rGO	NaOH (0.5 M)	Anodic	1	1.6	1.03	1800 s	[207]
Pd/Cu ₃ P/rGO	KOH (1 M)	Anodic	1	33.9	0.80	3600 s	[216]
Pd-Mn ₃ O ₄ /MWCNT	NaOH (0.5 M)	Anodic	1	50.5	0.77	1800 s	[217]
Pd/MnO ₂ -rGO	KOH (0.5 M)	Anodic	1	20.4	0.85	1800 s	[218]
Pd-Co ₃ O ₄ /C	KOH (1 M)	Anodic	1	65.1	0.81	28 800 s	[219]
Pd@Mo/MWCNTs	KOH (1 M)	Anodic	1	27.9	0.88	1000 s	[220]
FeCo@Fe@Pd/C	KOH (0.5 M)	Anodic & cathodic	1.5	8.0	0.85	-	[221]
Au@Pd/rGO	H ₂ SO ₄ (0.5 M)	Anodic	1	~28.0	~ 0.84 V	3000 s	[222]
Pd-Ni/TiO ₂	H ₂ SO ₄ (1 M)	Anodic	1	127.4	1.95	-	[208]

mainly in the provided situations. With the increased transport of electrons, the electrical conductivity increases; in another manner, the dispersion of materials depends on the surface area of support materials, and the increased distribution leads to the stability of materials. The conductive support material based on carbon, like carbon black, is a probable substance for the NPs having a suitable shape and size. The formation of a unique triple junction in carbon black because of the existence of several groups containing oxygen increases the electrochemical surface activity of carbon black. The performance and durability of catalysts also increase using graphitized CNF because it contains more nucleation sites which help in the good dispersal of catalysts on the supporting base surface. Functionalized MWCNTs consist of carboxyl groups, and some contents of nitrogen assists in the efficient distribution of the metal NPs by attaching them to the CNTs, which results in a high CD for methanol oxidation. CNTs mixed with nitrogen can help achieve efficient distribution of metals like Pt because a higher quantity of nitrogen provides an environment for better dispersion and attachment of NPs.

Carbon-based support material like graphene is also helpful for attaining structural elasticity, chemical durability, superior electricity conductance, and toxic resistivity. The performance of the MOR also improved by doping the catalyst with nitrogen and boron, which control the size of the particles and lead to the proper distribution of metals. Doping of nitrogen also enhances electrical conductivity by partial structural recovery. It gives different attaching sites for good distribution of material on the support [223]. In addition to that, conducting polymers like polyaniline (PANI) supporting material is conductive and responsible for increasing the electrocatalytic activity for FC application. The increased movement of ions, higher electrical conductivity, decreased methanol crossover and resistance to CO, and a larger ECSA. Further, it can upgrade the stability and performance of catalysts by using PPy as a polymer base with MWCNTs for the MeOH electro-oxidation reaction.

One such investigation using support material is by Galeano et al. [224], where the complete synthetic strategy for 15 nm Au, @C, was investigated. Primarily, the preparation observes the way illustrated within Fig. 18(a). Since the practice of the AuPt, @C yolk-shell particles apply different thermal processing phases (550 °C for synthesizing the absorbent silica shell, 1000 °C for carbonization/graphitization), the microstructure of the bimetallic core is anticipated to vary during the treatment. These modifications were followed by spatially determined elemental investigation, XRD and XPS. Fig. 18(b) exhibits the XRD patterns of a standard specimen after additional processing stages. Fig. 18(c-f) illustrates expected TEM pictures and nitrogen sorption isotherms of the exotemplate Au@Pt@SiO₂ @m-SiO₂ and the related representation AuPt, @C substances. The graphitization of the carbon shell was administered via Fe, as examined overhead. It may adjust the diameter of the Au@Pt@SiO₂ @m-SiO₂ by altering the number of silica

antecedents explained earlier. Fig. 18(c-f) shows that the exotemplate particles and the yolk-shell counterparts have consistent particle dimensions of about 70 nm. Few bimetallic centres have a greater particle size owing to the initial encapsulation of two and, rarely, more-bimetallic NPs within the exact silica exotemplate particle. Nevertheless, most surfaces possess just one core. The pores into the shell are more diminutive than the metal particles; therefore, encapsulation prevents particle coalescence.

Several Pt-carbon-based electrode catalysts, i.e. Pt-Ru/C [192], Pt-Ru-GMC (graphitic mesoporous carbons) [225], Pt-Ru/CNF, Pt-Ru-TiO₂, and Pt-Ru/(CTiO₂), Pt-Ru/TECNF [226], Bi-metal based Pt-NPs/dendritic Au nanostructures (Pt-NPs/DGNs) [227], Pt-Sn/carbon polyaniline (Pt-Sn/C-PANI) composite [193], Pt-Ni/C [228], Pt-Co/MWCNT [194], Pt-Co (bi-metal based) NPs supported on expanded graphite (EG) base (Pt-Co/EG electrocatalyst) [229], Pt-Co/rGO [195], a single 3D Pt-C/graphene aerogel mixture (Pt-C/GA) [230], Pt-Fe/MWCNTs [231], Pt-Ru-Ni (8:1:1)/MWCNTs NPs [232], Pt/Co-coal-CF electrode-catalyst for MOR [233], phosphorus doping, i.e. Pt/P-MCNTs [234], Pt-Pd/RGO [235], Pt and N-doped graphene (Pt/N-G) [236] and so on electrode catalyst was prepared by researchers time to time to enhance the catalytic oxidation of alcohols and hence the efficiency of fuel cells. It was found that by combining Pt with carbon-based materials or composites, fuel cells' electrocatalytic activity, durability, and resistance to carbon monoxide (CO) increase. It was also found that power density, mass activity, and the ECSA increase many times, leading to better cell performance at a lower potential.

Similarly, many fabricated catalysts based on Pd and carbon composite from time to time to enhance the electrooxidation of alcohol. Various catalyst like extremely small in size Pd-NPs on the exterior area of N-S blended graphene nanosheets, i.e. Pd/NS-G, shows outstanding performance for electrooxidation of MeOH in the basic medium [237], Bimetallic Pd₇Cu₃/rGO composite [238], Pd-MnO₂/MWCNT [239]. A three-component nanocomposite made up of MnO₂ nano-lamellas, Pd-NPs, and graphene sheets (Pd/MNL/GS) [240], bi-metal-based Pd-Ce NPs distributed on CNFs (Pd-Ce/CNFs) [118], Pd-Co (8:1)/C electrocatalyst [145], Pd_x Rh /C, (X = 1/3, 1, 3) [241], A nano-porous dandelion-shape Pd-NPs-supported graphitic carbon nitride nanoflakes rGO (CNNF-G) nanocatalyst [242], graphene-Pd-SnO₂ (G-Pd-SnO₂) composites [243], PdNPs-ZnO-gCN [244] were fabricated and had better performance for electrooxidation of MeOH in an alkaline environment. This electrocatalyst has a better electrochemical surface area, high power to oxidize CO to CO₂, high current density, and an extensive porous surface for FC. It leads to smooth diffusion of electrolytes and rapid removal of harmful materials during cell reactions, which leads to superiority in the working mechanism of the fuel cell. For the PEMFCs, loading Pt at the cathode to enhance its electrocatalytic activity is not easy because it is expensive. To overcome this situation, Ou et al. [245] fabricated Pt single atoms having ultrafine NPs (size 2.3 nm) that are

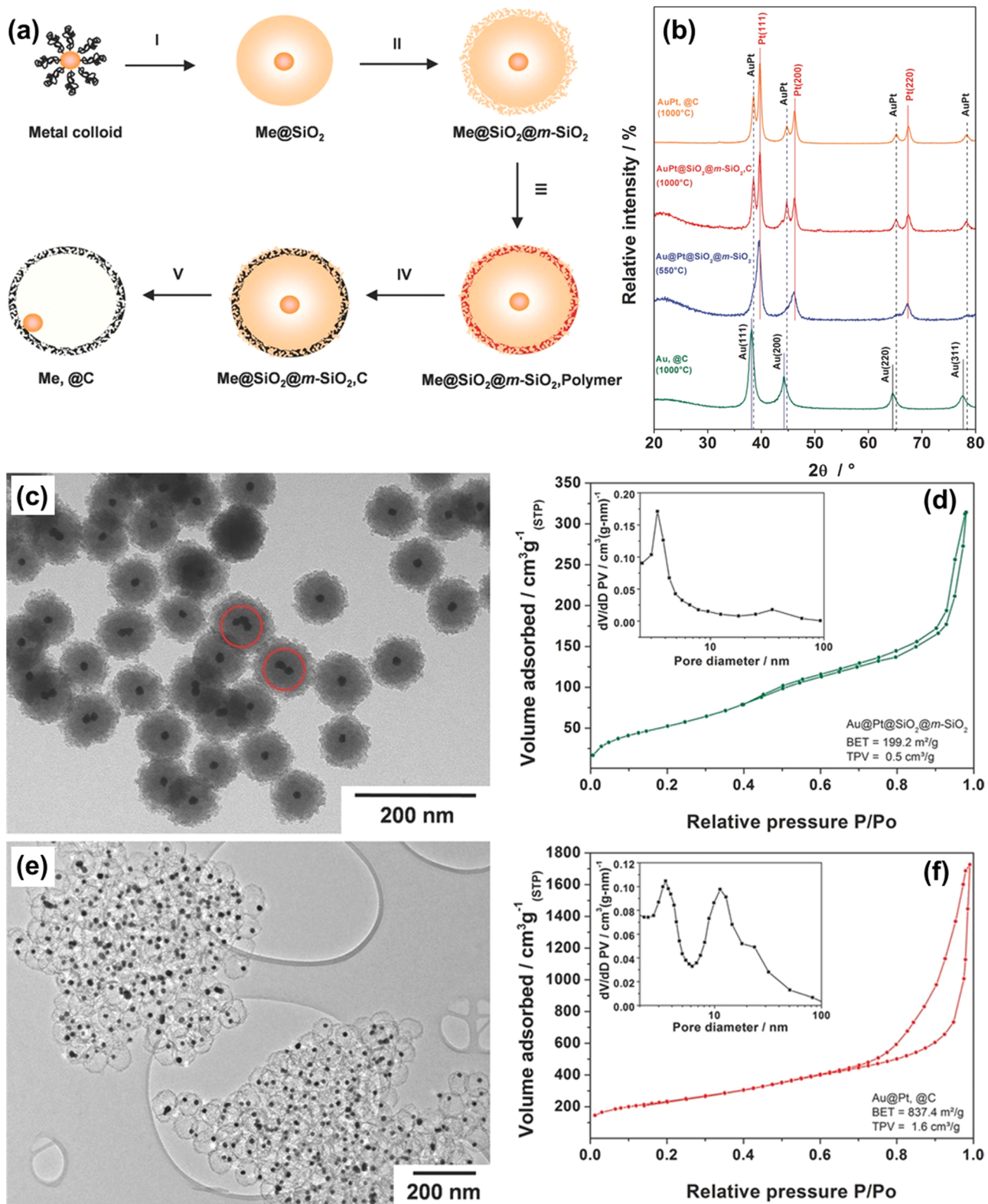


Fig. 18. (a) Process for preparing encapsulated metal NPs within porous carbon shells via nano casting utilizing the $\text{Me@SiO}_2@m\text{-SiO}_2$ as exotemplate. (b) XRD powder patterns of the materials involved in synthesizing the $\text{AuPt, } @\text{C}$ yolk-shell substance. The maximum heat each material was treated compared to the value within parenthesis. TEM pictures, nitrogen sorption isotherms, and communicating desorption BJH pore size allocations (inset) of (c, d) $\text{Au@Pt@SiO}_2@m\text{-SiO}_2$ core@shell substance and (e, f) corresponding $\text{AuPt, } @\text{C}$ yolk-shell substance after leaching of the silica. Au:Pt hypothetical molar proportion 1:3. Reproduced with permission from [224]. Copyright 2013 John Wiley and Sons.

engaged in a pore having 3D arrangement and are graphene-like carbon matrix, i.e., (Pt₁ + NP@3DPGC) with related nanoporous morphology for the loading of ultra-low Pt and PEMFCs. For this purpose, they used a novel transformative method. The fabricated material was loaded at the cathode of PEMFCs by ultra-low loading of 0.02 mg_{Pt} cm⁻². The mass activity of the catalyst increases 8.30 times from Commercially available Pt/C and 1.64 times from DOE 2025. The fabricated catalyst is highly durable with 70.8% power density retention when run for durability test.

4.2. Metal-organic framework (MOF) based catalyst

The Pt-based catalyst was replaced by some porous material made from transition metal at the anode for oxidation of MeOH in basic conditions such as metal-organic framework (MOF) and zeolites-based imidazolate frameworks (ZIFs) or support materials for FCs applications. This help to provide a template for catalyst because of their larger surface area and porosity. Also, help in the proper distribution of metal particles and accelerate the migration process of electroactive materials on the way to the surface of the electrode [246–250]. Nickel (Ni) incorporated MIL-110 electrocatalyst, fabricated by following the impregnation process, and used as an anode material in the MeOH oxidation. Ni/MIL-110 electrode-catalyst had a huge surface area and proper distribution of Ni. Though, the structure is destroyed due to a higher amount of Ni. Electrocatalytic performances examined by CA and CVs techniques show an excellent activity toward MeOH oxidation reaction in the basic medium [251]. In 2017, some researchers fabricated Co-BDC MOF hydrothermally having a cuboid shape, and their GO composites were further examined for MeOH oxidation in a basic environment. Out of 2 wt% and 5 wt% GO composites, the 5 wt% GO composites give a CD of 29.1 mA/cm² on a value of peak potential of 1.13 V vs RHE in CH₃OH (3 M)/KOH(1 M) solution. Lower resistance and the slightest Tafel slope show better conductivity and superior kinetics. On the other hand, maintaining 62% CD still later than 3600 s delivers the durability of the substance [252]. Different electrochemical studies of hydrothermally synthesized Cu-Benzene tricarboxylic acid MOF (Cu-BTC MOF) and with GO composites in the alkaline medium were discussed by Noor et al., [253]. The cubic-shaped porous 3D MOF shows excellent performance for MeOH oxidation. At a higher potential value of 1.84 V vs RHE, the synthesized composite sample Cu-BTC-5 wt % graphene oxide (GO) provides a CD of 120 mA/cm² from all the synthesized series. The formerly discussed substance had the highest coefficient of diffusion, smallest resistance of 20.52 Ω, and durability for 3600 s, which shows that it is the best substitute for the noble metal-based electrocatalyst.

Another MOF based composite NiO-MOF/rGO was reported where irregular-shaped NPs were synthesized hydrothermally that showed lower resistance of 252 Ω, a higher diffusion coefficient, and the highest CD of 275.8 mA/cm² for 3600 s in the basic environment [254]. Ni-BTC MOF & its rGO hybrid material was fabricated by Yaqoob et al. [255] using a one-pot solvothermal approach. It carefully tested prepared composite electrocatalytic performance for MeOH oxidation in a basic environment. Amongst the prepared MOF-rGO composites, the Ni-BTC 4 wt% rGO at a peak potential value of 1.65 V vs RHE gives a CD of 200.02 mA/cm². The Ni-BTC 4 wt% rGO material also shows a Tafel plot of 27.89 mV/dec with the least resistance of 18.12 Ω and durability of 3500 s.

In 2020, Yaqoob et al. [256] synthesized spherical shape NPs by using a solvothermal approach, i.e. Co BTC MOF series that was based on rGO for the oxidation of CH₃OH in a basic environment. These NPs were further characterized via diverse techniques like FTIR, XRD, SEM and EDX, and electrochemical activity was monitored by EIS, CA, and CV. Excellent electrochemical behavior displayed by Co-BTC 1 wt% rGO material (2.5 mg) by giving a CD of 130 mA/cm² at the value of the maximum potential of 1.59 V(RHE) having Tafel plots of 83.6 mV/dec, the resistance of 14.75 Ω, and are durable for 3500 s in potassium

hydroxide (1 M) and MeOH (2 M) homogeneous mixture. Maybodi et al. [250] fabricated a nonporous zinc-2-methylimidazole MOF (ZIF-8) NPs, by applying a facile template-free approach. Further, Ni was introduced to ZIF-8 to reduce the overvoltage of MeOH oxidation at the carbon paste electrode (CPE) so that Ni/ZIF-8CPE was prepared as an improved electrode. The CD in Ni/ZIF-8CPE was more than that of bare CPE in the oxidation peak case, as CV shows. Lower cost, easy electrode preparation, and superior durability are essential characteristics of the examined substance.

Hoseini et al. [257] described the supreme model of material ZIF-8 nano-structured layer on the oil-H₂O boundary. The fabricated substance shows the CD of 32.7 mA/cm² in methanol oxidation, somewhat better than Pt layer Pd/ZIF, Co-MOF-71 and Ni/ZIF-8. In contrast, the long-term toxicity time of the ZIF-8 layer (0.1%) & power amount (15.4 mW/cm²) made it a better option for the electrooxidation of methanol. A new three-dimensional porous substance that was based on Ni fabricated by Wu et al. [258] having cubane [Ni₄(OH)₄] & [Co₄(OH)₄] group & structurally characterized in 2019 for methanol oxidation reactions. The as-prepared Ketjen black (KB) & CTGU-15 (1:2) material shows the most electrocatalytic performance than the Ni-MOF-based catalyst. These enhanced activities for the MeOH oxidation process could result in the unique & energetic cubane [Ni₄(OH)₄] component and synergic consequence of KB & Ni-MOF. The validated material shows a CD of 29.8 mA/cm² at a higher potential value of 1.56 V vs RHE, which has 90 Ω resistance and is durable for 2 × 10³ sec. Liu et al. [259] 2019 fabricated a material using a simple stirring & sonication approach, namely MoS₂ @CoNi-ZIF composite having an external film of MoS₂ around an empty CoNi-ZIF NPs at room temperature.

Amongst the consecutive MoS₂ @CoNi-ZIF hybrids, necessary robustness in anodic CD was reported towards the MoS₂ @CoNi-ZIF (3:1), which provides a CD of 9 mA/cm² at a maximum potential value of 1.40 V vs RHE. Synthesized MoS₂ @CoNi-ZIF (3:1) electrode catalyst has 3 significant merits: (a) Bi-functional electro-catalytic performance for the degradation of & oxidation of methanol, (b) easy preparation without supplementary treatment and (c) much durability because of enhanced synergistic consequences between MoS₂ & CoNi-ZIF, metal-based oxide, and MoS₂. Novel pyridine enfolding MOF materials were synthesized to prepare N-doped porous carbon (NPC-800) by MOF carbonization. Prepared NPC-800 acted like a catalyst and supporting material for the catalyst. As a result of the interaction between Pt-NPs and N-doped support material, the Pt-catalyst decorated on NPC-800 exhibits superior electrocatalytic performance and higher durability for the MOR [260].

Vulcu et al. [261] in 2016, by using a two-step process, immobilized Cu-based MOF on gold electrolyte; as a result, the MOF's stability increased in an acidic environment and hence significantly used as a catalyst in the anode. The first step introduces the linker layer over the surface of the electrode. In contrast, in the subsequent step, this customized electrode was immersed in the chief solution of MOF at 25 °C for 96 h. The improved electrode exhibits good electrocatalytic performance in an acidic medium toward methanol oxidation at a low scan rate, as examined by EIS and CV. The modified electrode offered resistance of 27.4 Ω at 1.2 V. Simultaneously, retaining the highest electricity quantity for up to 3600 s. An easy procedure was presented by Zhang et al. (year 2020) to develop nanocrystals of Co-Zn-ZIF over MWCNTs which further changes into CNTs that are N-doped and carbon-coated nanomaterial and presented as CoP-NCZ/CNT. The material shows superior catalytic performance and greater-durability in an acid-based environment. The outstanding constancy and electrocatalytic performance of Pt-CoP-NCZ/CNT can be based on the combination of CNTs with Co-Zn-ZIF and the existence of carbon which is N-doped and accountable for higher electricity conductance; large specific surface areas with its N-doped arrangement useful in self-aggregation of NPs of Pt; the introduction of Zn NPs bound Co accumulation encourages uniform scattering of NPs of Co having much interaction with NPs of Pt and

increases tolerance for CO. Additionally, evaporation of Zn also keeps a higher specific surface area by enhancing porosity [262].

Yan et al. [263] proposed B-doped graphene quantum dots embedded within a bimetallic organic framework (BGQDs/MOF-t) as a positive active and cathodic solid material in the microbial fuel cell. A facile electro-deposition incorporates the BGQDs/MOF-t. Consequently, the in-situ development of FeCoMOF upon nickel foam may assist the building of nanoflowers with close associations, thus enhancing the electrochemical performance. Additionally, this nano-network may significantly support the implantation of BGQDs via the powerful interface of M-O-C bonding, bypassing π - π rearrangement and delivering effective charge transfer and ample edge available spots.

Based on the overhead explanation, it was synthesized BGQDs embedded within FeCoMOF (BGQDs/MOF-t) material through electro-deposition (Fig. 19(a)). Fig. 19(b) illustrates that multiple FeCoMOF were densely dispersed over the NF support. This 3D network was also tightly linked to the NF in BGQDs/MOF-t electrode substance, as demonstrated within Fig. 19(c). These pictures showed that the deposit of BGQDs on FeCoMOF induced no substantial morphology modification and minor element accumulation (Fig. 19(d-i)). Combined with SEM images, nanosheets may also be followed into FeCoMOF and BGQDs/ MOF-15 isolated from NF within the TEM pictures (Fig. 19(j and k)). The TEM picture of the BGQDs solution revealed that the dimensions of the BGQDs were within the spectrum of 1–4 nm with an average length

of 2.69 nm (Fig. 19(l)).

Apart from the morphology and synthesis procedures, the activity and long-term stability proved to be critical criteria for the experimental feasibility of materials. Therefore, the lengthy chronopotentiometry arcs of NF, FeCoMOF, BGQDs/MOF-15 and Pt/C stimuli were conducted at the voltage of -0.2 V in O_2 -saturated PBS, as illustrated within Fig. 19 (m). After 50 h of process, the electrochemical performance of the BGQDs/ MOF-15 cathode would hold at 91.2%, considerably higher than those of FeCoMOF (79.6%) and Pt/C (57.5%), where the NF showed shallow durability. Fig. 19(n) indicates the remarkable durability of BGQDs/ MOF-15 within the MFC after 800 h, and the highest potential output was held at approximately 0.6 V. In comparison, that from the Pt/C probe was 0.51 V and slowly decreased after 350 h. The BGQDs/ MOF-15 demonstrated exceptional power density and strength. HRTEM and XRD outcomes exhibited that the morphology of BGQDs/ MOF-15 was well preserved, and there were no other contaminant peaks in the XRD pattern, showing that no noticeable crystal configuration change happened (Fig. 19(o, p)). LSV and EIS estimated the electrochemical performances of different cathode catalysts. Within Fig. 19(q), BGQDs/ MOF-15 showed the most elevated current density among other cathode substances. It also observed identical movements upon EIS-relevant results. After the implantation of BGQDs, we may notice a substantial reduction in the diameter of the semicircle curve within Fig. 19(r).

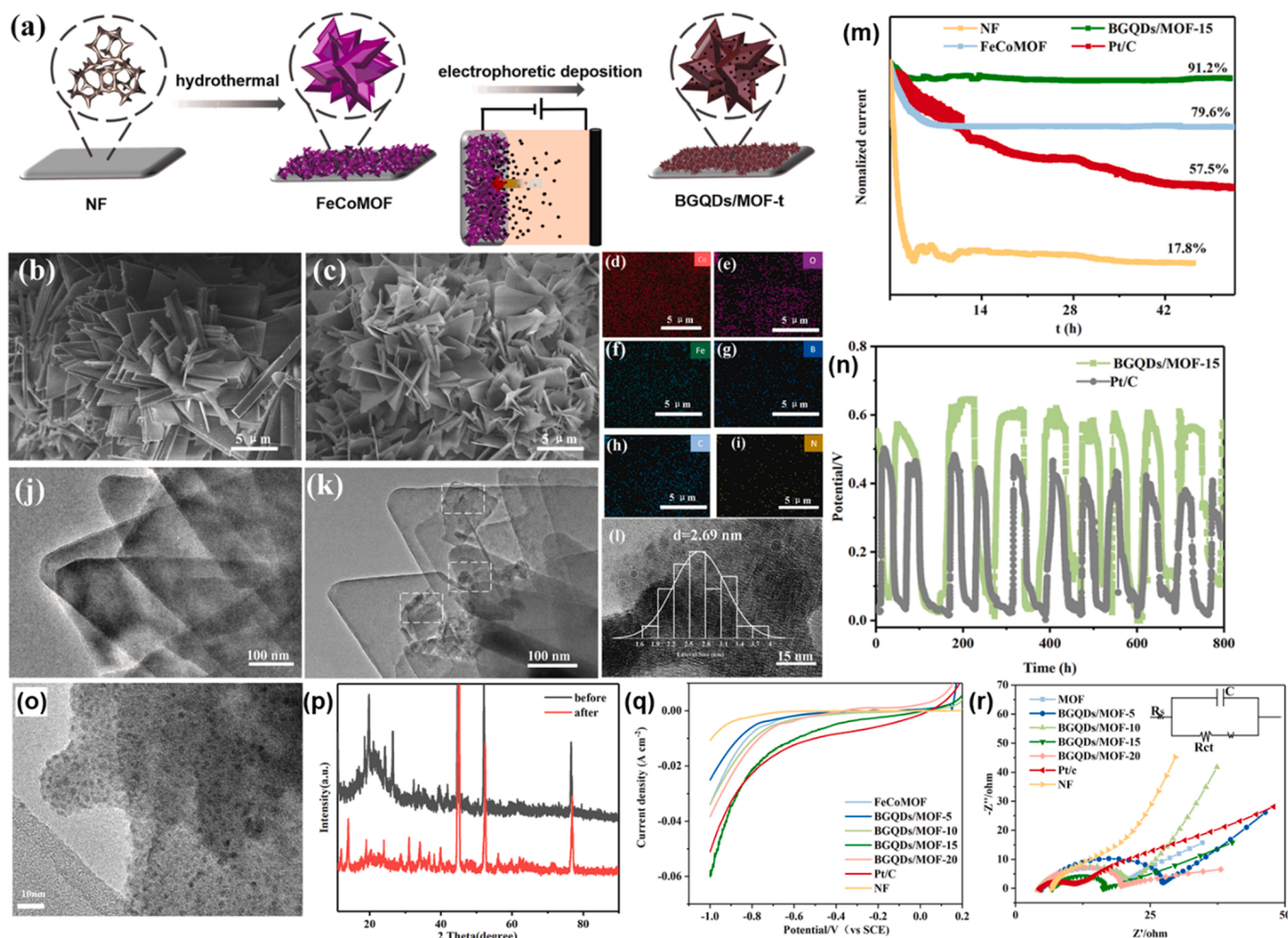


Fig. 19. (a) Graphic description of the incorporation method of the BGQDs/ MOF-t; SEM pictures of (b) FeCoMOF (c) BGQDs/ MOF-15; (d-i) EDS of BGQDs/ MOF-15; TEM pictures of (j) FeCoMOF (k) BGQDs/ MOF-15 (l) BGQDs solution. (m) Chronopotentiometry arcs of NF, FeCoMOF, BGQDs/ MOF-15 and Pt/C materials, (n) Cell potential of MFCs of BGQDs/ MOF-15, (o) HRTEM picture and (p) XRD of BGQDs/ MOF-15 after chronopotentiometry. (q) LSV arcs of different cathode materials within O_2 -saturated PBS solution, (r) EIS of diverse cathode stimuli. Reproduced with permission from [263]. Copyright 2022 Elsevier.

Further, Antony et al. [264] show the electrocatalytic performance of the MOF model design synthesized $\text{Ni}_x\text{Co}_{3-x}\text{O}_{4-y}$ for the CH_3OH oxidation reaction in a basic environment. MOF-based $\text{Ni}_x\text{Co}_{3-x}\text{O}_{4-y}$ nano-cages show an anodic CD of $\sim 250 \text{ A/g}$ at 0.57 V vs Hg/HgO , ~ 12 times greater than the parent Co_3O_4 . The enhanced catalytic performance was based on many active sites and non-stoichiometric composition. The lower charge transfer resistance displayed by the known material is also reliable with MOR consequences. The dependency of impedance upon potential indicates that the reaction's transition state favours the oxidation of methanol, where carbon monoxide and methanol are occupied on less-surrounded Co and Ni positions accordingly. N-doped carbon nanosheets (NCS) based on Pt-Co alloy NPs were effectively obtained by moderate pyrolysis of GO/ZIF-67/ H_2PtCl_6 materials by Lu et al. [265] in 2020. The great catalyst, Pt-Co/NCS-800, exhibits 2.6 times higher specific performance than Pt/C. This great activity was because of the electronic factor and the bi-functional process. Moreover, the size of the particle, the extent of alloying, and distribution also affect the catalytic mechanism. [Table 4](#).

4.3. Polymer-based catalysts

For the formation of a multifunctional composite, the NPs of metals combine with polymers take significant advantages in today's scenario in which the characteristics of the polymers are positively changed [266]. In this section of the review, we have discussed the polymer-based catalyst used in FC technology. Conductive polymers (CP) & metal NP (MN) separately have brilliant features. However, while they were added to each other, the resulting nanocomposite contains characteristics of both. CP and MN are used as superior substances because of their enhanced activity & multipurpose use [267]. The nanocomposites of conducting polymers and noble metals exhibit various outstanding features in blending various functional components [268].

The invention of multi-metal-based nanocatalysts with a convenient amount is always a dare for improving economic electrode catalysts. Further, nanomaterials with active carbon nanostructure show a suitable approach to boost the electrocatalytic activity of catalytic performance. Ghosh et al. synthesized a polymer-based electrocatalyst (Pd NPs-PPy) nanofibers through a colloidal radiolytic technique. They found that $\text{Pd}_{30}\text{Pt}_{29}\text{Au}_{41}/\text{PPy}$ nanohybrids ($\sim 8 \text{ nm}$) show better electrocatalytic performance (5.5 times higher than Pd/C) [269]. Pd-polypyrrole/nitrogen-mixed graphene (Pd-PPy/NGE) act as a ternary-nanocomposite fabricated using a single-step process. The prepared Pd-PPy/NGE nanocomposite material exhibited outstanding electrocatalytic performance for the electrooxidation of alcohols in a basic medium.

Remarkably, the fabricated Pd-PPy/NGE (1:50) catalyst having mass activity on electrooxidation of 2176.7 mgPd^{-1} (ethane-1,2-diol), 1192.7 mgPd^{-1} (MeOH) and $498.9 \text{ mA mgPd}^{-1}$ (EtOH), which are 4.3, 6.7 and 2.9 times respectively of those for commercially available Pd/C catalyst. However, the Pd-PPy/NGE (1:50) also exhibits

excellent anti-toxic capability and working stability compared to the Pd/C catalyst [270]. A transition metal-based electrode catalyst fabricated from the polymer 2,6-Diaminopyridine was used as a single repeating unit to prepare an N-rich network polymer. It makes self-sustaining sphere-shaped basic structures and has a higher number of metal-attaching sites. A Co-/Fe-coordinating pyrolyzed polymer shows oxygen reduction with a half-wave potential of 0.76 V vs RHE and the onset of 0.87 V vs RHE in neutral conditions [271].

For electrocatalytic applications, the CP is used as support to introduce the MNs. MNs supported on CP exhibit superior catalytic behavior due to the large surface area and the combined coupling consequence in both processes [272]. MNs show a higher surface area, those results in significant accumulation and imperfect colloidal constancy. To defeat these problems, metal NPs are externally covered by polymers [273] and give a steric obstacle in the accumulation process. MNs are traced over the polymer network using distinctive preparation methods and hence stay away from aggregation. The polymers also combine with the catalytic features of the MNs and therefore increase the catalytic performance.

In that manner, various chemical & physical methods are used to prepare the polymer-metal composites. In all used ways, the in-situ polymerization & composite formation (IPCF) approach [274] is extra capable. It shows a significant function when preparing metal NP-polymer-based composites with enhanced catalytic activity. By this method, the synthesized silver-poly-[4-(thiophene-3yl)-aniline], i.e., Ag (0)-pT3A, has been used as an electrode catalyst for the recognition of H_2O_2 , which is not an enzyme. When the composite is prepared using the IPCF method, the metal-NPs & polymer are formed collectively and come in close contact with each other. In this process, the metal salt starts the monomer's oxidative polymerization. It works as an oxidizing agent, while besides it, the MNPs are produced by the metal salt's direct reduction. Much effort has been made to illustrate the IPCF process & also maintain the reduction process of various dyes and the preparation of MNPs-based polymer nanocomposite [275,276].

It is proved that the fabricated MNPs enclosed polymers by using the IPCF procedure exhibit the outstanding electrooxidation capability of CH_3OH [138]. Polymers-supported PdNPs had also been prepared; those were efficiently utilized as electrode catalysts for the electrooxidation of methanol in the basic environment [137]. A suitable Pd catalyst at the CP-carbon structure was prepared for the oxidation of $\text{C}_2\text{H}_5\text{OH}$ and HCOOH . A carbon-dependent PPy composite was introduced inside the camphor sulfonic acid (CSA) [277]. Remarkable progress showed by the fabricated CSA-based PPy-carbon catalyst (PPyCC) towards the specific surface area and better electricity conduction interrelated with a PPyCC in the lack of PPyC. Pd-decorated on CSA-based PPy carbon materials exhibited a large electrochemically active surface area, which enhanced the catalyst performance and the oxidation of $\text{C}_2\text{H}_5\text{OH}$ and HCOOH . An emulsion in-situ polymerization approach used by Fard et al. [278] fabricated poly (pyrrole-co-aniline) (PPCA) hollow nanosphere (HN).

An approach free from template is used to synthesize Pd nanoflowers (Pd NFs) on a PPCA HN, increasing GCE by using a basic

Table 4
Metal-organic framework-based materials for methanol oxidation.

Electrocatalyst	Electrolyte	Type of catalyst	Molarity of methanol (M)	Support materials	Current density mA/cm ²	Peak potential mV (RHE) (V)	Stability (seconds)	Ref.
5 wt% GO/Co-MOF-71	KOH (1 M)	Anodic	3	Glassy carbon (GC)	29.1	1.13	3600 s	[252]
NiO-MOF/rGO	KOH (1 M)	Anodic	3	GC	275.9	1.83	3600 s	[254]
1 wt% rGO/Co BTC	KOH (1 M)	Anodic	2	GC	130.0	1.59	3500	[256]
ZIF-8 film	NaOH (0.5 M)	Anodic	0.5	GC	32.7	1.52	1200 s	[257]
MoS ₂ @CoNi-ZIF	KOH (1 M)	Anodic	0.5	GC	9.0	1.40	3000 s	[259]
Ni _x Co _{3-x} O _{4-y}	KOH (1 M)	Anodic	1	GC	17.6	1.54	1800 s	[264]
5 wt% GO/Cu-BTC	KOH (1 M)	Anodic	3	GC	120.0	1.84	3600 s	[253]
Ni/ZIF-8 CPE	NaOH (0.1 M)	Anodic	0.5	CPE	1.6	1.78	50 cycles	[250]

electrochemical method. The PPCA-supported Pd NFs have a superior electrochemically active surface area that increases the electrocatalytical activity compared to the oxidation process in a basic electrolyte. It could be responsible for the self-transfer of charges in the direction of conductive copolymer junctions, huge electrochemically present surface areas, and electrical conductivity. Those strategies provide a promising opinion for DAFCs.

Liu et al. [279] concluded that at the time of anode catalysis, the DMFC give some significant problems associated with new DMFC anode catalysts, i.e. (1) the implementation, covering performance, reliability and tolerance, and (2) price improvement. It proved that an adsorbed hydroxyl group is necessary for speed discovery levels of MeOH electrooxidation [280]. This hydroxyl group originated from the separation of H_2O at the catalyst's outer surface that occurs immediately on a considerable electrode potential at Pt. This makes oxidation of MeOH difficult near the Pt catalyst. Further, the removal of water occurs by lowering the Ru potential. That is why a bi-metal-based reaction starting agent contains both Pt & Ru on an anode electrode [281].

4.4. Non-noble metal-based catalyst

FC is an excellent technology to exchange the chemical form of fuel energy straight into electrical form by electrochemical reactions. There are many kinds of FC. Different noble metals, i.e., Pt and Pd-based electrode catalysts, are used to enhance the potential and efficiency of FCs. These noble metal-based catalysts are of high cost. Less expensive non-noble metal-based electrocatalysts are introduced, having good action and durability to overcome these situations [282]. For this

purpose, we mainly consider the TM-based catalyst. These TM-based catalysts are crystalline, but sometimes they also show crystalline behaviour that only depends on the fabrication condition. These TM-based catalysts are mainly synthesized using different approaches like pyrolysis, chemical etching, electrochemical, composition-tuned, etc. [283]. Gamil et al. [284] prepared non-noble metal nanocomposites like Co-Cr LDH, Ni-Co-Cr LDH, and Ni-Cr LDH that have high activity and more durability for FC application.

Wei et al. [285] synthesized a flower-like three-dimensional microsphere of $Ni_{0.6}Zn_{0.4}O$ by calcinations of Ni-Zn LDHs, which are manufactured hydrothermally. Flower-like structures provide a high surface area of contact between the reactant and catalyst, and Zn's introduction helps transfer electrons quickly. The prepared catalyst gives a CD of approximately 53 mA/cm^2 on a potential of 1.60 V in an alkaline medium. A low-cost electrocatalyst $Fe_2(MoO_4)_3$ is synthesized and confirmed the three distinct morphologies (such as nanorods, nanospheres, and nanotubes) have high current density due to their large surface area [286]. Some transition metal-based catalysts like $CoN@CMnN@C$ and $CuN@C$ are used in microbial fuel cells (MFCs) to boost the electrocatalytic activity of MFCs [287].

A nanosheet of $CuO/Co(OH)_2$ was fabricated for a MeOH oxidation reaction. The material has a high surface area, CD, maximum turnover potential, and binding energy. As the concentration of methanol increases, current density also increases [288]. Some Bi-doped cobalt oxide catalysts are prepared for methanol oxidation using the sol-gel method. The prepared electrode catalyst $Bi_{0.13}Co_{2.87}O-550$ has a more significant mass activity of 808.5 mA/mg with more durability in a basic medium. The prepared catalyst also exhibited the potential for

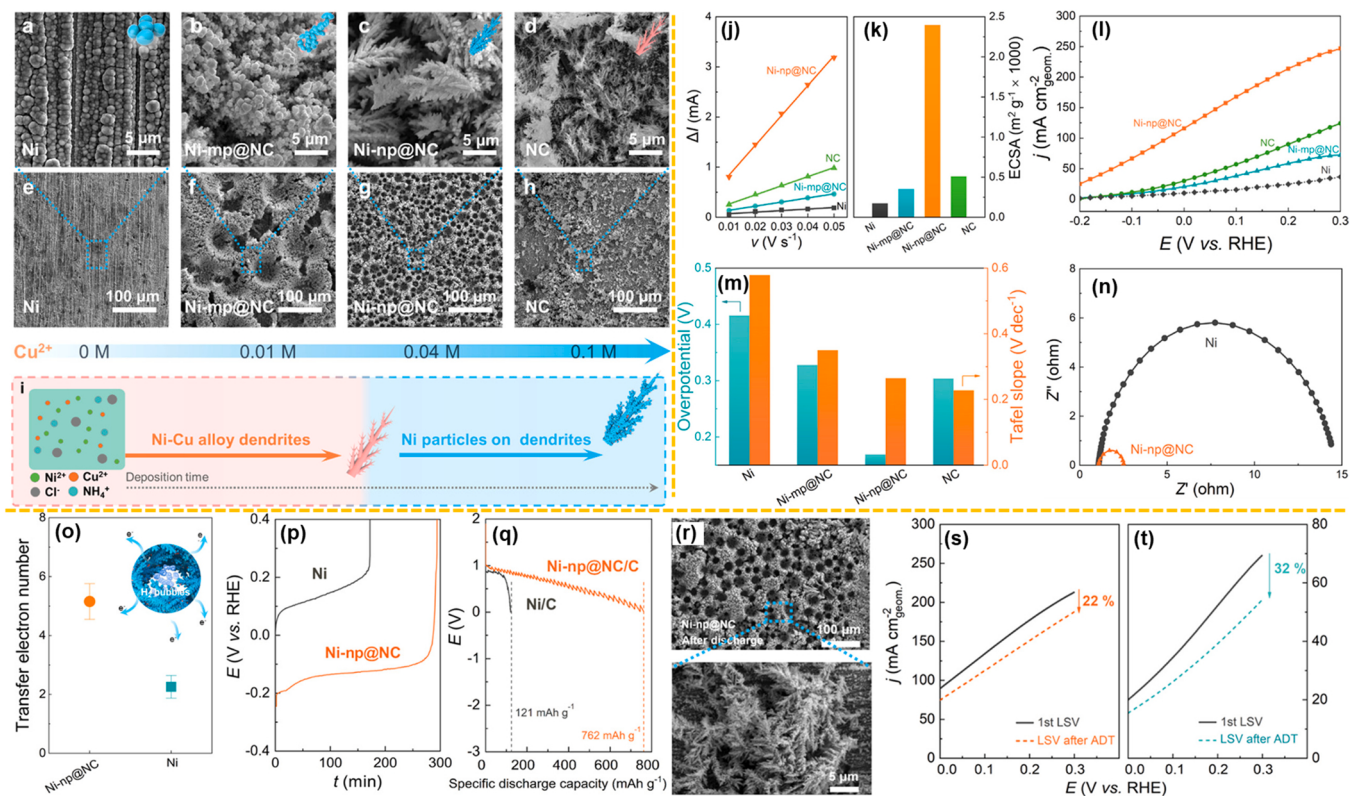


Fig. 20. HR-SEM pictures of (a) Ni, (b) Ni-mp@NC, (c) Ni-np@NC, and (d) NC substances. Low-resolution SEM pictures of (e) Ni, (f) Ni-mp@NC, (g) Ni-np@NC, and (h) NC compounds. (i) Representation diagram of the construction device of Ni-Cu amalgam catalyst surface throughout the electrodeposition procedure. (j) LSV arcs of BOR upon Ni, Ni-mp@NC, Ni-np@NC, and NC within KOH (1 M). (k) ECSA of diverse substances. (l) LSV arcs of BOR upon Ni, Ni-mp@NC, Ni-np@NC, and NC within NaOH (2 M) + $NaBH_4$ (0.135 M) on 298 K. (m) Overvoltage's at 10 mA cm^{-2} and Tafel plots upon Ni, Ni-mp@NC, Ni-np@NC, and NC. (n) Nyquist plots on the Ni and Ni-np@NC compounds. (o) Transfer electron quantity of BOR upon Ni-mp@NC and Ni compounds. (p) The discharge arcs of BOR at Ni-np@NC and Ni substances. (q) Discharge plots of DBFCs at 50 mA cm^{-2} by the Ni and Ni-np@NC anode substances, correspondingly. (r) SEM pictures of the Ni-np@NC substance after discharge. Steadiness assessment of BOR at (s) Ni-np@NC in addition (t) Ni compounds. Reproduced with permission from [290]. Copyright 2022 American Chemical Society.

electrooxidation of EtOH, glycol and glycerol [289].

A porous Cu-Ni alloy dendrite-like electrode catalyst decorated by NPs of Ni, i.e., Ni-*np*@NC, has been prepared with an ultrafast and handy approach. The Ni-*np*@NC electrocatalyst shows outstanding performance, like activity and selectivity for the oxidation reaction of borohydride. Additionally, the overpotential value of 169 mV at a CD of 10 mA cm⁻² for borohydride oxidation reaction and fuel effectiveness may attain up to 70%. The DBFC having the Ni-*np*@NC/C-based anode can provide the greatest CD of 218 mW cm⁻², more than the noble-based anode presented in the previous articles. The notable improvement of Ni-*np*@NC catalyst activity is on the back of the whole structure of porous dendrite decorated with NPs and the addition of Cu [290]. Fig. 20(a-h) displays the SEM pictures of catalysts simulated within additional Cu²⁺ concentration solutions. It may follow somewhat various surfaces of stimuli. It suggests that the introduction of Cu²⁺ mainly impacts the construction of the substance surface. As per the SEM pictures, two consequences of introducing Cu²⁺ on the catalysts' surface exist.

In contrast, the concentration of Cu²⁺ influences the selectivity catalyst of evolution to develop dendrites or particles. Thus, it can control the catalyst's surface by modifying the Cu²⁺ concentration. In summary, the substance surface's construction mechanism is shown in Fig. 20(i). In the subject of Cu²⁺ ions without the electrolyte, only Ni²⁺ ions are eased electrochemically to develop microparticles upon the surface of the Ni sheet support during the deposition procedure.

Furthermore, based upon the concern arcs of i_c and ν for synthesized materials from Fig. 20(j), the slant at Ni-*np*@NC is much more extensive than others, suggesting that it has an immense CDL. Thus, Ni-*np*@NC indicates the greatest ECSA of 2398 m² g⁻¹, which is 13-, 6-, and 4-times bigger than Ni, Ni-*mp*@NC, and NC, respectively, as illustrated in Fig. 20(k). This is attributed to the distinctive surfaces of the Ni-*np*@NC substance, spongy dendrites surrounded by NPs. Then, the performances of synthesized materials toward BOR are studied systematically. On Ni, Ni-*mp*@NC, Ni-*np*@NC, and NC materials, LSV graphs of BOR within NaBH₄ (0.135 M) and NaOH (2 M) combined solution are outlined in Fig. 20(l). Additionally, the lower overpotential of 169 mV at a CD of 10 mA cm⁻² is discovered on Ni-*np*@NC within Fig. 20(m), signifying that it is promising to the bond infringement of borohydride and has the highest catalytic performance to BOR. Similarly, the kinetics and interface reaction may also be studied through EIS. From Nyquist plots in Fig. 20(n), the charge transfer resistance (R_{ct}) drops strikingly after the foreword of Cu, representing much faster charge transfer kinetics of BOR on Ni-*np*@NC. It also indicates that introducing the Cu element improves the electrode interface's conductivity.

From Fig. 20(o), the numeral of transfer electrons upon Ni-*np*@NC is 5.15, constructing a breakthrough in the hypothetical 4-electron BOR on Ni-doped materials, where Ni is only 2.26. It can be why, on the Ni-*np*@NC material, borohydride hydrolysis and HER together through BOR are hindered, and the hydrogen developed from those side reactions is oxidized. The dendritic systems of Ni-*np*@NC may entangle and oxidize hydrogen drops to yield more electrons, as shown within the inset of Fig. 20(o). To verify the selectivity of prepared materials to BOR, persistent current discharge measures are brought out, and the discharge arcs of BOR at Ni-*np*@NC and Ni materials are shown in Fig. 20(p). Conferring to the analysis based on the discharge period, the fuel competence of BOR on Ni-*np*@NC is 70%, but that at Ni is just 40%. The higher fuel efficacy represents more borohydride being oxidized instantly rather than hydrolysis, suggesting a more suitable selectivity of Ni-*np*@NC to BOR.

Furthermore, it can assess the catalyst selectivity through the measure discharge capability of DBFC, which utilizes various designed materials as the anode. The discharge arcs of DBFC with Ni-*np*@NC anode and Ni anode are shown within Fig. 20(q). SEM illustrates the surface of the Ni-*np*@NC material to investigate the catalyst's resilience and durability on the surface of the Ni-*np*@NC material after discharging for

6 h. It may see from Fig. 20(r) that the spongy dendritic texture of Ni-*np*@NC is yet unchanged after an extended discharge. The ADTs are performed individually upon the Ni-*np*@NC and Ni stimuli. The test outcomes within Fig. 20(s, t) indicate that the catalytic performance of Ni-*np*@NC only reduces by around 22% after 500 CV scans, where that of the Ni material decreases by 32%, meaning that Ni-*np*@NC has a more suitable strength.

Feng et al. [299] have informed about several porous hollow nanocatalysts (PHNCs) based on Ir, i.e., IrNi, IrCo, and IrCoNi. Further, Gao et al. [300] described IrCoNi PHNCs fabricated by using a two-step process, (1) preparation of IrCoNi hollow nanocatalyst, (2) etching process as shown in Fig. 21(a). The TEM image shows the diverse hollow morphology of IrCoNi PHNCs (Fig. 21b); in the high-resolution TEM image (Fig. 21c), the rough outline, holes and central voids showed that result in higher numbers of active sites and hence increased the HER and OER catalysis. In addition, Density functional theory calculations were executed to clarify the intrinsic performance. The geometric optimization of the binding energies of oxygen-based intermediate moiety (Fig. 21d) and the projected density of states of the d band in Ir-based catalysts (Fig. 21e and f) displayed the reduction in the adsorption energy of IrCoNi catalysts. The schematic pictures of the reaction pathway also confirmed the weaker adsorption of oxygen-based intermediate moiety over the IrM nanocrystals, indicating their higher electrocatalytic activity.

Using the microwave-assisted reduction approach, the PtCo-based NPs in alloy form were fabricated by depositing them on various carbon-based supporting materials like rGO, rGO-Vulcan carbon, and activated carbon-Vulcan carbon, i.e., The NPs of PtCo was found to be 3.55 ± 0.64 nm in TEM analysis. The activity of these fabricated materials was checked for MOR, and out of all synthesized materials, the anodic peak current of PtCo@Activated carbon-Vulcan, hybrid, was found to be much higher, i.e., 73 mA/cm². The hybrid carbon support with PtCo NPs shows superior performance compared to single carbon support due to the synergistic effect of both [301].

Further, TM and N-C-based catalysts (M-NLPC) were fabricated using a ball mill with space-confinement pyrolysis. The catalysts have 3D-porous carbon with many active sites for effective ORR. Out of them, Fe-NLPC displayed excellent performance toward ORR at a half-wave potential of 0.88 V in a primary environment. The Fe-NLPC is highly durable and shows good tolerance for MeOH. It is used in DMFCs having no membrane and shows excellent activity [302]. An anode based on Si NWs is fabricated in a core-shell structure, i.e., SiNWs@ZnO, to know the activity of μ -DMFCs on exposure to light. For the SiNWs@ZnO heterojunction, the short circuit current is 100.5 μ A/cm², and the open circuit current is 0.7 V. The fabricated photoanode SiNWs@ZnO after the first use kept its 97.3% of current density for the next use. Using this catalyst, photo-assisted μ -DMFCs have 12 h discharge time with 0.7 V discharge voltage. Wisely planned core-shell structure and the corresponding energy levels among Si NWs and ZnO lead to important upgraded performances, where they can decrease the light reflexes of the polished Si, reinforce photos absorption and increase the charge transfer kinetics.

This research opens an exciting work related to the photo-assisted non-noble semiconductor anode for the high activity of μ -DMFC [303]. With the energy demand, the research in fuel cells increases with the fabrication of efficient electrode catalysts. Keeping this agenda in mind, novel nanocrystals based on two metal oxides with rGO are fabricated for the electrooxidation of methanol, i.e., MnCo₂O₄/NiCo₂O₄/rGO (MNR). The material MNR and MnCo₂O₄/NiCo₂O₄ are tested for MOR. It was found that adding rGO improves the electrocatalytic performance of catalysts due to the presence of a larger surface area and higher electrical conductivity. The excellent performance of MNR as compared to MnCo₂O₄/NiCo₂O₄ was because of the synergistic effect of MnCo₂O₄/NiCo₂O₄ and rGO. The current density for MnCo₂O₄/NiCo₂O₄ is 14.58 mA/cm². For MNR nanocatalysts, it is 24.76 mA/cm² with overvoltage of 0.6 and 0.58 V, and cyclic stability of

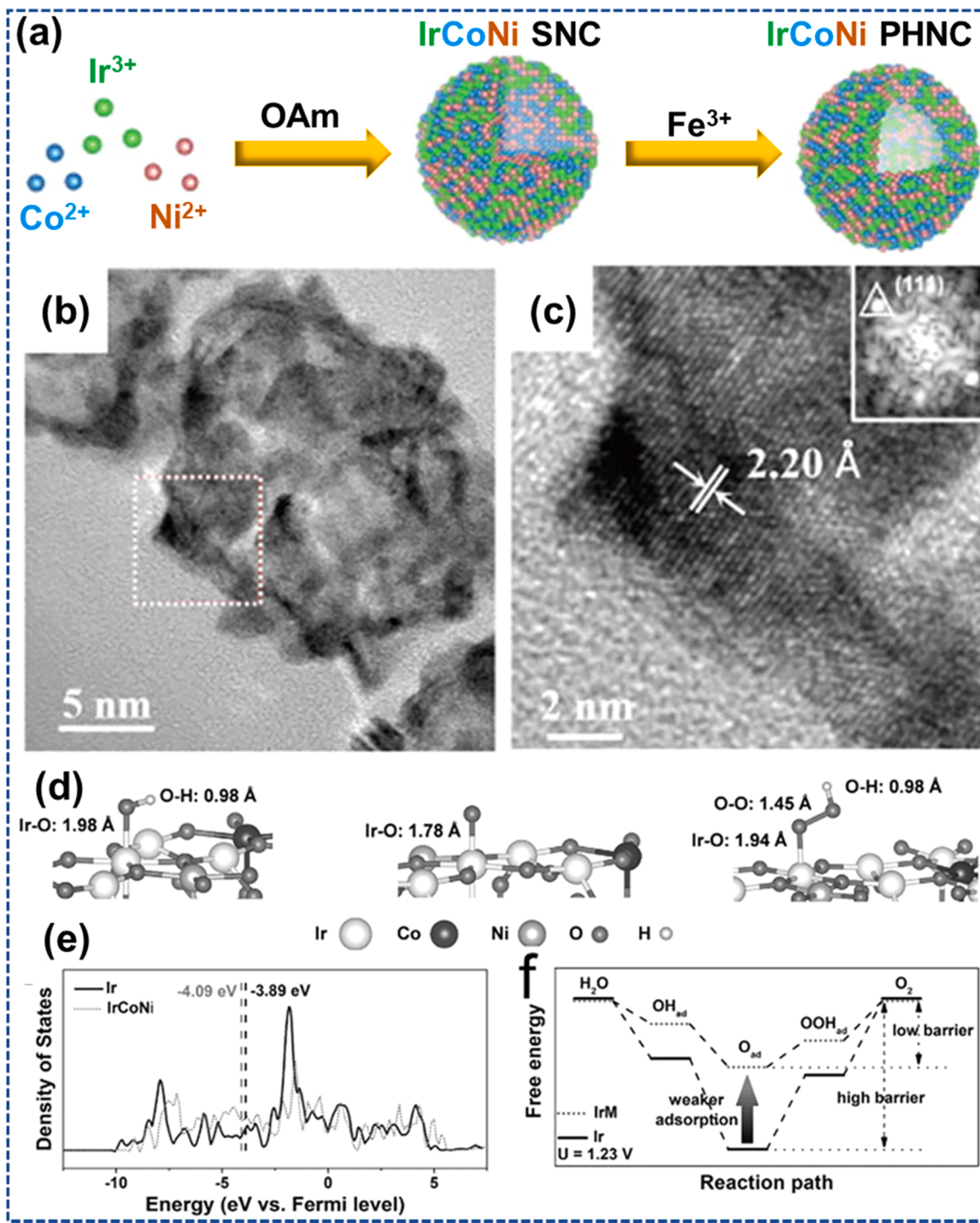


Fig. 21. (a) Schematic representation of the fabrication pathway of IrCoNi PHNCs, (b & c) High-resolution TEM pictures of as-fabricated IrCoNi PHNCs, the inset in (c) shows corresponding FFTpattern, (d) improved geometry of adsorption assembly of OH, O, and OOH mediates on IrCoNi, (e) DOS of d bands of Ir and IrCoNi with consistent d-band center represented through dash lines, (f) outline of OER reaction pathways.

Reproduced with permission from [300]. Copyright 2021 Elsevier.

98.3% and 99.7% for MnCo₂O₄/NiCo₂O₄ and MNR respectively (at optimum MeOH concentration/scan rate of 20 mV/S), can be capable and low-cost opportunities in the field of effective nanocatalysts for use in MeOH FC anodes [16].

5. Various methods of fabrication

Generally, the shape and size of metal NPs have a practical effect on their electrocatalytic behaviour. So, we need an effective catalyst

preparation method by which catalysts of desired surface properties are synthesized for FC reactions. Randomly, the deposition of NPs over the surface of some conductive or current-carrying supporting materials is the most hopeful method for alcohol oxidation reactions. As there is a good relation between surface coordination chemistry and synthetic methods, some of the techniques are successfully known for preparing metal NPs on conductive supporting materials surfaces having some reliable physical and chemical properties [223].

Assuming that the multiple typically utilized electrocatalysts are yet

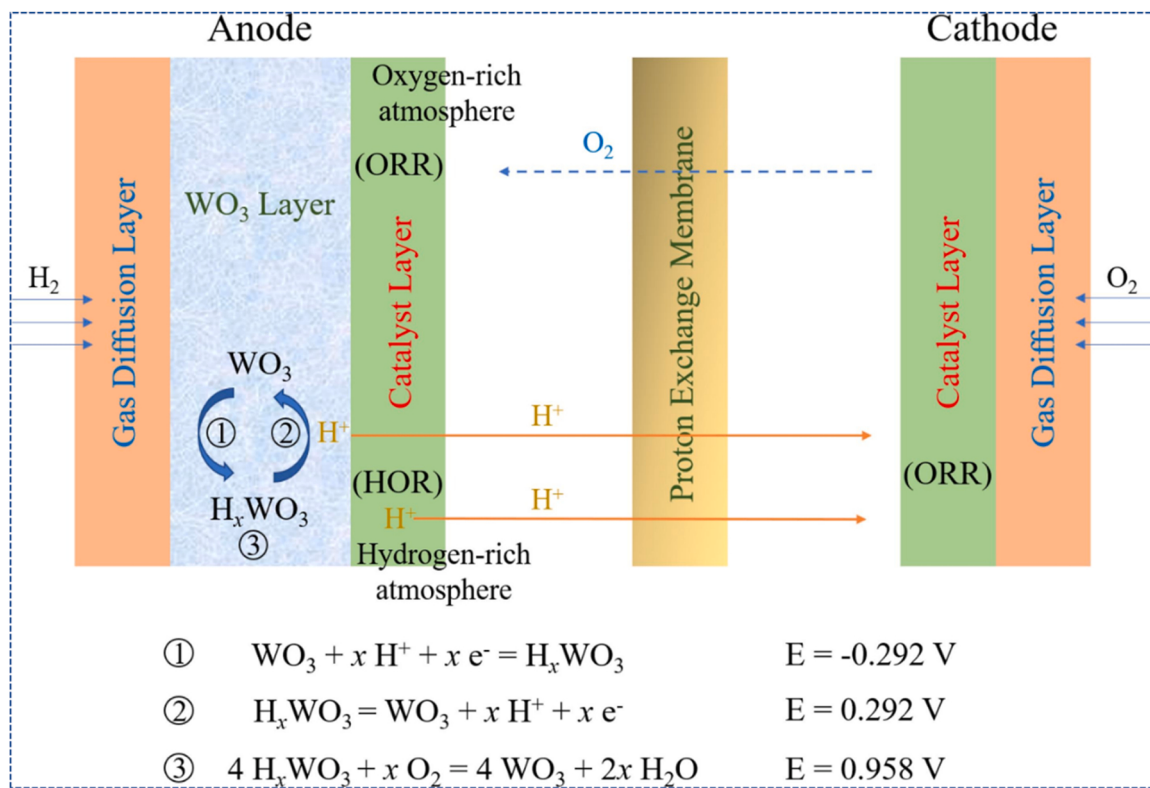


Fig. 22. Graphics of a MEA and the parts of anodic WO_3 coating within the hybrid PEMFC.
Reproduced with permission from [314]. Copyright 2021 Elsevier.

Pt or Pt-based substances within PEMFCs, several issues remain to be decoded before discovering their large-scale applications [304,305]. Foremost, the finite resources of Pt complete the Pt-based MEA (membrane electrode assembly) particularly expensive, pushing the investigators to pursue more effective and affordable catalysts [306]. Second, the electrocatalytic activity is unsatisfactory to get a high-enough power density consistent though noble Pt is utilized as an overwhelming cathode catalyst within appropriate PEMFCs [307]. Finally, the most severe barrier to the large-scale applications of PEMFCs is the inadequate long-term steadiness of Pt-based electrocatalysts. It has been often followed that the accumulation of Pt NPs and the electrochemical decomposition of carbon-based substrate will take place inevitably in the long-period process of PEMFCs, resulting within the degradation of catalysts and deterioration of activity [308].

Due to their abundant origins, cost-effectiveness and eco-friendly, transition metal oxides (TMO_x) are supposed up-and-coming prospects for different reactions within PEMFCs [309]. Similarly, oxides are an outstanding substrate that can interact with different metals, creating oxygen vacancies [310]. In the meantime, such intense relations among metal catalyst particles and oxide substrate may control metal particles' accumulation and sustain primarily metal particle dimensions [311].

Assuming the acidic media within PEMFCs, tungsten trioxide (WO_3) stands out among most TMO_x because of its superior strength in acidic solution [312]. Impressively, WO_3 may respond quickly with the available hydrogen to construct a unique hydrogen tungsten bronze (H_xWO_3 , $0.3 < x < 0.5$) network that is an acid-resistant metallic conductor completing it feasible to employ in highly acidic fuel cell media [313]. All these processes ensure WO_3 is essential in enhancing the transient power performance and stability of PEMFCs. The exact parts of WO_3 coating in the PEMFCs anode are graphically illustrated within Fig. 22 [314].

However, every parameter variation during the synthesis process affects the electrocatalytic behaviour of NPs. So researchers presented many methods like electrodeposition [315], electrospinning,

wet-chemical method, chemical vapour deposition method, solvothermal method, green hydrothermal method, hydrothermal synthesis, reduction, microwave-assisted polyol synthesis, hummer's method etc., for deposition of metal NPs over conductive supporting material surface. An exhaustive review of the material synthesis procedures for FCs applications has been provided in this section.

5.1. Electrodeposition method

For the electroplating purpose, generally, the electrodeposition method is used. In the electrodeposition process, the two electrodes of metal are put into a particular electrolyte. Then an electric field is applied from outside for the deposition of a desired metal layer over the cathode, i.e., the working electrode. This technique is usually used to get selected thin and thick layers of metal, nanomagnetic materials, supercapacitor materials etc. This method consists of both phase change and transfer of electrons and is studied under two categories, cathodic and anodic electrodeposition, depending on the reaction mechanism. The metal layer thickness is controlled by changing the CD and electrode potential [316,317]. Electrodeposition methods are of many types; they are also cost-effective and give pure nanomaterial deposition.

5.1.1. Galvanostatic electrodeposition (GED) method

This deposition is done by using three electrode systems, i.e., the working electrode (GCE), the reference electrode (Ag/AgCl), and the counter or auxiliary electrode (the Pt coil). In this, the uniform size of NPs is obtained by keeping the current constant by using this GED approach for the fabrication of spherical MnO_2 composite, which is coated with reduced graphene oxide (rGO), for ORR [318]. The complete process is shown in Fig. 23, given below [315].

Further, Pt-NPs were electro-deposited on the surface of carbon black and CNTs using the galvanostatic polarization method. This method allows controlling Pt-NPs morphology, i.e., dendritic, spherical and lamellar shapes. The electrocatalyst obtained by GED with three times

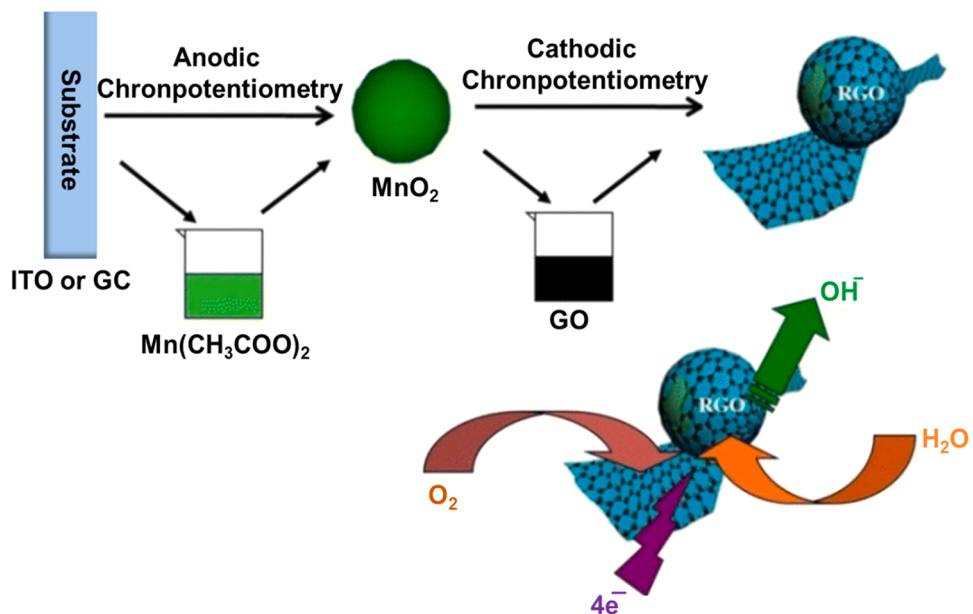


Fig. 23. Fabrication of MnO_2 @rGO electrocatalyst for ORR.
Reproduced with permission from [315]. Copyright 2021 John Wiley and Sons.

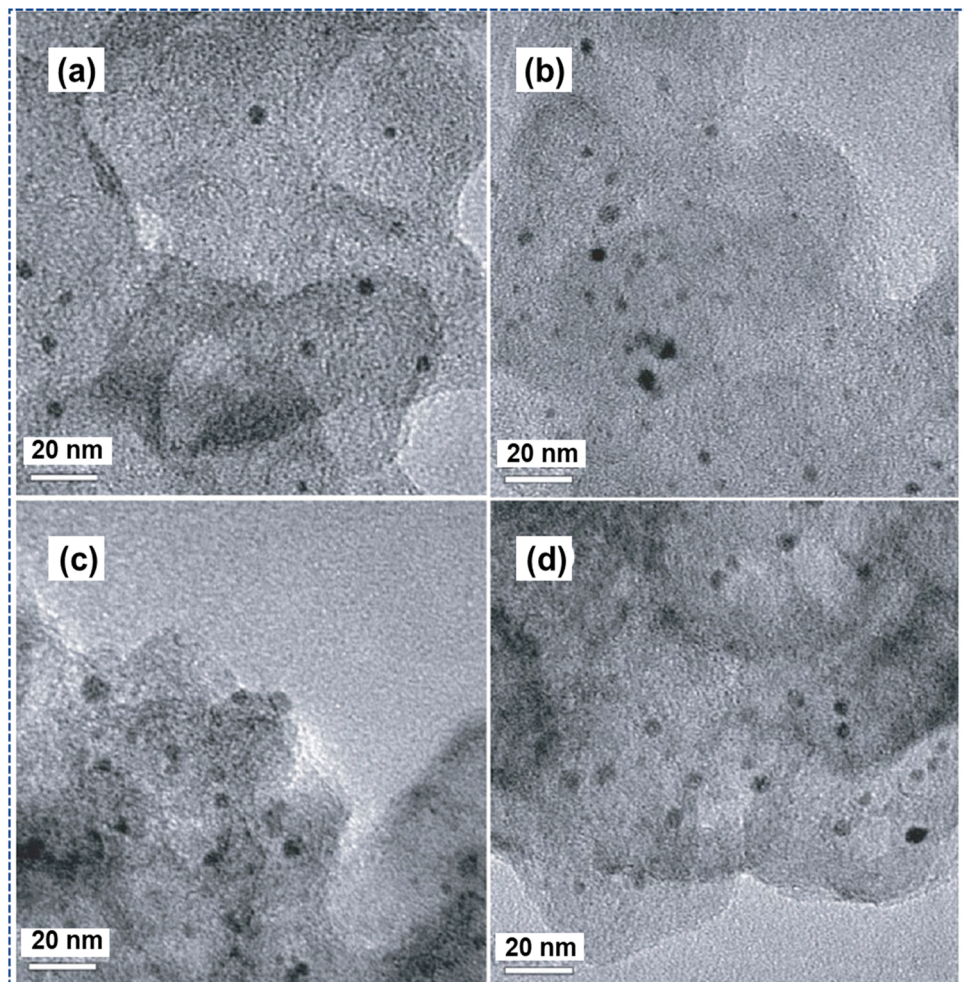


Fig. 24. TEM images of Pt particles that are electrodeposited by the GDE method over Vulcan XC-72 having various concentrations of PtCl_4^{2-} . (a) 10 mM, (b) 20 mM, (c) 40 mM, and (d) 80 mM.
Reproduced with permission from [320]. Copyright 2006 Elsevier.

more Pt loading, exhibits higher electrochemical real surface value and shows more activity toward MOR than commercial E-TEK [319]. Using the GDE (pulse) method low, Pt loading electrodes are fabricated over Nafion bonded C-layer (Vulcan XC-72). The deposition of Pt is done by using NaCl and K₂PtCl₄ salt at room temperature. The thickness of the catalyst layer and loading of Pt quantity are also reduced in aqueous solution because, in aqueous solution, the electrodeposition of Pt takes place only on the surface of carbon having slight conductivity of ion, i.e., Nafion-Na⁺ and provides maximum use of catalyst efficiency. The process proceeds in three steps:

1. Pt particles deposition on carbon layer that is Nafion-bonded
2. Treatment of layer with heat
3. Protonation of the layer

By using CV, we obtained the ECSA of the as-prepared catalyst. Fig. 24(a-d) represent the TEM image of Pt particles obtained by deposition over Vulcan XC-72 having a whole charge density of 1 C/cm² & concentration of Pt is 10, 20, 40, & 80 mM and displayed its morphology. Fig. 24(a-d) shows that a surge in the concentration of PtCl₄ has no binding effect on the size of particles. The prepared

materials have promising applications in PEMFCs [320].

The electrodeposition of Graphite felt (GF), having an approximate thickness of 3 mm in a normal state, was done by the GDE method using Triton X-102 micellar solution. A solution of PdCl₂ and SnCl₂ does the pre-treatment of GF, and in addition to getting the uniform dispersed NPs of Pt Triton, X-102 micellar media are also used. The diameter of Pd NPs is < 40 nm in diameter over the whole thickness of GF. The pre-treatment procedure stimulates the formation of Pd(PdO)-SnO₂ over the surface of Graphite. This work is an electrodeposition centre of Pd and produces another catalyst-support interaction effect. The Pd catalyst's oxidation of HCOOH is highly affected by the structure. The GF-based anode was demonstrated for direct formic acid FC and found to have many merits. As compared to the commercially available catalyst-coated membrane (CCM), having 40 g/m² Pd, the Pd/GF with 57 g/m² Pd, which was fabricated in the presence of Triton X-102 (12.5 vol%) and given pre-treatment 48 h gave a power output of 852 Wm⁻² at 333 K. On the other hand, the CCM gave a power output of 392 Wm⁻² at the same temperature [321].

5.1.2. Potentiostatic electrodeposition (PED) method

This method supplies a constant potential for some time during

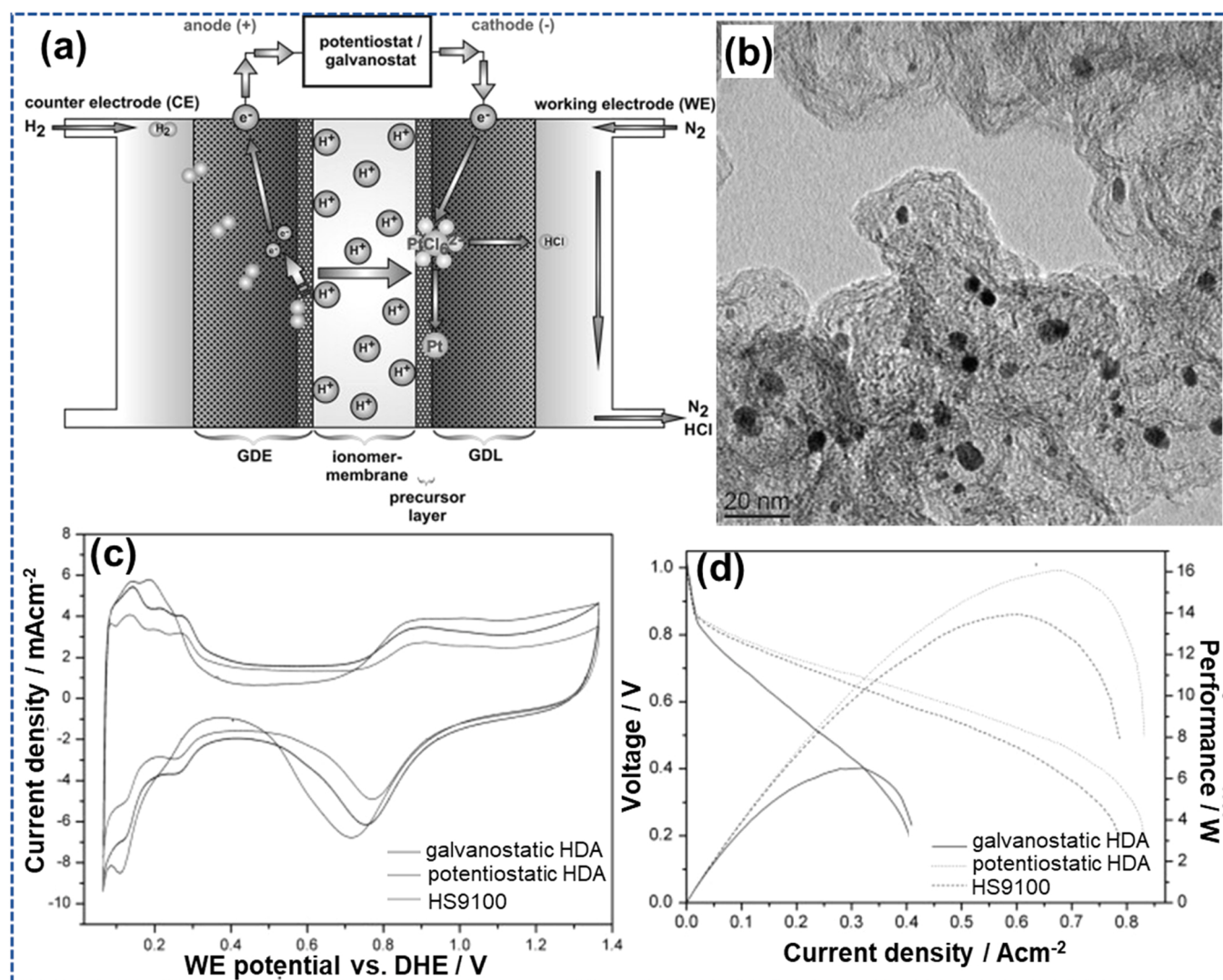


Fig. 25. (a) Schematic representation of electrodeposition cell having depolarized anode (HAD) (b) TEM images of Pt-catalyst PED over Vulcan XC-72 having particle size 4–10 nm, (c) CV curve of galvanostatic & PED HDA with HS9100, shows the higher electrochemical activity of PED Pt catalyst, (d) Current-voltage and current-performance curves that show higher performance in case of PED.

Reproduced with permission from [323]. Copyright 2012 Elsevier.

electrodeposition. On porous carbon support, MeOH electrooxidation was done using Pt NPs. These Pt NPs are obtained by the PED method. This experiment was done to know the characteristics of the electrodeposited Pt on several carbon support materials like graphite & conventional powder mixed with recast Nafion. The impact of the specific surface area of Pt on the electrooxidation of MeOH is observed over the number of Carbon supported Pt that was recast with Nafion. The results show that Pt's activity towards the electrooxidation of MeOH depends on the fine Pt surface and not on the particles' size. The fine structure of particles depends on the specific surface area of Pt, the preparation method and the nature of the substrate used [322]. The preparation of gas diffusion electrode (GDE) takes place by PED of Pt & Pd-nano alloy with hydrogen depolarized electrode at room temperature. For this purpose, a double pulse with nucleation and a growth phase is used. The setup for the electrodeposition is shown in Fig. 25(a). The TEM image of the electrodeposited Pt-catalyst on Vulcan-XC72 is displayed in Fig. 25(b). The particle size observed is 4–10 nm, and agglomeration size is observed at around 20 nm. It was observed that by PED of NPs, its electrochemical activity increases 2.5 times for fuel cell application compared to another electrodeposited method, as shown by the CV in Fig. 25(c). The current-voltage, as well as current performance characteristics, are shown in Fig. 25(d); the curve indicates that potentiostatically deposited GDE with 0.37 mg cm⁻² loading of Pt shows a higher activity of 16.0 W & 15.8 W at 500 mV, which is 2.5 times higher than GDE method [323].

5.1.3. Co-electrodeposition method

In this method, extremely porous nanocomposites having a more specific surface area are fabricated at 25 °C in a single step. The composition and the thickness of nanocomposites are controlled accordingly by changing the applied potential, the period for deposition and composition of used precursor materials. The prepared nanomaterials had short diffusion with path length for the reactants. The electrocatalyst prepared by this method is highly porous and has superior electrocatalytic activity. Ahn et al. [324] synthesized a Pt-Ru electrocatalyst (surface molar ratio of 51.7 Pt and 48.3 Ru) on carbon paper using a single-step co-electrodeposition approach with a three electrodes system. By altering time and deposition potential, the size of the particle and its density can be controlled.

All the electrochemical processes of this experiment were controlled by using a potentiostat. The field emission scanning electron microscope (SEM) image shows the deposition of Pt-Ru particles on carbon paper. The image shows that the size of particles decreases with an increase in density and negative potential. The synthesized Pt-Ru electrocatalyst exhibit superior electrocatalytic behaviour for MOR and good tolerance for carbon monoxide poisoning. A highly active and more selective CO₂ to CO Ag alloyed Zn dendritic electrode was fabricated using the co-electrodeposition method. The electrodeposition has been controlled to examine the electrode's porosity, surface area, silver content and thickness. An increase of 3133 cm²_{phy} cm⁻²_{geo} in the surface occurs by adding a small quantity of silver ion (Ag⁺) to the Zinc ion (Zn²⁺) solution. Without losing its selectivity, Ag and Zn electrocatalyst material produced carbon monoxide with 91% Faradic efficiency [325].

Wu et al. [326] fabricated Co₃O₄ nanoporous film using a two-step mechanism on a stainless steel substrate. In the first step, by using co-electrodeposition Co₃O₄-SiO₂ layer was synthesized. In the second step, the material Co₃O₄ was put under consecutive CV in a concentrated KOH solution to remove the SiO₂ part. As a result, the formation of the nanoporous-Co₃O₄ film takes place. Again, we used three-electrode systems in this process. The prepared electrocatalyst shows excellent electrocatalytic behaviour towards OER. The E-silica part enhances the surface roughness and helps transfer electrolyte ions and electrons when OER takes place. A Graphene-supported electrocatalyst of Pd and Ag NPs was fabricated on carbon cloth (CC) and represented as G-PdAg/CC. The fabricated electrocatalyst was compared with G-Pd/CC and G-Ag/CC using CV and showed superior electrocatalytic behaviour compared to

others [327].

3D ultra-fine Pt-nanoflowers are electrodeposited (by single step) on the carbon-deposited carbon diffusion layer electrode surface represented as C-GDL. This material is utilized in applications of polymer electrolyte FC. The surface structure, crystallinity, particle size distribution, and nanoflowers' oxidation state are inspected using different characteristic techniques. An increase in the current density from – 1.6 to – 32 mA/cm² was observed in nanoflowers showing the effect of Pt morphology on current density. During the analysis with a polymer electrolyte fuel cell, it was observed that Pt nanoflowers showed a higher peak power density of 660 mW/cm² at 0.6 V. The schematic representation of the synthesis of these nanoflowers is shown in Fig. 26(a). Further, the HR-TEM technique showed the Pt nanospheres dispersion & Pt nanoflowers mechanism of growth. The HR-TEM images of Pt-nanospheres at a CD – 3.2 mAcm⁻² are shown in Fig. 26(b-e) and at – 24 mAcm⁻² shown in Fig. 26(f-g). The formation of Pt nanospheres deposition is shown in Fig. 26(d), which was obtained grouping of NPs of 1 nm and 4 nm. The prominent lattice fringes of particular Pt nanodomains are shown in the inset of Fig. 26(e) having 2.28 ± 0.02 Å of d-spacing, which corresponds to (1 1 1). The formation of a flower-like structure is shown in Fig. 26(f), in which the petal's length is 50 nm and has a width of 10 nm on average. The Fig. 26(g) represents the Pt metal lattice plane (1 1 1) with a calculated d-space of 2.31 ± 0.02 Å. Moreover, the performance of the fuel cell is shown in Fig. 26(h-m). Fig. 26(h) represents the current-voltage curve of Pt-nanoflower and Pt-nanospheres, which shows better performance of Pt-nanoflowers toward polymer electrolyte fuel cells due to their higher surface area. The performance of polymer electrolyte fuel cells increases with an increase in CD, i.e., – 1.6 mA/cm² to – 24 mA/cm², due to enhancement in Pt loading and active catalyst sites. The decrease in the activity of polymer electrolyte FC is shown in Fig. 26(i), observed over 5 min and 30 min electrodeposition at the CD of – 24 mA/cm².

Further, electrodeposited Pt nanoflower showed enhanced performance at a CD of – 24 mA/cm² for 15 min having a peak power density of 660 mW/cm² over 0.6 V. Fig. 26(j) represents the mass activity of samples at various times and CD, and it was found that the nanoflower structure shows the highest mass activity at 0.6 V, i.e., 5500 mA mg/Pt (–24 mA/cm² and 15 min). The electrochemical impedance spectroscopy (EIS) of the sample is shown in Fig. 26(k) at 60 °C with H₂ (anode) and O₂ (cathode). The Nyquist plot shows that Ohmic resistance is the same for all, whereas variation is observed in charge transfer resistance (R_{CT}). This represents that R_{CT} depends on catalysts' electrodeposited layer over C-GDL at different CD. The resistance of the cell decreases with increases in current density for deposition of Pt. The CV of Fig. 26(l) shows the measurement of ECSA of fabricated catalyst at a potential range of 0.05–1.0 V vs. DHE over 25 °C. Fig. 26(m) represents Pt-deposited C-GDL steady-state current and durability test for 6 h. Initially, the highest CD was observed at 1 ± 0.05 A/cm² over 0.6 V, and after 2000 min it was 0.9 ± 0.05 A/cm² was observed. This shows that a minimum drop in CD occurs after 2000 min during start-up and shutdown [328].

Further, the coating of Ni-Cr-based alloy was done on copper substrate by co-electrodeposition method from a sulphate-chloride bath. The electrodeposition was done by direct-current (DC) and pulse-current (PC) methods. For this alloy composition, the efficiency of the cathode, crystallite size, structure and corrosive nature of Ni-Cr alloy deposition was examined, and it was found that the PC-electrodeposition method is suitable over DC. This is because desirable properties are obtained only from PC-electrodeposition, like a smooth coating surface without cracks, slim layer, high current density, high corrosion resistance due to forming a passive layer etc. [329]. The same effect was observed in the case of Ni-Co composite over ZnO NPs when done by Ghazanlou et al. [330]. Table 5.

5.1.4. Hydrothermal electrodeposition method

It is another well-known electrodeposition method. Firstly Mengqi

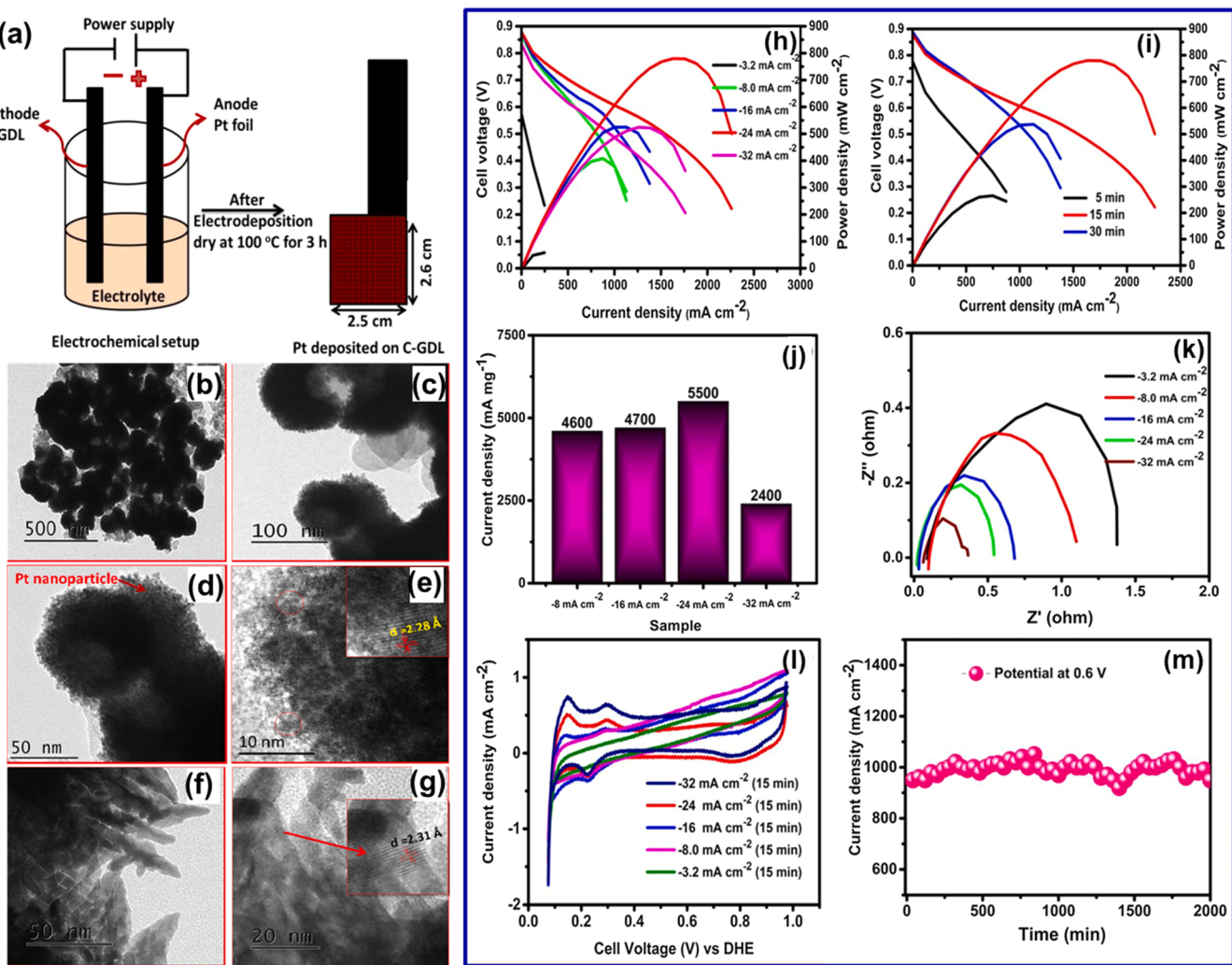


Fig. 26. (a) The schematic representation of Pt NPs decorated on the C-GDL with its surface structure; (b-g) HR-TEM image of electrodeposited Pt over C-GDL for 15 min at CD – 3.2 mA/cm²(b-e) and – 24 mA/cm²(f-g); (h) Electrodeposited Pt-polarization curve at various CD; (i) At a CD of – 24 mA/cm² for various time interval electrodeposited Pt; (j) At 0.6 V CD/gm of electrodeposited Pt-samples shows its mass activity; (k) At 0.4 V EIS of electrodeposited Pt samples; (l) CV shows ECSA of Pt H₂ adsorption-desorption area; (m) durability test of electrodeposited Pt for 33 h at a CD of – 24 mA/cm² for 15 min.

Table 5
The non-metal-based electrode catalyst for methanol oxidation.

Electrocatalyst	electrolyte	Type of catalyst	Molarity of methanol (M)	Electrode used	Current density mA/cm ²	Peak potential mV (RHE) (V)	Stability (sec)	Ref.
Ni _{0.6} Zn _{0.4} O/GCE	KOH (0.1 M)	Anodic	0.1	GC	~53	1.60	36000 s	[285]
Ni _{0.5} Co _{0.5} alloy	NaOH (0.1 M)	Cathodic	0.1	Ti foil	821.0	1.71	1200 s	[291]
NiCo ₂ O ₄ /SS (1 M)	KOH	Anodic	0.5	Stainless steel	905.0	1.56	1050 s	[292]
ZnO-CeO ₂ nanodots@CNFs (1 M)	KOH	Anodic	3	GC	~16.0	~1.88 V	500 s	[293]
Cu ₂ O/PPy-GO	H ₂ SO ₄ (0.05 M)	Anodic	2	GC	115.0	1.71	900 s	[294]
Co ₃ O ₄ -rGO	KOH (0.1 M)	Anodic	0.1	Pt	0.38	0.88	2000 s 100 cycles	[295]
Fe ₂ (MoO ₄) ₃ /GCE	KOH (0.1 M)	Anodic	1	GC	3.27	1.06	200 cycles	[286]
Cu-Ni/GCE	NaOH (1 M)	Anodic	0.3	GC	138.0	1.61	120 s for Dual step	[296]
Ni Sn (2:1)	NaOH (0.5 M)	Anodic	0.5	GC	50.0	1.66	5000 s	[297]
Ni-Co alloy (1:4)	NaOH (0.1 M)	Anodic	0.1	GC	821.0	1.72	200 s For dual step	[298]

Yao et al. [331] fabricated mesoporous Ni_{0.8}Fe_{0.2} film, self-supported on SLS as an OER electrocatalyst. This method has some advantages over other methods: (1) high temperature (110 °C), which leads to the

generation of H₂ gas at the cathode to overflow faster and helps to plate solution convert into gas; as a result, high pressure is created inside Teflon autoclave. Due to gas at the cathode and high pressure inside the

autoclave, the coated film contains a more active site at its surface, enhancing OER. (2) coating of crystallization is further improved by hydrothermal conditions, which leads to electrode stability. The fabricated film shows a larger electrochemical active surface area of 25.3 mF cm^{-2} . Further, MnO_2 interlinked NWs on carbon fabric were synthesized by hydrothermal electrodeposition followed by CVD polymerization of polypyrrole (PPy), i.e., $\text{PPy}@\text{MnO}_2$. The fabricated one-dimensional material shows high electrical conductivity, fast electrochemical kinetics and more structure stability [332].

5.1.5. Microwave electrodeposition method

It is another method to deposit nanomaterials over conducting surface as an electrocatalyst. Microwave-assisted methods have been used for the reactions requiring localized heating with an inverted temperature gradient. These processes generally occur in dry conditions or a closed reactor. Cu metal was electrodeposited on the surface of Pt, Au and carbon electrodes by using microwave radiation, and their effect was studied using CV and SEM. The experiment was done in an electrochemical cell with three electrodes and in a 2.45 GHz microwave cavity [333].

5.2. Electrospinning method

Electrospinning (ES) is an excellent method to synthesize 1D nanofibrous materials. The ES setup consists of three main components, a spinneret, a higher-voltage energy supplier, and a conductive collector. ES method is very cost-effective in producing fibrous nanomaterials and can control fibrous nanomaterials' size, diameter, and aspect ratio [334]. This process enhances stability, electrocatalytic performance, and nanomaterials' electrical and thermal conductivities. Amorphous Ni-iron oxide/C composite NFs are highly stable and synthesized using the ES method as an electrocatalyst for OER. This procedure involved two methods: (1) ES fabrication of Polyvinylpyrrolidone (PVP) polymer NFs that carry Ni and Fe inside and act as a precursor. (2) Ni-iron oxide/C composite NFs are synthesized thermally in the air at 250°C using a precursor. The fabricated NFs have a Ni/Fe molar ratio of 1:2, with a short overpotential of 310 mV and a CD of 10 mA/cm^2 . The NFs also exhibit higher catalytic stability $> 15 \text{ h}$, and the Faradic yield is $> 90\%$ for OER [335].

Principally, electrospinning has been utilized for PEMFC electrode incorporation within two distinct methods: (1) for the synthesis of compound reliance, where electrospun fibres are pyrolyzed or

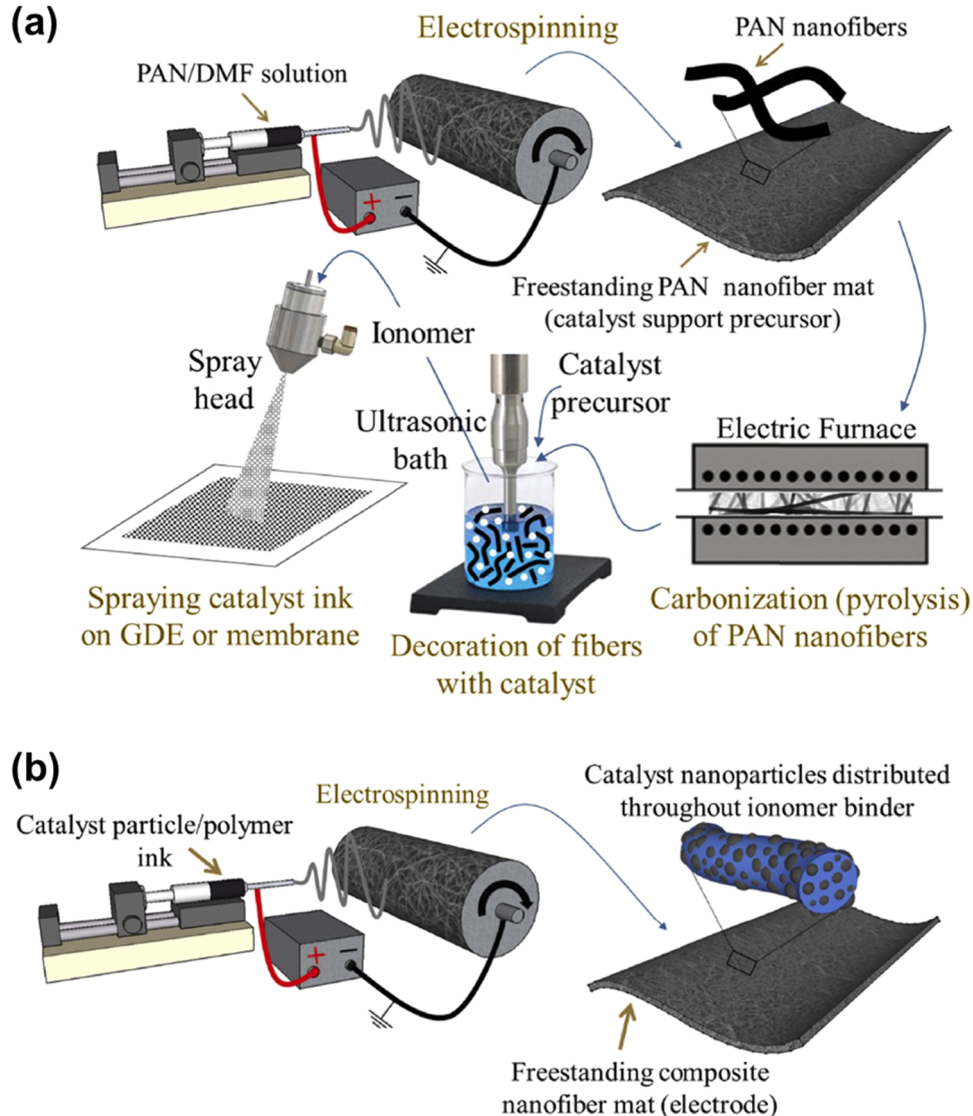


Fig. 27. (a) Using the ES approach of polyacrylonitrile (PAN) NF, an electrode of carbon fibres is fabricated, followed by carbonization, dispersion with NPs and deposition done by ionomer binder over GDE layers. (b) ES of a catalytic material ink into free-standing electrodes. Reproduced with permission from [336]. Copyright 2020 Elsevier.

calcinated to deliver carbon or metal oxide fibres which are then segmented, adorned with catalyst, distributed with a binder, and combined within a traditional covered or sprinkled probe MEA, and (2) for explicit incorporation of fibre rug electrodes, where polymer fibres are utilized as-spun into the electrode, and retail catalyst may be either contained into the electrospinning ink or sprinkled upon the fibres. The foremost approach is displayed within Fig. 27(a), where carbon or inorganic asset is first constructed from an electrospun and pyrolyzed predecessor, observed by noble metal deposit. The mat is then pulverized into a short-fibre powder, combined with an ionomer solution. The resultant ink is deposited upon a PEM or GDL utilizing traditional slurry layer/spraying techniques. An illustration of the second approach is shown in Fig. 27(b), where traditional FC catalyst powder (e.g., Pt on carbon asset) is merged with an ionomer, a carrier polymer, and solvent to assemble an ink that is then electrospun within a fibre mat electrode [336].

Using ES and underpotential deposition method, Hong et al. [337] fabricated a new PEMFC electrode known as E-U electrode with Pd/C@Pt_{skin} core-shell Catalyst with meagre Pt amount, i.e., 19 $\mu\text{g cm}^{-2}$. The higher porosity and more electrochemical active surface area of the E-U electrode also reduce the resistivity for oxygen transfer in the catalyst layer. This increases the performance of FC at a higher CD. A non-noble metal-based catalyst was prepared that was

made up of pyrolyzed Fe and Co that was co-doped with electrospun carbon nanofibers (CNFs). The ORR and OER of the fabricated catalyst are studied in alkaline and acidic environments, and it was found that the catalyst shows excellent performance toward ORR. Due to this, it is used in anion exchange membrane FCs applications. In anion exchange membrane FC investigation, a cathode is present that was based on an NF catalyst. The cathode catalyst is made up of ionic liquid, i.e., (Fe/Co/IL-CNF-800b) displayed a higher power density of 195 mW/cm [338]. The ES synthesis of Cobalt oxide/Carbon NFs (CNFs) and Nano-composite based polyvinyl alcohol (PVA) was done, and some researchers investigated their electrocatalytic performance for FC applications. In this work, the surface structure of the PVA NF and CNF electrodes is characterised by SEM images and shown in Fig. 28(a, b) and Fig. 28(c, d), respectively. Uniform and bead-free NFs have an approximate diameter between 200 and 300 nm. Using CV, investigated the fabricated materials' electrochemical performance in a homogeneous mixture of H_2SO_4 (0.5 M) and CH_3OH (0.6 M) at 25 °C. The set potential window is -0.6 to $+0.6$ V (vs SCE) in KOH (1 M), having a scan rate of 100 mV s⁻¹. Fig. 28(e) shows the CV of CNF with and without cobalt oxide. The curve with cobalt oxide/CNF has a larger CV area that represents higher specific conductance of material than bare CNF. Further, Fig. 28(f) illustrates the stability of the cobalt oxide/CNF catalyst. The repeated CV of cobalt oxide/CNF at a scan rate of 50 mV s⁻¹

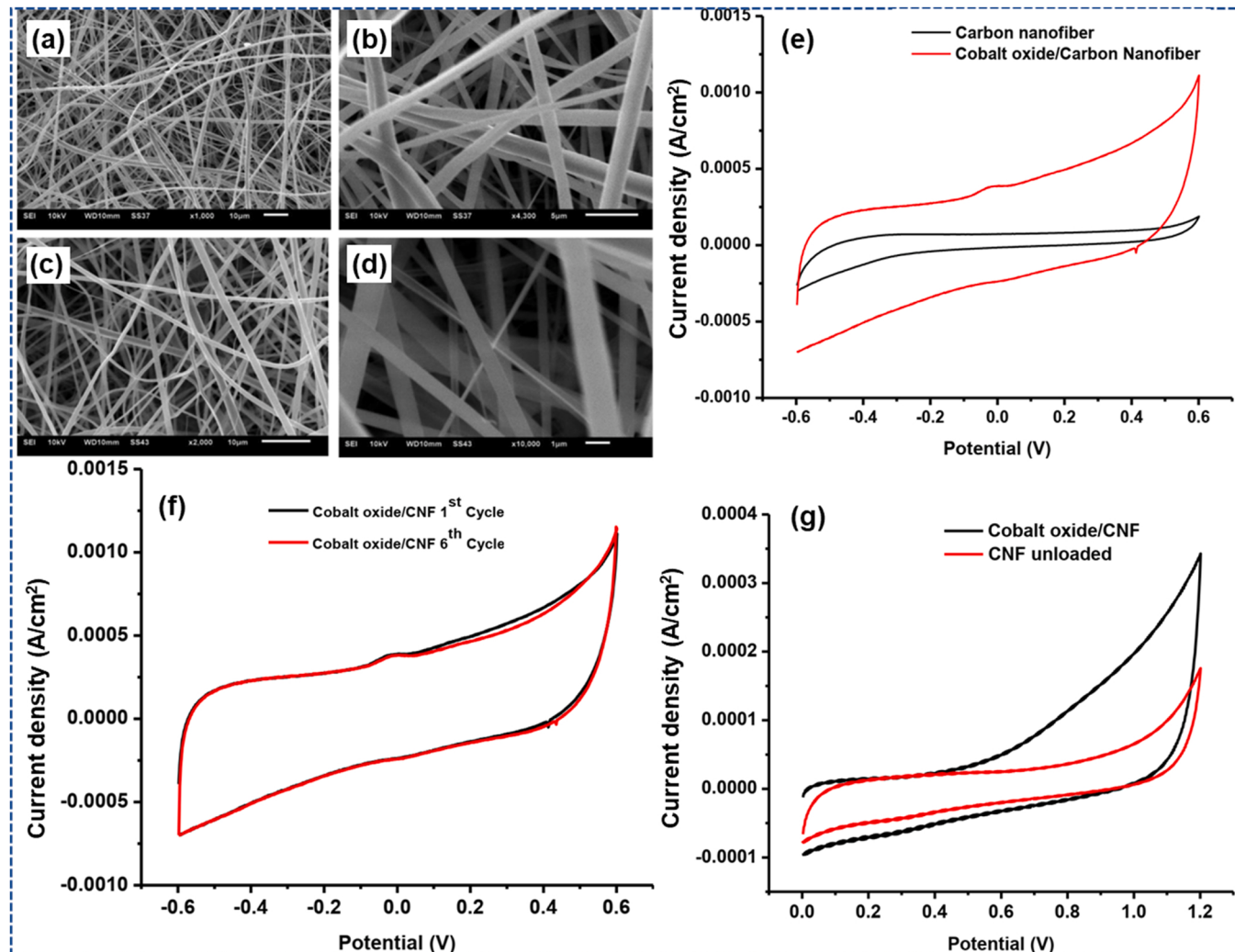


Fig. 28. SEM pictures of PVAs (a, b) before carbonization, (c, d) after carbonization, (e) CV of CNF and cobalt oxide/CNF at a scan rate of 50 mV s⁻¹, (f) Repeated CVs to check the stability of CNF and cobalt oxide/CNF at a scan rate 100 mV s⁻¹ in 1 M KOH, (g) CVs of CNF & cobalt oxide/CNF in a solution of H_2SO_4 and MeOH to check activity toward MOR at a potential range 0 to $+1.2$ V at a scan rate of 100 mV s⁻¹.
 Reproduced with permission from [339]. Copyright 2012 ESG.

in KOH (1 M) showed more stability after 6 cycles. Fig. 28(g) displayed the electrochemical performance of cobalt oxide loaded and unloaded CNF in H_2SO_4 (0.5 M) with MeOH. The CV curve shows CNF with cobalt oxide has a higher peak CD than bare CNF and shows high catalytic activity for MOR in DMFC. This is due to the presence of cobalt oxide, which can enhance the performance by (1) cobalt oxide and CNF synergistic effect, which gives the development of active sites, and (2) an increase in electronic continuity [339].

5.3. Wet-chemical method

The size and shape of nanostructured materials are better controlled using a wet chemical approach. Further, the shape and size of NPs depend on the conditions in which they are synthesized, like temperature, heating and cooling time, type of precursor used, mixing methods etc. This method is started by forming metal atoms via noble metals reduction or thermal decomposition; after that, aggregation of NPs occurs in a controlled manner. The reactions of the wet chemical method take place in the solution phase. Nikam et al. [340] described three types of wet chemical methods for the synthesis of NPs of metal oxide: (1) Solvothermal, (2) Microwave-assisted synthesis and (3) Thermal decomposition. Further, CuO NWs are fabricated using a wet chemical method with a diameter of 90 nm and a length of micrometres [341]. By the reduction of Platinum-2,4-pentanedionate in dibenzyl ether over 200 °C, the dendritic Pt NPs are synthesized. The synthesized Pt NPs are multi-faceted. The reduction occurs in the presence of oleic acid and oleylamine in the solution phase. The diagrammatic presentation of preparation is shown in Fig. 29(a). Fig. 29(b-g) obtained NPs electron microscopy study overview is displayed in a synoptic manner. High-angle annular dark field scanning TEM and TEM pictures (Fig. 29(b, c, respectively) showed uniform shape, small size and reasonable distribution of prepared dendritic NPs. As represented in Fig. 29(d), known as the particle size distribution histogram, the approximate 400

particles' mean diameter is measured at about 52 ± 2 nm. The most prominent characteristic of NPs is their regular/consistent edges that cover the surface of the nano-object, as shown in Fig. 29(c, e). The micrograph of a single particle in high-magnification displayed in Fig. 29(e) shows the presence of particular shape crystals in the approximate dimension of 10 ± 1 nm and explores its porous morphology. Fig. 29(f) shows the HR-TEM image of the crystallites that give the knowledge about exact terraces made from similar lower-indexed planes. However, regular decks lead on NPs surfaces. In the selected area electron diffraction outline shown in Fig. 29(g), it can observe the face-centred cubic lattice (111), (200), and (220) planes from the main diffraction ring of the first most reflection. The system is based on three electrodes, a GCE (working electrode), a saturated calomel electrode (reference electrode) and a Pt-wire (counter electrode). The result shows that the prepared nanomaterials are electrochemically more active toward ORR (Fig. 29(h)), MOR (Fig. 29(i)), having high mass activity and surface performance in comparison to Pt/C which present commercially as shown in CV [342].

Ganguli et al. [343], in 2021, provided various design principles of selenide-rich materials like $NiCo_2Se_4$ and Co_3Se_4 by wet chemical method for oxygen evolution reaction. A probable 2,6-dinitrophenol (2,6-DNP) based sensor probe was synthesized using differential pulse voltammetry (DPV). Electrocatalyst PbO -doped with ZnO nanomaterial, synthesized by wet chemical method and decorated on GCE, was used in this study. Different techniques, field emission-SEM (FESEM), XRD, FTIR, X-ray photoelectron spectroscopy (XPS), and UV-vis, are used to know the various properties of nanomaterial like optical, morphological, elemental, structural, and functional. The peak currents found in the DPV study of 2,6-DNP by using PbO -doped ZnO nanomaterial over GCE were plotted vs the applied potential to give calibration of the 2,6-DNP sensor represented by $ip(\mu A) = 1.0171 C(\mu M) + 22.312 (R^2 = 0.9951$; regression coefficient). 2,6-DNP sensor probe sensitivity was known by the curve of the calibration graph, and the vital range for 2,6-DNP

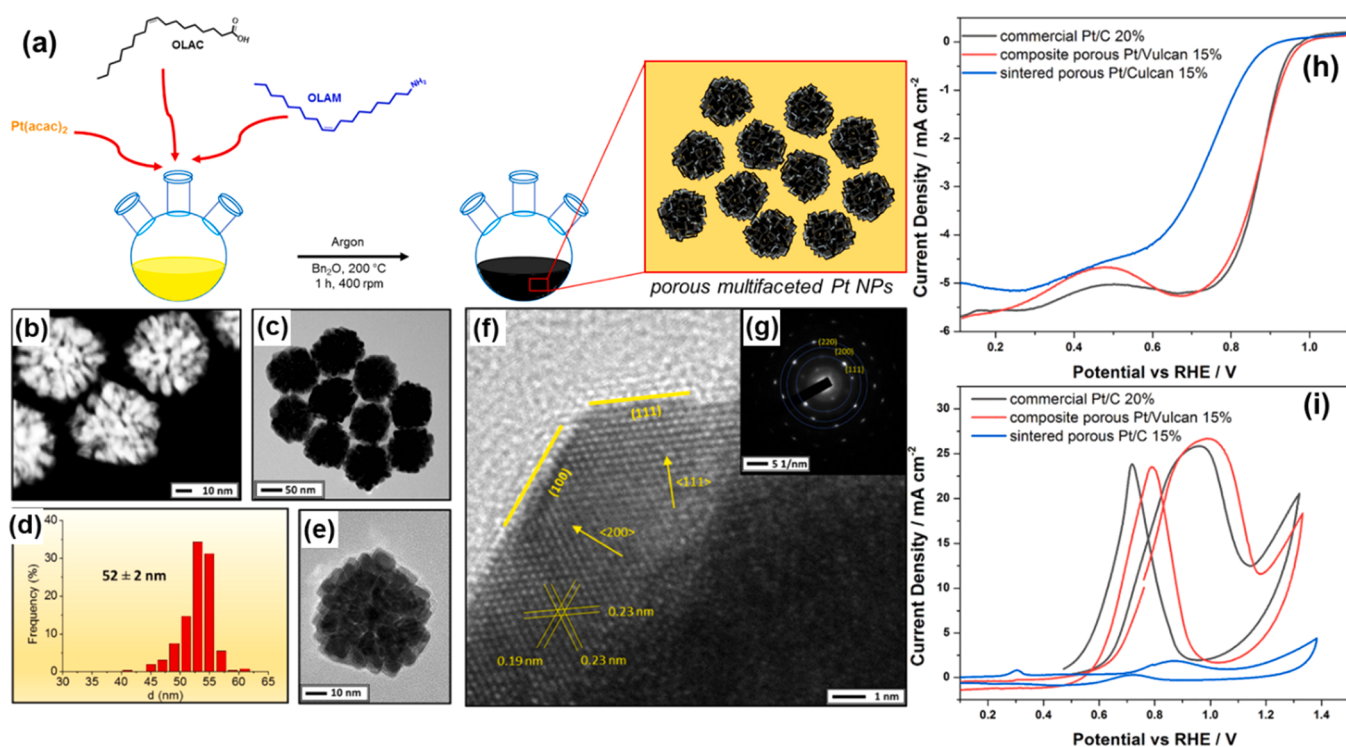


Fig. 29. (a) Porous Multifaceted Pt NPs fabrication scheme. Representative high-angle annular dark field-scanning TEM image of the Pt NPs (b); lower magnification (c), dimensional analysis (d), and higher magnification (e) TEM images of the NPs; HR-TEM image of the Pt crystallite (f) and selected-area electron diffraction patterns (g). LSV diagram of synthesized nanomaterial shows the electrocatalytic activity as compared to other materials (h) ORR, (i) MOR. Reproduced with permission from [342]. Copyright 2022 American Chemical Society.

recognition was found as $32.1867 \mu\text{A}\mu\text{M}^{-1} \text{cm}^{-2}$ and $3.23\text{--}16.67 \mu\text{M}$, respectively [344]. A bi-metal-based Pt-Au alloyed nano chains are fabricated by using a single-step wet chemical co-reduction approach fixed on rGO and represented as Pt-Au NCs/rGO. As a morphology-guiding and capping agent, caffeine is used. The fabricated nanocomposite showed a large surface area, efficient catalytic behaviour and much durability toward ethylene glycol and MOR as a comparison to commercially available Pt-C (Pt 50 wt%), PtRu-C (Pt 30 wt% and Ru 15 wt%) and Pt black [345].

5.4. The chemical vapour deposition method

In the chemical vapour deposition (CVD) method, a thin film of materials is formed on a heated substrate by using a chemical reaction in which precursors are used in the gaseous phase. In CVD, high-quality material having good conformation is formed, and the deposition rate is also reasonable. The CVD process consists of some basic steps: (1) the reactant in the gaseous phase is transferred into the reactor, and (2) gaseous reactants then react to form intermediate reactants and products in the gaseous state by using a homogeneous reaction pathway or these gaseous reactants may directly diffuse through the substrate's boundary layer, (3) the obtained substances then adsorb at the heated substrate & diffuses onto the surface, (4) Formation of thin layer takes place at the solid-gas interface by nucleation, combination & growth, (5) reaction by-product is formed, (6) the unreacted materials desorb from surface and move from reaction zone [346].

Further, Duverneuil et al. [347] deposited SnO_2 coating on Ti plates by metal-organic CVD. For this purpose, a reactive mixture of SnEt_4 and dioxygen is used. Through this process, $\text{Ti}/\text{IrO}_x/\text{SnO}_2$ electrodes are prepared; these electrodes are used for the electrooxidation of biodegradable contaminants present in wastewater of industries. The electrodes show a higher overpotential for OER and excellent capacity to eliminate total organic carbon from wastewater.

García-Contreras et al. [348] deposited Pt, Pt-Ni, and Pt-Co-Ni film on GCE using metal-organic CVD. During CVD, the interaction took place among product and reactants and formed an intermediate; as a result, a film containing crystalline NPs was present in more than one phase, which XRD, SEM and TEM proved. All the deposited film shows higher catalytic activity in 0.5 M KOH, but Pt-Co-Ni film shows the most increased electrocatalytic activity toward ORR.

5.5. Solvothermal method

In the solvothermal process, to enhance the autogenous pressure inside the reactor, the organic solvents are heated up above their boiling point [349], and by changing some variables like type of solvent, temperature, pressure etc., the characteristics like purity, crystalline, extent, dispersion of particles also modified [350]. Using such techniques, low-priced, environmentally friendly carbons synthesis from organic matter became possible [351].

The solvothermal method is also helpful in preparing many crystalline micro and NPs [352]. The reactions occur in water, known as hydrothermal, ammonia, or ammonothermal, and ethylene glycol is saccharotheramal. To differentiate this particular reaction from those reactions in various solvents, the common term "solvothermal" was used in the early 1980 s [353]. A novel electrocatalyst Pd decorated on Ni and Co NPs on rGO ($\text{Pd}_{10}\text{-Ni}_{45}\text{-Co}_{45}/\text{rGO}$) was fabricated using a solvothermal approach. The prepared material shows vigorous borohydride oxidation reaction activity with a CD of 108 mAcm^{-2} higher than $\text{Pd}_{10}\text{-Ni}_{45}/\text{rGO}$ and 185 mAcm^{-2} higher than $\text{Pd}_{10}\text{Co}_{90}/\text{rGO}$ at 0.5 V [354].

Further, using a solvothermal approach, various electrocatalysts like $\text{Pd}_{1.87}\text{Cu}_{0.11}\text{Sn}$ ternary NPs electrocatalysts [355] for alkaline DEFC applications. Highly porous Zirconium metal-organic framework (Zr-MOF) [356] cage-like electrocatalyst for ORR in microbial FC application, Pd-decorated rGO (Pd/rGO) and Pd-decorated

nitrogen-doped rGO (Pd/N-rGO) [357] NPs for DEFCs, Zn Phthalocyanine (ZnPc) nanoarchitecture and their composites with rGO [358] for ORR in alkaline FC etc. are synthesized. These nanostructured materials show higher electrocatalytic activity with higher CD at the low potential in alkaline or acidic medium.

5.6. Reduction method

This method involved the reduction of metal salts in several solvents and reducing agents [359]. Metal NPs and conductive supports are prepared by using this method. To synthesize the NPs by reduction method, we required: a metal salt as a precursor, a reductant, and a stabilizer. The commonly used reducing agent is ethylene glycol, sodium borohydride, potassium borohydride etc. The development of NPs on the surface of the support is due to the interaction between both [223].

Ayesha khan et al. fabricated starch-protected zero-valent Cu & Cu_2O NPs using a reduction approach in which using ascorbic acid as a reductant at 80°C . The mean size of NPs is 28.73 nm (Cu) & 25.19 nm (Cu_2O), which is obtained by using the Scherrer formula on diffraction peaks [360]. A bi-metallic Pt-Pd alloy-based NPs decorated on rGO (rGO/Pt-Pd) was fabricated by a hydrothermal-assisted chemical reduction process in which HCOOH act as a reductant. In this process, no stabilizer, as well as no capping agent, is used. The fabricated electrocatalyst rGO/Pt-Pd has a sizeable ECSA, lower onset potential, excellent electrocatalytic behaviour, more stability and a high peak current value for MOR. This is used in DMFC applications [361].

Yang et al. [362] fabricated Pd nanoplates with graphene (PdNPs/G) using the reduction method, with ascorbic acid as a reductant. Pd nanoplates have a higher surface-to-mass ratio and active prominent crystal faces, i.e. (110); conversely, graphene can transfer electrons rapidly. Due to these properties, PdNPs/G electrocatalyst exhibited superior electrocatalytic performance and more tolerance and durability for MOR and is a good candidate in applications of DMFCs. For the electrooxidation of EtOH in sulphuric acid, PtRuMo/C and PtRu/C NPs electrocatalyst was fabricated by chemical reduction of inorganic precursor salt, in which sodium borohydride act as a reductant. The catalyst shows excellent electrocatalytic activity, durability, and tolerance toward CO poisoning. PtRuMo/C shows superior activity as compared to PtRu/C NPs [363].

5.7. The microwave-assisted polyol synthesis method

Polyol-based methods fabricate metal and nanostructured alloy particles of controlled size. Polyol means polyalcohol's like glycol, glycerol etc., having a high boiling point and the ability to dissolve inorganic salts. Due to its chelating effect and average reducing nature, which prevent cluster formation of NPs during the process, the polyol method is used to prepare metal NPs. This method helps to prepare high-purity NPs with a size in nanometre, sub-micrometre, etc. Using microwave-assisted polyol synthesis, Cu nanosuspension is prepared in diethylene glycol, ascorbic acid and PVP. The size of Cu particles in nanosuspension is $45\text{--}130 \text{ nm}$ and stable for many months [364].

Using the polyol process, a Pt/C electrocatalyst having 40 wt% is fabricated for the cathode electrode without any stabilizer. Pt NPs are approximately 2.9 nm and exhibit outstanding performance for DMFC [365]. A bimetallic PdAu on a carbon support, i.e., PdAu/C electrocatalyst, was fabricated by NH_3 modified pulse microwave-assisted polyol synthesis for glucose electrooxidation in an alkaline environment and abbreviated as PdAu/C- NH_3 . The material shows excellent electrocatalytic activity and good sensitivity toward the electro-oxidation of glucose [366]. Further, by using the microwave-assisted polyol process, many electrocatalysts were fabricated for an FC application, i.e., Bimetallic Pt-Zn on CNT support (Pt-Zn/CNT) for MOR [196], Pt NPs 60 wt% on MWCNTs for DMFC application [367], CoSe catalyst supported on carbon (CoSe/C) for ORR [368], Pt/CNT for ORR in PEMFC [369], etc. and shows good electrocatalytic activity, stability,

tolerance for CO poisoning.

The electrode catalyst Pt NPs decorated on CNTs and Vulcan XC-72 were synthesized using the microwave-assisted polyol technique. As-prepared catalyst techniques like XRD, TEM, & XPS are considered for characterisation purposes. The size of Pt NPs that was uniformly scattered onto carbon support (Pt/C) was found to be a diameter of 2–6 nm. The characteristic diffraction peaks for Pt/C electrocatalyst were observed for face centred cubic arrangement of Pt. The XPS analysis shows that Pt (0) is present in bulk with a slight quantity of Pt (IV) and Pt (II). Fig. 30(a, b) shows the TEM images of a catalyst supported on Vulcan carbon and CNT. The images displayed the higher and uniform dispersal of metal NPs over the surface of the carbon. The approximate diameters are 3.8 ± 0.3 nm for Pt/Vulcan carbon and 3.6 ± 0.3 nm for Pt/CNT, which is obtained by measurement of the size of haphazardly selected 150 particles. Fig. 30(c) is the CV that shows the actual surface area of Pt/CNT and Pt/Vulcan by integrating charge in the area of hydrogen absorption. A shaded area in the voltammogram represented them.

Fig. 30 (d) represents a voltammogram of Pt/Vulcan and Pt/CNT electrodes in H_2SO_4 (1 M) at 25 °C, having a scan rate of 50 mV s⁻¹. This graph compares current produce during ORR of Pt/Vulcan & Pt/CNT. At 0.1 V and 0.5 V, a significantly higher oxygen reduction wave

was obtained for these two materials, representing the electrocatalysis by Pt in solution. High electrocatalytic performance was indicated by more value of cathodic current of the as-prepared catalyst in ORR. The Pt/C catalyst show elevated electrocatalytic performance toward ORR, as proved by CV studies. A prepared catalyst is an excellent material for proton exchange membrane FC applications [370].

The microwave-assisted polyol method is also used to fabricate nanoarchitecture Pd that is decorated on graphene nanosheets (Pd@GN). This was done at pH values of 7, 9 and 11. Pd NPs are obtained in 10 min, highly crystalline by conducting pulse microwave irradiation. By performing CV, EIS and single-cell test, the stability and electrocatalytic performance of the Pd@GN catalyst at 30–75 °C. At pH 9, the surface utilization is 94.7%, and the electrochemically active surface area is 72.2 m²/g for the fabricated Pd@GN catalyst. The maximum power density of the Pd@GN catalyst is 1.75 kW/g for a single cell at 75 °C and shows higher performance for FC applications [371].

Various methods of electrocatalyst fabrication, i.e., electrodeposition, electrospinning, wet-chemical, chemical vapour deposition, solvothermal, reduction and microwave-assisted polyol synthesis, are discussed above. Every method has its advantage for synthesising electrode catalysts, like the electrodeposition method gives a variety of NPs

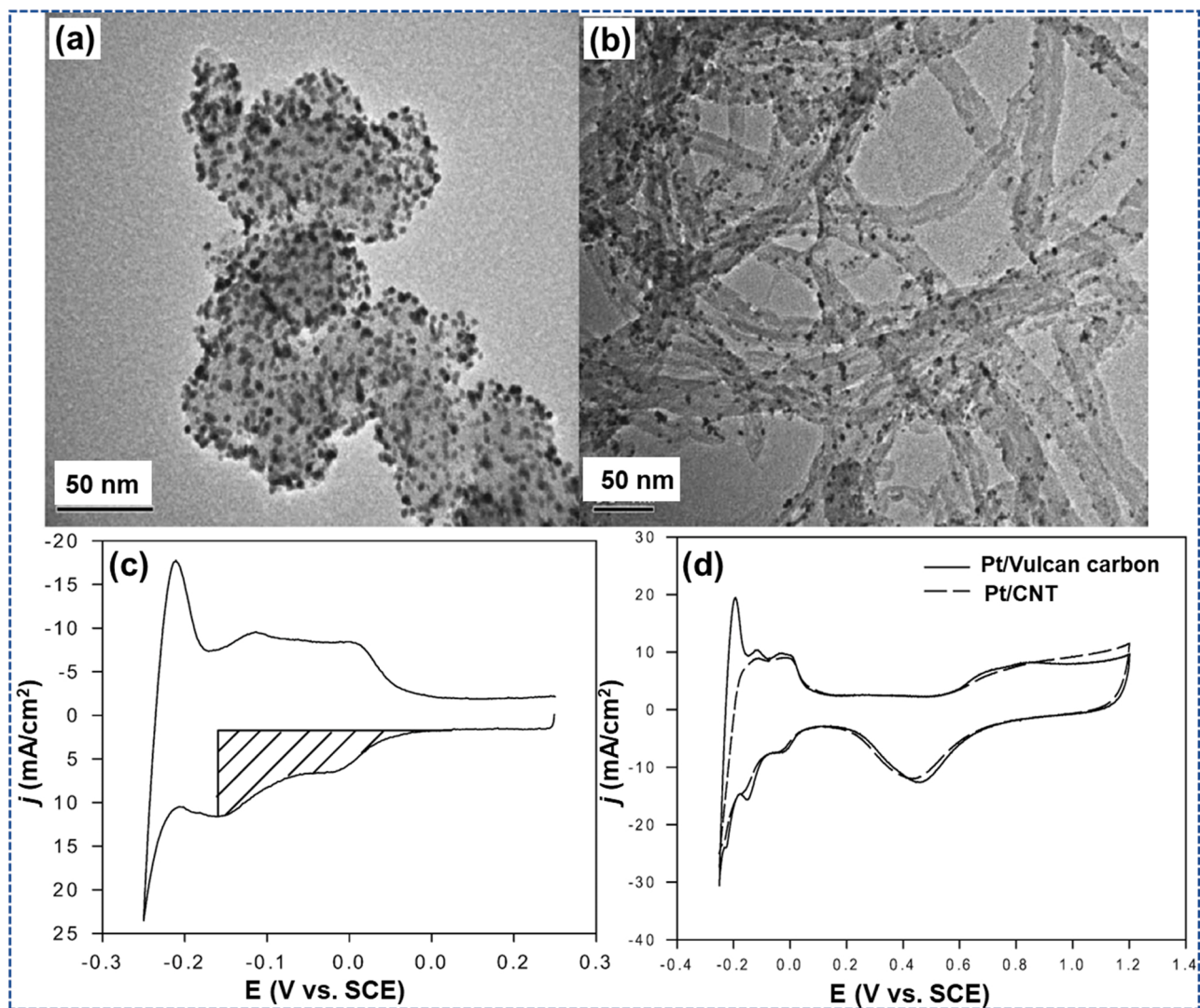


Fig. 30. (a, b) TEM images for Pt/Vulcan XC-72 carbon (a), Pt/CNT (b) having Pt loading 20 wt%; (c) Voltammetric diagram for electro absorption of hydrogen for Pt/CNT in H_2SO_4 (1 M) having scan rate 50 mV/S; (d) CV of Pt/CNT and Pt/Vulcan electrode at 25 °C having scan rate 50 mV s⁻¹ in 1 M H_2SO_4 . Reproduced with permission from [370]. Copyright 2005 Elsevier.

with improved durability and conductivity. Electrodeposition desirable qualities added to the catalyst or electrodes with improved function. On the other hand, this method is costly and harms the environment by producing harmful by-products.

In the same manner, electrospinning has much control over the morphology, porosity and composition of NPs. Still, its residual solvent has a toxic impact and is mainly used to fabricate nanofibers. The wet chemical method is used primarily to fabricate two-dimensional nanomaterials with tuned shape and size and requires a template for synthesis; on the other hand wet chemical method requires a higher temperature for reaction, uses surfactants and is not suitable for commercialization [372]. In addition, this CVD method produces a thin and uniform film with higher purity, low porosity and selective deposition, but its by-product is toxic, and instrumentation is expensive [373]. Further, solvothermal/hydrothermal methods are used to fabricate mono-dispersed and homogenous nanomaterials. This method dissolves several materials in the solvent to fabricate NPs. Good control over the size and shape of NPs is done by adjusting the reaction condition, but the autoclave used in the solvothermal process is very expensive [374].

In addition to these methods, the microwave-assisted polyol method is also used to fabricate nanomaterials because it combines the speed and homogeneous heating of precursor material. The reaction requires a short time to fabricate NPs because the electric and magnetic components combine, an effect that creates friction and collision in molecules [375]. From the above discussion, it is clear that each method has its advantages and selectivity. A suitable method is used depending on the type of nanomaterial to be fabricated.

6. Relationship between morphology, synthesis and composition of catalysts

Catalysts play an important and major role in the working of FCs. They enhance fuel cell activity by increasing the electrochemically active surface area. In this manner, the morphology of the catalyst has an essential role in the working of FCs. The process of electrocatalysis is a surface reaction for a particular catalyst. The active sites present over the catalyst show their electrocatalytic performance. By modifying the catalyst's surface and shape of catalyst in a reactive atmosphere, the activity of the catalyst is increased. As we know, by changing into different morphology, the number of active sites over catalysts also increases, increasing the activity of the catalyst. In this way, forming a porous catalyst is a more suitable option [376–378]. The catalytic activity of the catalyst is improved by increasing the number of active sites and modifying electronic structure by changing into different morphology. The method of synthesis plays a major role in the morphology of catalysts.

7. Challenges and future technology in fuel cell

FCs have various advantages in transportation, stationary, defence and portable power applications. Besides this, it also enhances the efficiency of cells over ancient used techniques. FC is twice as efficient as internal combustion engines, by the ability more significant than the effectiveness of 80% in collective heat and power arrangements. Additionally, FC-based vehicles put forward the potential for significantly less or zero emissions of harmful substances from the cars. Besides all these benefits, there are also some hurdles with fuel cell technology. Some of these are (i) Cost, i.e.; current approximation shows that at a higher amount of manufacturing (500,000 units), the price of an 80-kW direct H₂ FC application meant for transport would be \$73/kW [379]. Also, the high cost of its catalyst like Pt, Pd etc., affects this factor, (ii) Durability, (iii) Two-phase flow, (iv) Control of heat and water, (v) removal of poisonous gases like CO, (vi) pollutants impurities etc.

As FC technology grows daily, its genetic merit makes it suitable for quick adaptation, mainly in many power-consuming applications,

including trains, long-haul trucks, buses, and maritime. In the current scenario, more attention is given to developing highly durable and efficient light- to heavy-duty vehicles for fuel cells, which is a challenge. Hence, there is the requirement for essential material and the invention of a system that originates novel classes of hydrogen-based vehicles that advance this technology's higher potential, power density and versatility. For the adoption of heavy-duty FC electric vehicles on the road, essential infrastructure is required for hydrogen production, storage, and distribution. The US department of energy, H₂ @Scale, took the initiative to adopt widespread light-duty FC electric vehicles [380].

Nowadays, researchers are entirely devoted to discovering new and low-cost electrolytes and electrode materials that can maintain electrochemical properties even at low temperatures with either similar or high efficiency compared to traditional high-temperature materials. To robust the durability and power competence of FCs, the fabrication of new materials and customization in pre-existing materials is done by researchers and still focus [381].

Future investigations should be devoted to the wide-scale preparation of stable, inexpensive metal-based nanocrystals with different sizes, forms, and compositions. This study leads to the introduction of a novel, much more significant electrocatalyst for FC applications. However, it is not possible that same catalyst material work in all situations for the proper functioning of DAFCs, mainly in various operation states for numerous uses. As a result, there is a need for broad and advanced research ventures in the laboratory, which will lead to commercializing DAFCs in the coming years [15].

8. Conclusion

This review article mainly focused on synthesizing various electrode catalysts for FC applications. Pt-based, Pd-based, carbon composite-based, MOF-based and polymer-based catalysts are considered together with their specific significance on electrooxidation of alcohols in FC technology. Using Pt as a catalyst is a good option to overcome the catalyst loading and exhausted FC problem. The advancement in the area of FC catalysts has taken much concern in investigating an alternative. The advancement in the field of nanotechnology provides exceptionally stable and various support material-based catalysts.

Further, this article also describes the different types of FC with their operating temperature, type of electrolyte and working principles. In addition to these, various applications of FC, like in defense, transportation, portable devices etc., are considered, which lighten the advanced fields of FC technology and their importance. The research gap shows by this topic thorough study of the present situations of the investigational survey in FC technology.

Declaration of Competing Interest

The authors declare that they have no known competing financial interests that could have appeared to influence the work reported in this paper. All authors agreed on this submission. The paper is not considered by any other journal at this moment.

Data Availability

Data will be made available on request.

Acknowledgements

The authors acknowledge the support from the Department of Chemistry and Research & Development Cell of Maharishi Markandeshwar (Deemed to be University), Mullana, Ambala, Haryana, India.

References

- [1] Y. Zhang, F. Gao, H. You, Z. Li, B. Zou, Y. Du, Recent advances in one-dimensional noble-metal-based catalysts with multiple structures for efficient fuel-cell electrocatalysis, *Coord. Chem. Rev.* 450 (2022) 214244.
- [2] H. Fei, J. Dong, D. Chen, T. Hu, X. Duan, I. Shakir, Y. Huang, X. Duan, Single atom electrocatalysts supported on graphene or graphene-like carbons, *Chem. Soc. Rev.* 48 (2019) 5207–5241.
- [3] S. Ma, M. Lin, T.-E. Lin, T. Lan, X. Liao, F. Maréchal, J. Van herle, Y. Yang, C. Dong, L. Wang, Fuel cell-battery hybrid systems for mobility and off-grid applications: a review, *Renew. Sustain. Energy Rev.* 135 (2021) 110119.
- [4] H. Xing, C. Stuart, S. Spence, H. Chen, Fuel cell power systems for maritime applications: progress and perspectives, *Sustainability* 13 (2021).
- [5] H. Kaur, S.S. Siwal, R.V. Saini, N. Singh, V.K. Thakur, Significance of an electrochemical sensor and nanocomposites: toward the electrocatalytic detection of neurotransmitters and their importance within the physiological system, *ACS Nanosci. Au* 3 (2023) 1–27.
- [6] H. Kaur, K. Sheoran, S.S. Siwal, R.V. Saini, A.K. Saini, W.F. Alsanie, V.K. Thakur, Role of silver nanoparticle-doped 2-aminodiphenylamine polymeric material in the detection of dopamine (DA) with uric acid interference, *Materials* 15 (2022).
- [7] H. Lei, X. Li, C. Sun, J. Zeng, S.S. Siwal, Q. Zhang, Galvanic replacement-mediated synthesis of Ni-supported Pd nanoparticles with strong metal-support interaction for methanol electro-oxidation, *Small* 15 (2019), 1804722.
- [8] K. Mishra, N. Devi, S.S. Siwal, Q. Zhang, W.F. Alsanie, F. Scarpa, V.K. Thakur, Ionic liquid-based polymer nanocomposites for sensors, energy, biomedicine, and environmental applications: roadmap to the future (n/a), *Adv. Sci.* (2022), 2202187.
- [9] L.-X. Ding, A.-L. Wang, G.-R. Li, Z.-Q. Liu, W.-X. Zhao, C.-Y. Su, Y.-X. Tong, Porous Pt-Ni-P composite nanotube arrays: highly electroactive and durable catalysts for methanol electrooxidation, *J. Am. Chem. Soc.* 134 (2012) 5730–5733.
- [10] A.-L. Wang, X.-J. He, X.-F. Lu, H. Xu, Y.-X. Tong, G.-R. Li, Palladium-cobalt nanotube arrays supported on carbon fiber cloth as high-performance flexible electrocatalysts for ethanol oxidation, *Angew. Chem. Int. Ed.* 54 (2015) 3669–3673.
- [11] A.-L. Wang, H. Xu, J.-X. Feng, L.-X. Ding, Y.-X. Tong, G.-R. Li, Design of Pd/PANI/Pd sandwich-structured nanotube array catalysts with special shape effects and synergistic effects for ethanol electrooxidation, *J. Am. Chem. Soc.* 135 (2013) 10703–10709.
- [12] Z. Zhang, G. Liu, X. Cui, B. Chen, Y. Zhu, Y. Gong, F. Saleem, S. Xi, Y. Du, A. Borgna, Z. Lai, Q. Zhang, B. Li, Y. Zong, Y. Han, L. Gu, H. Zhang, Crystal phase and architecture engineering of lotus-thalamus-shaped Pt-Ni anisotropic superstructures for highly efficient electrochemical hydrogen evolution, *Adv. Mater.* 30 (2018), 1801741.
- [13] L. Mond, C. Langer, F. Quincke, L.—Action of carbon monoxide on nickel, *J. Chem. Soc. Trans.* 57 (1890) 749–753.
- [14] L.G. Austin, Fuel cells—A review of government-sponsored research, 1950–1964, (1967).
- [15] S.S. Siwal, S. Thakur, Q.B. Zhang, V.K. Thakur, Electrocatalysts for electrooxidation of direct alcohol fuel cell: chemistry and applications, *Mater. Today Chem.* 14 (2019), 100182.
- [16] M.B. Askari, S. Azizi, M.T. Moghadam, M. Seifi, S.M. Rozati, A. Di, Bartolomeo, MnCo2O4/NiCo2O4/rGO as a catalyst based on binary transition metal oxide for the methanol oxidation reaction, *Nanomaterials* (2022).
- [17] O.Z. Sharaf, M.F. Orhan, An overview of fuel cell technology: fundamentals and applications, *Renew. Sustain. Energy Rev.* 32 (2014) 810–853.
- [18] L. Carrette, K.A. Friedrich, U. Stimming, Fuel cells – fundamentals and applications, *Fuel Cells* 1 (2001) 5–39.
- [19] Y. Cui, J. Zhang, G. Zhang, J. Huang, P. Liu, M. Antonietti, X. Wang, Synthesis of bulk and nanoporous carbon nitride polymers from ammonium thiocyanate for photocatalytic hydrogen evolution, *J. Mater. Chem.* 21 (2011) 13032–13039.
- [20] X. Li, J. Wei, Y. Chai, S. Zhang, Carbon nanotubes/tin oxide nanocomposite-supported Pt catalysts for methanol electro-oxidation, *J. Colloid Interface Sci.* 450 (2015) 74–81.
- [21] S.S. Mahapatra, J. Datta, Characterization of Pt-Pd/C electrocatalyst for methanol oxidation in alkaline medium, *Int. J. Electrochem.* 2011 (2011), 563495.
- [22] C. Lamy, E.M. Belgsir, J.M. Léger, Electrocatalytic oxidation of aliphatic alcohols: application to the direct alcohol fuel cell (DAFC), *J. Appl. Electrochem.* 31 (2001) 799–809.
- [23] C. Hu, X. Wang, Highly dispersed palladium nanoparticles on commercial carbon black with significantly high electro-catalytic activity for methanol and ethanol oxidation, *Int. J. Hydrog. Energy* 40 (2015) 12382–12391.
- [24] K. Sundmacher, T. Schultz, S. Zhou, K. Scott, M. Ginkel, E.D. Gilles, Dynamics of the direct methanol fuel cell (DMFC): experiments and model-based analysis, *Chem. Eng. Sci.* 56 (2001) 333–341.
- [25] K. Maheshwari, S. Sharma, A. Sharma, S. Verma, Technology, fuel cell and its applications: a review, *Int. J. Eng. Res. Technol.* 7 (2018).
- [26] S.S. Siwal, A.K. Saini, S. Rarotra, Q. Zhang, V.K. Thakur, Recent advancements in transparent carbon nanotube films: chemistry and imminent challenges, *J. Nanostruct. Chem.* 11 (2021) 93–130.
- [27] H. Lei, S. Singh Siwal, X. Zhang, Q. Zhang, Compositional and morphological engineering of in-situ-grown Ag nanoparticles on Cu substrate for enhancing oxygen reduction reaction activity: a novel electrochemical redox tuning approach, *J. Colloid Interface Sci.* 571 (2020) 1–12.
- [28] W. Hong, J. Wang, E. Wang, Facile synthesis of highly active PdAu nanowire networks as self-supported electrocatalyst for ethanol electrooxidation, *ACS Appl. Mater. Interfaces* 6 (2014) 9481–9487.
- [29] S.J. Peighambardoust, S. Rowshan Zamir, M. Amjadi, Review of the proton exchange membranes for fuel cell applications, *Int. J. Hydrog. Energy* 35 (2010) 9349–9384.
- [30] G. Merle, M. Wessling, K. Nijmeijer, Anion exchange membranes for alkaline fuel cells: a review, *J. Membr. Sci.* 377 (2011) 1–35.
- [31] C. Rice, S. Ha, R.I. Masel, P. Waszczuk, A. Wieckowski, T. Barnard, Direct formic acid fuel cells, *J. Power Sources* 111 (2002) 83–89.
- [32] D. Leech, P. Kavanagh, W. Schuhmann, Enzymatic fuel cells: recent progress, *Electrochim. Acta* 84 (2012) 223–234.
- [33] D. Frattini, G. Accardo, A. Moreno, S.P. Yoon, J.H. Han, S.W. Nam, A novel nickel-aluminum alloy with titanium for improved anode performance and properties in molten carbonate fuel cells, *J. Power Sources* 352 (2017) 90–98.
- [34] D. Cao, Y. Sun, G. Wang, Direct carbon fuel cell: fundamentals and recent developments, *J. Power Sources* 167 (2007) 250–257.
- [35] V.S. Bagotsky, Fuel cells: problems and solutions, John Wiley & Sons, 2012.
- [36] R.M. Ormerod, Solid oxide fuel cells, *Chem. Soc. Rev.* 32 (2003) 17–28.
- [37] N. Shaari, S.K. Kamarudin, R. Bahru, S.H. Osman, N.A.I. Md Ishak, Progress and challenges: review for direct liquid fuel cell, *Int. J. Energy Res.* 45 (2021) 6644–6688.
- [38] S.Q. Song, W.J. Zhou, Z.H. Zhou, L.H. Jiang, G.Q. Sun, Q. Xin, V. Leontidis, S. Kontou, P. Tsaikaras, Direct ethanol PEM fuel cells: the case of platinum based anodes, *Int. J. Hydrog. Energy* 30 (2005) 995–1001.
- [39] X. Geng, H. Zhang, W. Ye, Y. Ma, H. Zhong, Ni-Pt/C as anode electrocatalyst for a direct borohydride fuel cell, *J. Power Sources* 185 (2008) 627–632.
- [40] A. Serov, C. Kwak, Recent achievements in direct ethylene glycol fuel cells (DEGFC), *Appl. Catal. B: Environ.* 97 (2010) 1–12.
- [41] V. Cigolotti, M. Genovese, P.J.E. Fragiocomo, Comprehensive review on fuel cell technology for stationary applications as sustainable and efficient poly-generation energy systems, *Energies* 14 (2021) 4963.
- [42] M.P. Hogarth, G.A. Hards, Direct methanol fuel cells technological advances and further requirements, *Platin. Met. Rev.* 40 (1996) 150.
- [43] M. Watanabe, S. Saegusa, P. Stonehart, High platinum electrocatalyst utilizations for direct methanol oxidation, *J. Electroanal. Chem. Interfacial Electrochem.* 271 (1989) 213–220.
- [44] M.Z.F. Kamarudin, S.K. Kamarudin, M.S. Masdar, W.R.W. Daud, Review: direct ethanol fuel cells, *Int. J. Hydrog. Energy* 38 (2013) 9438–9453.
- [45] Y.S. Li, T.S. Zhao, Z.X. Liang, Performance of alkaline electrolyte-membrane-based direct ethanol fuel cells, *J. Power Sources* 187 (2009) 387–392.
- [46] A.S. Lin, A.D. Kowalak, W.E. O’Grady, Studies of the role of water in the electrocatalysis of methanol oxidation, *J. Power Sources* 58 (1996) 67–72.
- [47] J.F.E. Gootzen, A.H. Wonders, W. Visscher, J.A.R. van Veen, Adsorption of C3 alcohols, 1-butanol, and ethene on platinumized platinum as studied with FTIRS and DEMS, *Langmuir* 13 (1997) 1659–1667.
- [48] L. Nan-Hai, S. Shi-Gang, In situ FTIR spectroscopic studies of the electrooxidation of C4 alcohol on a platinum electrode in acid solutions Part I. Reaction mechanism of 1-butanol oxidation, *J. Electroanal. Chem.* 436 (1997) 65–72.
- [49] S. Patra, N. Munichandraiah, Electrocatalysis of methanol on Pt-modified conductive polymer PEDOT, *Langmuir* 25 (2009) 1732–1738.
- [50] G. Wu, Y.-S. Chen, B.-Q. Xu, Remarkable support effect of SWNTs in Pt catalyst for methanol electrooxidation, *Electrochim. Commun.* 7 (2005) 1237–1243.
- [51] J.S. Lee, K.I. Han, S.O. Park, H.N. Kim, H. Kim, Performance and impedance under various catalyst layer thicknesses in DMFC, *Electrochim. Acta* 50 (2004) 807–810.
- [52] M. Uchida, Y. Aoyama, M. Tanabe, N. Yanagihara, N. Eda, A. Ohta, Influences of both carbon supports and heat-treatment of supported catalyst on electrochemical oxidation of methanol, *J. Electrochim. Soc.* 142 (1995) 2572–2576.
- [53] J. Solla-Gullon, F.J. Vidal-Iglesias, A. Lopez-Cudero, E. Garnier, J.M. Feliu, A. Aldaz, Shape-dependent electrocatalysis: methanol and formic acid electrooxidation on preferentially oriented Pt nanoparticles, *Phys. Chem. Chem. Phys.* 10 (2008) 3689–3698.
- [54] J. Garche, L. Juissen, Applications of fuel cell technology: status and perspectives, *Interface Mag.* 24 (2015) 39–43.
- [55] J. Markard, B. Truffer, Actor-oriented analysis of innovation systems: exploring micro-meso level linkages in the case of stationary fuel cells, *Technol. Anal. Strateg. Manag.* 20 (2008) 443–464.
- [56] T. Thampam, D. Shah, C. Cook, J. Novoa, S. Shah, Development and evaluation of portable and wearable fuel cells for soldier use, *J. Power Sources* 259 (2014) 276–281.
- [57] F. Barbir, Fuel cell stack design principles with some design concepts of micro-mini fuel cells, in: S. Kakaç, A. Pramuanjaroenkij, L. Vasiliev (Eds.), *Mini-Micro Fuel Cells*, Springer Netherlands, Dordrecht, 2008, pp. 27–46.
- [58] M. Broussely, G. Archdale, Li-ion batteries and portable power source prospects for the next 5–10 years, *J. Power Sources* 136 (2004) 386–394.
- [59] G. Zubi, R.S. Adhikari, N.E. Sánchez, W. Acuña-Bravo, Lithium-ion battery-packs for solar home systems: layout, cost and implementation perspectives, *J. Energy Storage* 32 (2020), 101985.
- [60] Y. Xie, J. Xiao, Q. Liu, X. Wang, J. Liu, P. Wu, S. Ouyang, Highly efficient utilization of walnut shell biochar through a facile designed portable direct carbon solid oxide fuel cell stack, *Energy* 227 (2021), 120456.
- [61] P. Boldrin, N.P. Brandon, Progress and outlook for solid oxide fuel cells for transportation applications, *Nat. Catal.* 2 (2019) 571–577.

[62] Y. Balali, S. Stegen, Review of energy storage systems for vehicles based on technology, environmental impacts, and costs, *Renew. Sustain. Energy Rev.* 135 (2021), 110185.

[63] S.S. Siwal, H. Kaur, A.K. Saini, V.K. Thakur, Recent progress in carbon dots-based materials for electrochemical energy storage toward environmental sustainability, *advanced energy and sustainability* (n/a), *Research* (2022), 2200062.

[64] J. Kast, R. Vijayagopal, J.J. Gangloff, J. Marcinkoski, Clean commercial transportation: medium and heavy duty fuel cell electric trucks, *Int. J. Hydrol. Energy* 42 (2017) 4508–4517.

[65] M.F. Ezzat, I. Dincer, Development and assessment of a new hybrid vehicle with ammonia and hydrogen, *Appl. Energy* 219 (2018) 226–239.

[66] P.E.V. de Miranda, E.S. Carreira, U.A. Icardi, G.S. Nunes, Brazilian hybrid electric-hydrogen fuel cell bus: improved on-board energy management system, *Int. J. Hydrol. Energy* 42 (2017) 13949–13959.

[67] E. Ogungbemi, T. Wilberforce, O. Ijaodola, J. Thompson, A.G. Olabi, Selection of proton exchange membrane fuel cell for transportation, *Int. J. Hydrol. Energy* 46 (2021) 30625–30640.

[68] N.-C. Shih, B.-J. Weng, J.-Y. Lee, Y.-C. Hsiao, Development of a 20 kW generic hybrid fuel cell power system for small ships and underwater vehicles, *Int. J. Hydrol. Energy* 39 (2014) 13894–13901.

[69] J.J. de-Troya, C. Alvarez, C. Fernández-Garrido, L. Carral, Analysing the possibilities of using fuel cells in ships, *Int. J. Hydrol. Energy* 41 (2016) 2853–2866.

[70] A.S. Patil, T.G. Dubois, N. Sifer, E. Bostic, K. Gardner, M. Quah, C. Bolton, Portable fuel cell systems for America's army: technology transition to the field, *J. Power Sources* 136 (2004) 220–225.

[71] J. Narayana Das, Fuel cell technologies for defence applications, in: K. V. Raghavan, P. Ghosh (Eds.), *Energy Engineering*, Springer Singapore, Singapore, 2017, pp. 9–18.

[72] A.S. Aricò, S. Srinivasan, V. Antonucci, DMFCs: from fundamental aspects to technology development, *Fuel Cells* 1 (2001) 133–161.

[73] A.S. Aricò, P. Creti, P.L. Antonucci, J. Cho, H. Kim, V. Antonucci, Optimization of operating parameters of a direct methanol fuel cell and physico-chemical investigation of catalyst–electrolyte interface, *Electrochim. Acta* 43 (1998) 3719–3729.

[74] P.K. Shen, C. Xu, Alcohol oxidation on nanocrystalline oxide Pd/C promoted electrocatalysts, *Electrochim. Commun.* 8 (2006) 184–188.

[75] C. Xu, Pk Shen, Y. Liu, Ethanol electrooxidation on Pt/C and Pd/C catalysts promoted with oxide, *J. Power Sources* 164 (2007) 527–531.

[76] E. Habibi, H. Razmi, Glycerol electrooxidation on Pd, Pt and Au nanoparticles supported on carbon ceramic electrode in alkaline media, *Int. J. Hydrol. Energy* 37 (2012) 16800–16809.

[77] R. Pattabiraman, Electrochemical investigations on carbon supported palladium catalysts, *Appl. Catal. A*: Gen. 153 (1997) 9–20.

[78] F. Hu, F. Ding, S. Song, P.K. Shen, Pd electrocatalyst supported on carbonized TiO₂ nanotube for ethanol oxidation, *J. Power Sources* 163 (2006) 415–419.

[79] K. Kakaei, M. Dorraji, One-pot synthesis of Palladium Silver nanoparticles decorated reduced graphene oxide and their application for ethanol oxidation in alkaline media, *Electrochim. Acta* 143 (2014) 207–215.

[80] K.L.K. Yeung, A.C.C. Tseung, The reduction of oxygen on teflon-bonded perovskite oxide electrodes, *J. Electrochem. Soc.* 125 (1978) 878–882.

[81] R. Zeis, Materials and characterization techniques for high-temperature polymer electrolyte membrane fuel cells, *Beilstein J. Nanotechnol.* 6 (2015) 68–83.

[82] A. Chandan, M. Hattenberger, A. El-kharouf, S. Du, A. Dhir, V. Self, B.G. Pollet, A. Ingram, W. Bujalski, High temperature (HT) polymer electrolyte membrane fuel cells (PEMFC) – a review, *J. Power Sources* 231 (2013) 264–278.

[83] E. Antolini, J.R.C. Salgado, E.R. Gonzalez, The stability of Pt–M (M=first row transition metal) alloy catalysts and its effect on the activity in low temperature fuel cells: a literature review and tests on a Pt–Co catalyst, *J. Power Sources* 160 (2006) 957–968.

[84] H.R. Colón-Mercado, B.N. Popov, Stability of platinum based alloy cathode catalysts in PEM fuel cells, *J. Power Sources* 155 (2006) 253–263.

[85] C.V. Rao, J. Parrondo, S.L. Ghatty, B. Rambabu, High temperature polymer electrolyte membrane fuel cell performance of PtxCoy/C cathodes, *J. Power Sources* 195 (2010) 3425–3430.

[86] H.A. Gasteiger, S.S. Kocha, B. Sompalli, F.T. Wagner, Activity benchmarks and requirements for Pt, Pt-alloy, and non-Pt oxygen reduction catalysts for PEMFCs, *Appl. Catal. B: Environ.* 56 (2005) 9–35.

[87] Y. Bing, H. Liu, L. Zhang, D. Ghosh, J. Zhang, Nanostructured Pt-alloy electrocatalysts for PEM fuel cell oxygen reduction reaction, *Chem. Soc. Rev.* 39 (2010) 2184–2202.

[88] L. Dubau, T. Asset, R. Chattot, C. Bonnaud, V. Vanpeene, J. Nelayah, F. Maillard, Tuning the performance and the stability of porous hollow PtNi/C nanostructures for the oxygen reduction reaction, *ACS Catal.* 5 (2015) 5333–5341.

[89] C. Chen, Y. Kang, Z. Huo, Z. Zhu, W. Huang, H.L. Xin, J.D. Snyder, D. Li, J. A. Herron, M. Mavrikakis, M. Chi, K.L. More, Y. Li, N.M. Markovic, G.A. Somorjai, P. Yang, V.R. Stamenkovic, Highly crystalline multimetallic nanoframes with three-dimensional electrocatalytic surfaces, *Science* 343 (2014) 1339–1343.

[90] C. Cui, L. Gan, H.-H. Li, S.-H. Yu, M. Heggen, P. Strasser, Octahedral PtNi nanoparticle catalysts: exceptional oxygen reduction activity by tuning the alloy particle surface composition, *Nano Lett.* 12 (2012) 5885–5889.

[91] N. Bevilacqua, T. Asset, M.A. Schmid, H. Markötter, I. Manke, P. Atanassov, R. Zeis, Impact of catalyst layer morphology on the operation of high temperature PEM fuel cells, *J. Power Sources Adv.* 7 (2021), 100042.

[92] N. Bevilacqua, M.A. Schmid, R. Zeis, Understanding the role of the anode on the polarization losses in high-temperature polymer electrolyte membrane fuel cells using the distribution of relaxation times analysis, *J. Power Sources* 471 (2020), 228469.

[93] Y. Yang, T. Yue, Y. Wang, Z. Yang, X. Jin, Effects of morphology on electrocatalytic activity of CeO₂ nanomaterials, *Microchem. J.* 148 (2019) 42–50.

[94] C.B. Sun, M.W. Guo, S.S. Siwal, Q.B. Zhang, Efficient hydrogen production via urea electrolysis with cobalt doped nickel hydroxide-riched hybrid films: cobalt doping effect and mechanism aspect, *J. Catal.* 381 (2020) 454–461.

[95] C. Li, V. Malgras, S.M. Alshehri, J.H. Kim, Y. Yamauchi, Electrochemical synthesis of mesoporous Pt nanowires with highly electrocatalytic activity toward methanol oxidation reaction, *Electrochim. Acta* 183 (2015) 107–111.

[96] B. Jiang, C. Li, V. Malgras, M. Imura, S. Tominaka, Y.J.Cs Yamauchi, Mesoporous Pt nanospheres with designed pore surface as highly active electrocatalyst, *Chem. Sci.* 7 (2016) 1575–1581.

[97] L. Wang, Y. Yamauchi, Synthesis of mesoporous Pt nanoparticles with uniform particle size from aqueous surfactant solutions toward highly active electrocatalysts, *Chem. – A Eur. J.* 17 (2011) 8810–8815.

[98] D. Wang, Y. Zhang, Z. Li, Z. Wu, S. Hata, F. Gao, Y. Shiraishi, Y. Du, One-pot synthesis of PdPtAg porous nanospheres with enhanced electrocatalytic activity toward polyalcohol electrooxidation, *J. Colloid Interface Sci.* 636 (2023) 602–609.

[99] F. Gao, Y. Zhang, P. Song, J. Wang, B. Yan, Q. Sun, L. Li, X. Zhu, Y. Du, Shape-control of one-dimensional PtNi nanostructures as efficient electrocatalysts for alcohols electrooxidation, *Nanoscale* 11 (2019) 4831–4836.

[100] L. Gao, X. Li, Z. Yao, H. Bai, Y. Lu, C. Ma, S. Lu, Z. Peng, J. Yang, A. Pan, H. Huang, Unconventional p–d hybridization interaction in PtGa ultrathin nanowires boosts oxygen reduction electrocatalysis, *J. Am. Chem. Soc.* 141 (2019) 18083–18090.

[101] Z. Chen, D. Higgins, Z. Chen, Electrocatalytic activity of nitrogen doped carbon nanotubes with different morphologies for oxygen reduction reaction, *Electrochim. Acta* 55 (2010) 4799–4804.

[102] M. Zhang, Y. Yan, K. Gong, L. Mao, Z. Guo, Y. Chen, Electrostatic layer-by-layer assembled carbon nanotube multilayer film and its electrocatalytic activity for O₂ reduction, *Langmuir* 20 (2004) 8781–8785.

[103] S.S. Siwal, Q. Zhang, N. Devi, K.V. Thakur, Carbon-based polymer nanocomposite for high-performance energy storage applications, *Polymers* 12 (2020).

[104] S. Karamveer, V.K. Thakur, S.S. Siwal, Synthesis and overview of carbon-based materials for high performance energy storage application: A review, *Mater. Today.: Proc.* 56 (2022) 9–17.

[105] S.S. Siwal, W. Yang, Q. Zhang, Recent progress of precious-metal-free electrocatalysts for efficient water oxidation in acidic media, *J. Energy Chem.* 51 (2020) 113–133.

[106] J. Zhang, Y. Cheng, S. Lu, L. Jia, P.K. Shen, S.P. Jiang, Significant promotion effect of carbon nanotubes on the electrocatalytic activity of supported Pd NPs for ethanol oxidation reaction of fuel cells: the role of inner tubes, *Chem. Commun.* 50 (2014) 13732–13734.

[107] A.A. El Mel, R. Nakamura, C. Bittencourt, The Kirkendall effect and nanoscience: hollow nanospheres and nanotubes, *Beilstein J. Nanotechnol.* 6 (2015) 1348–1361.

[108] S. Sakurai, M. Inaguma, D.N. Futaba, M. Yumura, K. Hata, Diameter and density control of single-walled carbon nanotube forests by modulating ostwald ripening through decoupling the catalyst formation and growth processes, *Small* 9 (2013) 3584–3592.

[109] F. Xiong, F. Lv, C. Tang, P. Zhang, S. Tan, Q. An, S. Guo, L. Mai, In situ construction of amorphous hierarchical iron oxyhydroxide nanotubes via selective dissolution-regrowth strategy for enhanced lithium storage, *Sci. China Mater.* 63 (2020) 1993–2001.

[110] M. Beltrán-Gastélum, M.I. Salazar-Gastélum, R.M. Félix-Navarro, S. Pérez-Sicairos, E.A. Reynoso-Soto, S.W. Lin, J.R. Flores-Hernández, T. Romero-Castañón, I.L. Albarrán-Sánchez, F. Paraguay-Delgado, Evaluation of PtAu/MWCNT (Multiwalled Carbon Nanotubes) electrocatalyst performance as cathode of a proton exchange membrane fuel cell, *Energy* 109 (2016) 446–455.

[111] S. Matuost, N. Pongpichayakul, P. Waenkaew, N. Promsawan, S. Themsirimongkon, J. Jakmunee, S. Saipanya, Electrocatalytic activity of bimetallic PtPd on cerium oxide-modified carbon nanotube for oxidation of alcohol and formic acid, *J. Electroanal. Chem.* 895 (2021), 115445.

[112] S. Lu, K. Eid, D. Ge, J. Guo, L. Wang, H. Wang, H. Gu, One-pot synthesis of PtRu nanodendrites as efficient catalysts for methanol oxidation reaction, *Nanoscale* 9 (2017) 1033–1039.

[113] H.Q. Pham, T.T. Huynh, Platinum–copper bimetallic nanodendritic electrocatalyst on a tio₂-based support for methanol oxidation in alkaline fuel cells, *ACS Appl. Nano Mater.* 4 (2021) 4983–4993.

[114] T. Sun, J. Chen, X. Lao, X. Zhang, A. Fu, W. Wang, P. Guo, Unveiling the synergistic effects of monodisperse sea urchin-like PdPb alloy nanodendrites as stable electrocatalysts for ethylene glycol and glycerol oxidation reactions, *Inorg. Chem.* 61 (2022) 10220–10227.

[115] B.-Q. Miao, Y.-C. Liu, Y. Ding, P.-J. Jin, P. Chen, Y. Chen, Rhodium nanodendrites catalyzed alkaline methanol oxidation reaction in direct methanol fuel cells, *Sustain. Mater. Technol.* 31 (2022), e00379.

[116] M. Nasrollahzadeh, M.S. Sajadi, M. Atarod, M. Sajjadi, Z. Isaabadi, An introduction to green nanotechnology, Academic Press, 2019.

[117] Y.L. Hsin, K.C. Hwang, C.-T. Yeh, Poly(vinylpyrrolidone)-modified graphite carbon nanofibers as promising supports for ptRu catalysts in direct methanol fuel cells, *J. Am. Chem. Soc.* 129 (2007) 9999–10010.

[118] M.A. Alvi, M.S. Akhtar, An effective and low cost PdCe bimetallic decorated carbon nanofibers as electro-catalyst for direct methanol fuel cells applications, *J. Alloy. Compd.* 684 (2016) 524–529.

[119] S. Xue, Q. Wang, G. Dai, M. Zhao, S. Sun, N. Yu, Q. Huang, Y. Zhu, L. Fu, Y. Wu, Titanium carbide/carbon nanofibers film as flexible gas diffusion layers for passive direct methanol fuel cells, *Int. J. Energy Res.* 46 (2022) 10919–10929.

[120] M. Yaldagard, M. Nazoktabar, M. Jahanshahi, Fabrication of platinum/polypyrolytic carbon nanofiber nanocomposite electrocatalyst for direct methanol fuel cells, *J. Nano Res. Trans. Tech. Publ.* (2021) 101–117.

[121] X. Peng, D. Lu, Y. Qin, M. Li, Y. Guo, S. Guo, Pt-on-Pd dendritic nanosheets with enhanced bifunctional fuel cell catalytic performance, *ACS Appl. Mater. Interfaces* 12 (2020) 30336–30342.

[122] F. Gao, Y. Zhang, F. Ren, Y. Shiraishi, Y. Du, Universal surfactant-free strategy for self-standing 3D tremella-like Pd–M (M = Ag, Pb, and Au) nanosheets for superior alcohols electrocatalysis, *Adv. Funct. Mater.* 30 (2020), 2000255.

[123] F. Zhao, L. Zheng, Q. Yuan, X. Yang, Q. Zhang, H. Xu, Y. Guo, S. Yang, Z. Zhou, L. Gu, X. Wang, Ultrathin PdAuBiTe nanosheets as high-performance oxygen reduction catalysts for a direct methanol fuel cell device, *Adv. Mater.* 33 (2021), 2103383.

[124] S.S. Siwal, Q. Zhang, 3 - Classification and application of redox-active polymer materials for energy storage nanoarchitectonics, in: V. Kumar, K. Sharma, R. Sehgal, S. Kalia (Eds.), *Conjugated Polymers for Next-Generation Applications*, Woodhead Publishing, 2022, pp. 91–113.

[125] W. Yang, X. Yang, J. Jia, C. Hou, H. Gao, Y. Mao, C. Wang, J. Lin, X. Luo, Oxygen vacancies confined in ultrathin nickel oxide nanosheets for enhanced electrocatalytic methanol oxidation, *Appl. Catal. B: Environ.* 244 (2019) 1096–1102.

[126] I.E.L. Stephens, A.S. Bondarenko, U. Grønbjerg, J. Rossmeisl, I. Chorkendorff, Understanding the electrocatalysis of oxygen reduction on platinum and its alloys, *Energy Environ. Sci.* 5 (2012) 6744–6762.

[127] C. Alegre, M.E. Gálvez, R. Moliner, V. Baglio, A.S. Aricò, M.J. Lázaro, Towards an optimal synthesis route for the preparation of highly mesoporous carbon xerogel-supported Pt catalysts for the oxygen reduction reaction, *Appl. Catal. B: Environ.* 147 (2014) 947–957.

[128] M. Kim, J.-N. Park, H. Kim, S. Song, W.-H. Lee, The preparation of Pt/C catalysts using various carbon materials for the cathode of PEMFC, *J. Power Sources* 163 (2006) 93–97.

[129] E. Antolini, Carbon supports for low-temperature fuel cell catalysts, *Appl. Catal. B: Environ.* 88 (2009) 1–24.

[130] W. Yang, Y. Wang, J. Li, X. Yang, Polymer wrapping technique: an effective route to prepare Pt nanoflower/carbon nanotube hybrids and application in oxygen reduction, *Energy Environ. Sci.* 3 (2010) 144–149.

[131] H.-S. Oh, H. Kim, Efficient synthesis of Pt nanoparticles supported on hydrophobic graphitized carbon nanofibers for electrocatalysts using noncovalent functionalization, *Adv. Funct. Mater.* 21 (2011) 3954–3960.

[132] R. Kou, Y. Shao, D. Wang, M.H. Engelhard, J.H. Kwak, J. Wang, V. Viswanathan, C. Wang, Y. Lin, Y. Wang, I.A. Aksay, J. Liu, Enhanced activity and stability of Pt catalysts on functionalized graphene sheets for electrocatalytic oxygen reduction, *Electrochim. Commun.* 11 (2009) 954–957.

[133] S.H. Kang, T.-Y. Jeon, H.-S. Kim, Y.-E. Sung, W.H. Smyrl, Effect of annealing PtNi nanophases on extended TiO₂ nanotubes for the electrochemical oxygen reduction reaction, *J. Electrochem. Soc.* 155 (2008) B1058.

[134] C.V. Subban, Q. Zhou, A. Hu, T.E. Moylan, F.T. Wagner, F.J. DiSalvo, Sol–gel synthesis, electrochemical characterization, and stability testing of Ti0.7W0.3O2 nanoparticles for catalyst support applications in proton-exchange membrane fuel cells, *J. Am. Chem. Soc.* 132 (2010) 17531–17536.

[135] M. Rezaei, S.H. Tabaee, D.F. Haghshenas, Electrochemical nucleation and growth of Pd/PdCo core–shell nanoparticles with enhanced activity and durability as fuel cell catalyst, *J. Mater. Chem. A* 2 (2014) 4588.

[136] S. Siwal, N. Devi, V.K. Perla, S.K. Ghosh, K. Mallick, Promotional role of gold in electrochemical methanol oxidation, *Catalysis, Struct. React.* 5 (2019) 1–9.

[137] S. Siwal, S. Matseke, S. Mpelane, N. Hooda, D. Nandi, K. Mallick, Palladium–polymer nanocomposite: an anode catalyst for the electrochemical oxidation of methanol, *Int. J. Hydrog. Energy* 42 (2017) 23599–23605.

[138] S. Siwal, M. Choudhary, S. Mpelane, R. Brink, K. Mallick, Single step synthesis of a polymer supported palladium composite: potential anode catalyst for the application of methanol oxidation, *RSC Adv.* 6 (2016) 47212–47219.

[139] X. Liu, D. Wang, Y. Li, Synthesis and catalytic properties of bimetallic nanomaterials with various architectures, *Nano Today* 7 (2012) 448–466.

[140] L.F. Brown, A comparative study of fuels for on-board hydrogen production for fuel-cell-powered automobiles, *Int. J. Hydrog. Energy* 26 (2001) 381–397.

[141] E.H. Yu, U. Kreuer, K. Scott, Principles and materials aspects of direct alkaline alcohol fuel cells, *Energies* 3 (2010) 1499.

[142] A. Chen, C. Ostrom, Palladium-based nanomaterials: synthesis and electrochemical applications, *Chem. Rev.* 115 (2015) 11999–12044.

[143] Y. Zhang, Q. Huang, G. Chang, Z. Zhang, T. Xia, H. Shu, Y. He, Controllable synthesis of palladium nanocubes/reduced graphene oxide composites and their enhanced electrocatalytic performance, *J. Power Sources* 280 (2015) 422–429.

[144] N.-F. Yu, N. Tian, Z.-Y. Zhou, T. Sheng, W.-F. Lin, J.-Y. Ye, S. Liu, H.-B. Ma, S.-G. Sun, Pd nanocrystals with continuously tunable high-index facets as a model nanocatalyst, *ACS Catal.* 9 (2019) 3144–3152.

[145] Y. Wang, X. Wang, C.M. Li, Electrocatalysis of Pd–Co supported on carbon black or ball-milled carbon nanotubes towards methanol oxidation in alkaline media, *Appl. Catal. B: Environ.* 99 (2010) 229–234.

[146] Y. Ren, S. Zhang, R. Lin, X. Wei, Electro-catalytic performance of Pd decorated Cu nanowires catalyst for the methanol oxidation, *Int. J. Hydrog. Energy* 40 (2015) 2621–2630.

[147] M.G. Hosseini, M. Abdolmaleki, S. Ashrafpoor, Methanol electro-oxidation on a porous nanostructured Ni/Pd-Ni electrode in alkaline media, *Chin. J. Catal.* 34 (2013) 1712–1719.

[148] Z. Yin, Y. Zhang, K. Chen, J. Li, W. Li, P. Tang, H. Zhao, Q. Zhu, X. Bao, D. Ma, Monodispersed bimetallic PdAg nanoparticles with twinned structures: formation and enhancement for the methanol oxidation, *Sci. Rep.* 4 (2014).

[149] S.R. Chowdhury, P. Mukherjee, Sk Bhattacharya, Palladium and palladium–copper alloy nano particles as superior catalyst for electrochemical oxidation of methanol for fuel cell applications, *Int. J. Hydrog. Energy* 41 (2016) 17072–17083.

[150] E.J.E. Antolini, E. Science, Palladium in fuel cell catalysis, 2 (2009) 915–931.

[151] G. Wang, L. Lei, J. Jiang, Y. Zhou, Q. Huang, Z. Zou, S.P. Jiang, H. Yang, An ordered structured cathode based on vertically aligned Pt nanotubes for ultra-low Pt loading passive direct methanol fuel cells, *Electrochim. Acta* 252 (2017) 541–548.

[152] S.K. Desai, M. Neurock, K. Kourtakis, A periodic density functional theory study of the dehydrogenation of methanol over Pt(111), *J. Phys. Chem. B* 106 (2002) 2559–2568.

[153] G.T. Burstein, C.J. Barnett, A.R. Kucernak, K.R. Williams, Aspects of the anodic oxidation of methanol, *Catal. Today* 38 (1997) 425–437.

[154] V.S. Bagotzky, Y.B. Vassilyev, Mechanism of electro-oxidation of methanol on the platinum electrode, *Electrochim. Acta* 12 (1967) 1323–1343.

[155] G.A. Planes, G. García, E. Pastor, High performance mesoporous Pt electrode for methanol electroxidation. A DEMS study, *Electrochim. Commun.* 9 (2007) 839–844.

[156] Y.-B. He, G.-R. Li, Z.-L. Wang, Y.-N. Ou, Y.-X. Tong, Pt nanorods aggregates with enhanced electrocatalytic activity toward methanol oxidation, *J. Phys. Chem. C* 114 (2010) 19175–19181.

[157] Y. Bi, G. Lu, Control growth of uniform platinum nanotubes and their catalytic properties for methanol electroxidation, *Electrochim. Commun.* 11 (2009) 45–49.

[158] Z. Yan, B. Li, D. Yang, J. Ma, Pt nanowire electrocatalysts for proton exchange membrane fuel cells, *Chin. J. Catal.* 34 (2013) 1471–1481.

[159] R.M. Antoniassi, J.C.M. Silva, A. Oliveira Neto, E.V. Spinacé, Synthesis of Pt+SnO₂/C electrocatalysts containing Pt nanoparticles with preferential (100) orientation for direct ethanol fuel cell, *Appl. Catal. B: Environ.* 218 (2017) 91–100.

[160] M. Cao, D. Wu, R. Cao, Recent advances in the stabilization of platinum electrocatalysts for fuel-cell reactions, *ChemCatChem* 6 (2014) 26–45.

[161] L. Huang, S. Zaman, X. Tian, Z. Wang, W. Fang, B.Y. Xia, Advanced platinum-based oxygen reduction electrocatalysts for fuel cells, *Acc. Chem. Res.* 54 (2021) 311–322.

[162] N. Kristian, X. Wang, Ptshell–Aucore/C electrocatalyst with a controlled shell thickness and improved Pt utilization for fuel cell reactions, *Electrochim. Commun.* 10 (2008) 12–15.

[163] H. Ataei-Esfahani, J. Liu, M. Hu, N. Miyamoto, S. Tominaka, K.C.W. Wu, Y. Yamauchi, Mesoporous metallic cells: design of uniformly sized hollow mesoporous Pt–Ru particles with tunable shell thicknesses, *Small* 9 (2013) 1047–1051.

[164] V.R. Stamenkovic, B.S. Mun, M. Arenz, K.J.J. Mayrhofer, C.A. Lucas, G. Wang, P. N. Ross, N.M. Markovic, Trends in electrocatalysis on extended and nanoscale Pt–bimetallic alloy surfaces, *Nat. Mater.* 6 (2007) 241–247.

[165] F. Taufany, C.-J. Pan, H.-L. Chou, J. Rick, Y.-S. Chen, D.-G. Liu, J.-F. Lee, M.-T. Tang, B.-J. Hwang, Relating structural aspects of bimetallic Pt3Cr1/C nanoparticles to their electrocatalytic activity, stability, and selectivity in the oxygen reduction reaction, *Chem. – A Eur. J.* 17 (2011) 10724–10735.

[166] L. Liu, E. Pippel, R. Scholz, U. Gösele, Nanoporous Pt–Co alloy nanowires: fabrication, characterization, and electrocatalytic properties, *Nano Lett.* 9 (2009) 4352–4358.

[167] H. Abe, F. Matsumoto, L.R. Alden, S.C. Warren, H.D. Abruña, F.J. DiSalvo, Electrocatalytic performance of fuel oxidation by Pt3Ti nanoparticles, *J. Am. Chem. Soc.* 130 (2008) 5452–5458.

[168] Y. Kang, L. Qi, M. Li, R.E. Diaz, D. Su, R.R. Adzic, E. Stach, J. Li, C.B. Murray, Highly active Pt3Pb and core–shell Pt3Pb–Pt electrocatalysts for formic acid oxidation, *ACS Nano* 6 (2012) 2818–2825.

[169] T. Ghosh, Q. Zhou, J.M. Gregoire, R.B. van Dover, F.J. DiSalvo, Pt–Cd and Pt–Hg phases As high activity catalysts for methanol and formic acid oxidation, *J. Phys. Chem. C* 114 (2010) 12545–12553.

[170] Z.-Z. Jiang, Z.-B. Wang, W.-L. Qu, H. Rivera, D.-M. Gu, G.-P. Yin, Carbon-riveted Pt catalyst supported on nanocapsule MWCNTs–Al2O3 with ultrahigh stability for high-temperature proton exchange membrane fuel cells, *Nanoscale* 4 (2012) 7411–7418.

[171] J. Wu, J. Zhang, Z. Peng, S. Yang, F.T. Wagner, H. Yang, Truncated octahedral Pt3Ni oxygen reduction reaction electrocatalysts, *J. Am. Chem. Soc.* 132 (2010) 4984–4985.

[172] J.W. Hong, S.W. Kang, B.-S. Choi, D. Kim, S.B. Lee, S.W. Han, Controlled synthesis of Pd–Pt Alloy hollow nanostructures with enhanced catalytic activities for oxygen reduction, *ACS Nano* 6 (2012) 2410–2419.

[173] Y. Kang, X. Ye, J. Chen, Y. Cai, R.E. Diaz, R.R. Adzic, E.A. Stach, C.B. Murray, Design of Pt–Pd binary superlattices exploiting shape effects and synergistic effects for oxygen reduction reactions, *J. Am. Chem. Soc.* 135 (2013) 42–45.

[174] P. Karthika, H. Ataei-Esfahani, H. Wang, M.A. Francis, H. Abe, N. Rajalakshmi, K. S. Dhatathreyan, D. Arivuoli, Y. Yamauchi, Synthesis of mesoporous Pt–Ru alloy

particles with uniform sizes by sophisticated hard-templating method, *Chem. – Asian J.* 8 (2013) 902–907.

[175] Y. Yamauchi, A. Tonegawa, M. Komatsu, H. Wang, L. Wang, Y. Nemoto, N. Suzuki, K. Kuroda, Electrochemical synthesis of mesoporous Pt–Au binary alloys with tunable compositions for enhancement of electrochemical performance, *J. Am. Chem. Soc.* 134 (2012) 5100–5109.

[176] X. Cao, N. Wang, Y. Han, C. Gao, Y. Xu, M. Li, Y. Shao, PtAg bimetallic nanowires: facile synthesis and their use as excellent electrocatalysts toward low-cost fuel cells, *Nano Energy* 12 (2015) 105–114.

[177] M. Watanabe, S. Motoo, Electrocatalysis by ad-atoms: Part II. Enhancement of the oxidation of methanol on platinum by ruthenium ad-atoms, *J. Electroanal. Chem. Interfacial Electrochem.* 60 (1975) 267–273.

[178] J.K. Nørskov, T. Bligaard, J. Rossmeisl, C.H. Christensen, Towards the computational design of solid catalysts, *Nat. Chem.* 1 (2009) 37–46.

[179] J. Rossmeisl, G.S. Karlberg, T. Jarailillo, J.K. Nørskov, Steady state oxygen reduction and cyclic voltammetry, *Faraday Discuss.* 140 (2009) 337–346.

[180] T. Frelink, W. Visscher, J.A.R. van Veen, On the role of Ru and Sn as promoters of methanol electro-oxidation over Pt, *Surf. Sci.* 335 (1995) 353–360.

[181] Y. Dai, B. Lim, Y. Yang, C.M. Cobley, W. Li, E.C. Cho, B. Grayson, P.T. Fanson, C. T. Campbell, Y. Sun, Y. Xia, A. Sinter-Resistant, Catalytic system based on platinum nanoparticles supported on TiO₂ nanofibers and covered by porous silica, *Angew. Chem. Int. Ed.* 49 (2010) 8165–8168.

[182] S.-Y. Huang, C.-M. Chang, C.-T. Yeh, Promotion of platinum–ruthenium catalyst for electro-oxidation of methanol by ceria, *J. Catal.* 241 (2006) 400–406.

[183] Y.-Y. Chu, Z.-B. Wang, Z.-Z. Jiang, D.-M. Gu, G.-P. Yin, A. Novel, Structural design of a Pt/CeO₂ catalyst with improved performance for methanol electro-oxidation by β -cyclodextrin carbonization, *Adv. Mater.* 23 (2011) 3100–3104.

[184] K. Sasaki, L. Zhang, R.R. Adzic, Niobium oxide-supported platinum ultra-low amount electrocatalysts for oxygen reduction, *Phys. Chem. Chem. Phys.* 10 (2008) 159–167.

[185] S.-Y. Huang, P. Ganesan, S. Park, B.N. Popov, Development of a titanium dioxide-supported platinum catalyst with ultrahigh stability for polymer electrolyte membrane fuel cell applications, *J. Am. Chem. Soc.* 131 (2009) 13898–13899.

[186] J. Ding, K.-Y. Chan, J. Ren, F.-s Xiao, Platinum and platinum–ruthenium nanoparticles supported on ordered mesoporous carbon and their electrocatalytic performance for fuel cell reactions, *Electrochim. Acta* 50 (2005) 3131–3141.

[187] M. Oezaslan, P. Strasser, Activity of dealloyed PtCo3 and PtCu3 nanoparticle electrocatalyst for oxygen reduction reaction in polymer electrolyte membrane fuel cell, *J. Power Sources* 196 (2011) 5240–5249.

[188] H. Adabi, A. Shakouri, A. Zitolo, T. Asset, A. Khan, J. Bohannon, R. Chattot, C. Williams, F. Jaouen, J.R. Regalbuto, W.E. Mustain, Multi-atom Pt and PtRu catalysts for high performance AEMFCs with ultra-low PGM content, *Appl. Catal. B: Environ.* 325 (2023), 122375.

[189] E. Daş, S. Alkan Gürsel, A. Bayrakçeken, Yurtcan, Pt-alloy decorated graphene as an efficient electrocatalyst for PEM fuel cell reactions, *J. Supercrit. Fluids* 165 (2020), 104962.

[190] D.K. Kang, C.S. Noh, N.H. Kim, S.-H. Cho, J.M. Sohn, T.J. Kim, Y.-K. Park, Effect of transition metals (Ni, Sn and Mo) in Pt5Ru4M alloy ternary electrocatalyst on methanol electro-oxidation, *J. Ind. Eng. Chem.* 16 (2010) 385–389.

[191] M.-R. Gao, Q. Gao, J. Jiang, C.-H. Cui, W.-T. Yao, S.-H. Yu, A. Methanol-Tolerant, Pt/CoSe₂ nanobelt cathode catalyst for direct methanol fuel cells, *Angew. Chem. Int. Ed.* 50 (2011) 4905–4908.

[192] O. Sahin, H. Kivrak, A comparative study of electrochemical methods on Pt–Ru DMFC anode catalysts: the effect of Ru addition, *Int. J. Hydrol. Energy* 38 (2013) 901–909.

[193] M. Amani, M. Kazemeini, M. Hamedanian, H. Pahlavanzadeh, H. Gharibi, Investigation of methanol oxidation on a highly active and stable Pt–Sn electrocatalyst supported on carbon–polyaniline composite for application in a passive direct methanol fuel cell, *Mater. Res. Bull.* 68 (2015) 166–178.

[194] J.-M. Zhang, S.-N. Sun, Y. Li, X.-J. Zhang, P.-Y. Zhang, Y.-J. Fan, A strategy in deep eutectic solvents for carbon nanotube-supported PtCo nanocatalysts with enhanced performance toward methanol electrooxidation, *Int. J. Hydrol. Energy* 42 (2017) 26744–26751.

[195] R. Baronia, J. Goel, S. Tiwari, P. Singh, D. Singh, S.P. Singh, S.K. Singhal, Efficient electro-oxidation of methanol using PtCo nanocatalysts supported reduced graphene oxide matrix as anode for DMFC, *Int. J. Hydrol. Energy* 42 (2017) 10238–10247.

[196] C.-T. Hsieh, W.-M. Hung, W.-Y. Chen, J.-Y. Lin, Microwave-assisted polyol synthesis of Pt–Zn electrocatalysts on carbon nanotube electrodes for methanol oxidation, *Int. J. Hydrol. Energy* 36 (2011) 2765–2772.

[197] X.T. Li, H. Lei, C. Yang, Q.B. Zhang, Electrochemical fabrication of ultra-low loading Pt decorated porous nickel frameworks as efficient catalysts for methanol electrooxidation in alkaline medium, *J. Power Sources* 396 (2018) 64–72.

[198] H. Wang, J. Zheng, F. Peng, H. Yu, Pt/IrO₂/CNT anode catalyst with high performance for direct methanol fuel cells, *Catal. Commun.* 33 (2013) 34–37.

[199] X. Peng, Y. Zhao, D. Chen, Y. Fan, X. Wang, W. Wang, J. Tian, One-pot synthesis of reduced graphene oxide supported PtCu_y catalysts with enhanced electrocatalytic activity for the methanol oxidation reaction, *Electrochim. Acta* 136 (2014) 292–300.

[200] B. Luo, X. Yan, J. Chen, S. Xu, Q. Xue, PtFe nanotubes/graphene hybrid: Facile synthesis and its electrochemical properties, *Int. J. Hydrol. Energy* 38 (2013) 13011–13016.

[201] R. Ahmadi, M.K. Amini, Synthesis and characterization of Pt nanoparticles on sulfur-modified carbon nanotubes for methanol oxidation, *Int. J. Hydrol. Energy* 36 (2011) 7275–7283.

[202] X. Wang, X. Li, D. Liu, S. Song, H. Zhang, Green synthesis of Pt/CeO₂/graphene hybrid nanomaterials with remarkably enhanced electrocatalytic properties, *Chem. Commun.* 48 (2012) 2885–2887.

[203] J.R. Rodriguez, S. Fuentes-Moyado, T.A. Zepeda, J.N. Díaz de León, J. Cruz-Reyes, M.T. Oropeza-Guzman, G. Berhault, G. Alonso-Núñez, Methanol electro-oxidation with alloy nanoparticles of Pt10–x–Fe_x supported on CNTs, *Fuel* 182 (2016) 1–7.

[204] L. Dong, R.R.S. Gari, Z. Li, M.M. Craig, S. Hou, Graphene-supported platinum and platinum–ruthenium nanoparticles with high electrocatalytic activity for methanol and ethanol oxidation, *Carbon* 48 (2010) 781–787.

[205] W. Li, W. Zhou, H. Li, Z. Zhou, B. Zhou, G. Sun, Q. Xin, Nano-structured Pt–Fe/C as cathode catalyst in direct methanol fuel cell, *Electrochim. Acta* 49 (2004) 1045–1055.

[206] S. Khammarnia, A. Akbari, M.-S. Ekrami-Kakhki, J. Saffari, Enhanced catalytic activity of Pt–NdFeO₃ nanoparticles supported on polyaniline–chitosan composite towards methanol electro-oxidation reaction, *J. Nanostruct.* 10 (2020) 239–257.

[207] H. Li, G. Chang, Y. Zhang, J. Tian, S. Liu, Y. Luo, A.M. Asiri, A.O. Al-Youbi, X. Sun, Photocatalytic synthesis of highly dispersed Pd nanoparticles on reduced graphene oxide and their application in methanol electro-oxidation, *Catal. Sci. Technol.* 2 (2012) 1153–1156.

[208] J. Yu, Y. Shi, D. Wu, TiO₂ nanotube supported PdNi catalyst for methanol electro-oxidation, *Powder Technol.* 230 (2012) 252–256.

[209] M.G. Hosseini, M.M. Momeni, H. Khalilpur, Synthesis and characterization of palladium nanoparticles immobilized on TiO₂ nanotubes as a new high active electrode for methanol electro-oxidation, *Int. J. Nanosci.* 11 (2012), 1250016.

[210] K. Mandal, D. Bhattacharjee, P.S. Roy, S.K. Bhattacharya, S. Dasgupta, Room temperature synthesis of Pd–Cu nanoalloy catalyst with enhanced electrocatalytic activity for the methanol oxidation reaction, *Appl. Catal. A: Gen.* 492 (2015) 100–106.

[211] X. Niu, H. Zhao, M. Lan, Palladium deposits spontaneously grown on nickel foam for electro-catalyzing methanol oxidation: Effect of precursors, *J. Power Sources* 306 (2016) 361–368.

[212] S. Cao, W. Xu, S. Zhu, Y. Liang, Z. Li, Z. Cui, X. Yang, A. Inoue, Synthesis of TiO₂nanoparticles loaded Pd/CuO nanoporous catalysts and their catalytic performance for methanol, ethanol and formic acid electro-oxidations, *J. Electrochem. Soc.* 163 (2016) E263–E271.

[213] R. Kannan, A.R. Kim, K.S. Nahm, D.J. Yoo, Manganese–titanium–oxide–hydroxide-supported palladium nanostructures – a facile electrocatalysts for the methanol, ethylene glycol and xylitol electrooxidation, *Int. J. Hydrol. Energy* 41 (2016) 6787–6797.

[214] Q. Tan, H. Zhu, S. Guo, Y. Chen, T. Jiang, C. Shu, S. Chong, B. Hultman, Y. Liu, G. Wu, Quasi-zero-dimensional cobalt-doped CeO₂ dots on Pd catalysts for alcohol electro-oxidation with enhanced poisoning-tolerance, *Nanoscale* 9 (2017) 12565–12572.

[215] Z. Cui, M. Yang, F.J. DiSalvo, Mesoporous Ti0.5Cr0.5N supported PdAg nanoalloy as highly active and stable catalysts for the electro-oxidation of formic acid and methanol, *ACS Nano* 8 (2014) 6106–6113.

[216] K. Zhang, Z. Xiong, S. Li, B. Yan, J. Wang, Y. Du, Cu3P/RGO promoted Pd catalysts for alcohol electro-oxidation, *J. Alloy. Compd.* 706 (2017) 89–96.

[217] Y. Zhao, S. Nie, H. Wang, J. Tian, Z. Ning, X. Li, Direct synthesis of palladium nanoparticles on Mn3O4 modified multi-walled carbon nanotubes: a highly active catalyst for methanol electro-oxidation in alkaline media, *J. Power Sources* 218 (2012) 320–330.

[218] R. Liu, H. Zhou, J. Liu, Y. Yao, Z. Huang, C. Fu, Y. Kuang, Preparation of Pd/MnO₂-reduced graphene oxide nanocomposite for methanol electro-oxidation in alkaline media, *Electrochim. Commun.* 26 (2013) 63–66.

[219] K.H. Ye, S.A. Zhou, X.C. Zhu, C.W. Xu, P.K. Shen, Stability analysis of oxide (CeO₂, NiO, Co₃O₄ and Mn3O4) Effect on Pd/C for methanol oxidation in alkaline medium, *Electrochim. Acta* 90 (2013) 108.

[220] N. Kakati, J. Maiti, S.H. Lee, Y.S. Yoon, Core shell like behavior of PdMo nanoparticles on multiwall carbon nanotubes and their methanol oxidation activity in alkaline medium, *Int. J. Hydrol. Energy* 37 (2012) 19055–19064.

[221] O. Fashedemi, K.I. Ozoemena, Enhanced methanol oxidation and oxygen reduction reactions on palladium-decorated FeCo@Fe/C core–shell nanocatalysts in alkaline medium, *Phys. Chem. Chem. Phys.* 15 (2013) 20982–20991.

[222] L.-L. He, P. Song, J.-J. Feng, R. Fang, D.-X. Yu, J.-R. Chen, A.-J. Wang, Porous dandelion-like gold@ palladium core-shell nanocrystals in-situ growth on reduced graphene oxide with improved electrocatalytic properties, *Electrochim. Acta* 200 (2016) 204–213.

[223] L. Yaqoob, T. Noor, N. Iqbal, Recent progress in development of efficient electrocatalyst for methanol oxidation reaction in direct methanol fuel cell, *Int. J. Energy Res.* 45 (2021) 6550–6583.

[224] C. Galeano, C. Baldizzone, H. Bongard, B. Spliethoff, C. Weidenthaler, J.C. Meier, K.J.J. Mayrhofer, F. Schüth, Carbon-based yolk–shell materials for fuel cell applications, *Adv. Funct. Mater.* 24 (2014) 220–232.

[225] J. Qi, L. Jiang, Q. Tang, S. Zhu, S. Wang, B. Yi, G. Sun, Synthesis of graphitic mesoporous carbons with different surface areas and their use in direct methanol fuel cells, *Carbon* 50 (2012) 2824–2831.

[226] Y. Ito, T. Takeuchi, T. Tsujiguchi, M.A. Abdelkareem, N. Nakagawa, Ultrahigh methanol electro-oxidation activity of PtRu nanoparticles prepared on TiO₂-embedded carbon nanofiber support, *J. Power Sources* 242 (2013) 280–288.

[227] H. Hu, H. Cheng, J. Zhou, Q. Zhu, Y. Yu, Hierarchical porous Fe2O3 assisted with graphene-like carbon as high-performance lithium battery anodes, *Mater. Today Phys.* 3 (2017) 7–15.

[228] L.P.A. Guerrero-Ortega, A. Manzo-Robledo, E. Ramírez-Meneses, J. Mateos-Santiago, L. Lartundo-Rojas, V. Garibay-Fébres, Methanol electro-oxidation

reaction at the interface of (bi)-metallic (PtNi) synthesized nanoparticles supported on carbon Vulcan, *Int. J. Hydrol. Energy* 43 (2018) 6117–6130.

[229] M. Chen, B. Lou, Z. Ni, B. Xu, PtCo nanoparticles supported on expanded graphite as electrocatalyst for direct methanol fuel cell, *Electrochim. Acta* 165 (2015) 105–109.

[230] L. Zhao, Z.-B. Wang, J.-L. Li, J.-J. Zhang, X.-L. Sui, L.-M. Zhang, Hybrid of carbon-supported Pt nanoparticles and three dimensional graphene aerogel as high stable electrocatalyst for methanol electrooxidation, *Electrochim. Acta* 189 (2016) 175–183.

[231] J.R. Rodriguez, R.M. Félix, E.A. Reynoso, Y. Gochi-Ponce, Y.V. Gómez, S. F. Moyado, G. Alonso-Núñez, Synthesis of Pt and Pt-Fe nanoparticles supported on MWCNTs used as electrocatalysts in the methanol oxidation reaction, *J. Energy Chem.* 23 (2014) 483–490.

[232] Y. Zhao, L. Fan, J. Ren, B. Hong, Electrodeposition of Pt–Ru and Pt–Ru–Ni nanoclusters on multi-walled carbon nanotubes for direct methanol fuel cell, *Int. J. Hydrol. Energy* 39 (2014) 4544–4557.

[233] X. Mu, Z. Xu, Y. Xie, H. Mi, J. Ma, Pt nanoparticles supported on Co embedded coal-based carbon nanofiber for enhanced electrocatalytic activity towards methanol electro-oxidation, *J. Alloys. Compd.* 711 (2017) 374–380.

[234] Z. Liu, Q. Shi, F. Peng, H. Wang, R. Zhang, H. Yu, Pt supported on phosphorus-doped carbon nanotube as an anode catalyst for direct methanol fuel cells, *Electrochem. Commun.* 16 (2012) 73–76.

[235] Y. Lu, Y. Jiang, H. Wu, W. Chen, Nano-PtPd cubes on graphene exhibit enhanced activity and durability in methanol electrooxidation after CO stripping–cleaning, *J. Phys. Chem. C* 117 (2013) 2926–2938.

[236] B. Xiong, Y. Zhou, Y. Zhao, J. Wang, X. Chen, R. O’Hayre, Z. Shao, The use of nitrogen-doped graphene supporting Pt nanoparticles as a catalyst for methanol electrocatalytic oxidation, *Carbon* 52 (2013) 181–192.

[237] X. Zhang, J. Zhu, C.S. Tiwary, Z. Ma, H. Huang, J. Zhang, Z. Lu, W. Huang, Y. Wu, Palladium nanoparticles supported on nitrogen and sulfur dual-doped graphene as highly active electrocatalysts for formic acid and methanol oxidation, *ACS Appl. Mater. Interfaces* 8 (2016) 10858–10865.

[238] X. Cui, X. Wang, X. Xu, S. Yang, Y. Wang, One-step stabilizer-free synthesis of porous bimetallic PdCu nanofinger supported on graphene for highly efficient methanol electro-oxidation, *Electrochim. Acta* 260 (2018) 47–54.

[239] Y. Zhao, L. Zhan, J. Tian, S. Nie, Z. Ning, MnO₂ modified multi-walled carbon nanotubes supported Pd nanoparticles for methanol electro-oxidation in alkaline media, *Int. J. Hydrol. Energy* 35 (2010) 10522–10526.

[240] H. Huang, X. Wang, Design and synthesis of Pd–MnO₂ nanolamella–graphene composite as a high-performance multifunctional electrocatalyst towards formic acid and methanol oxidation, *Phys. Chem. Chem. Phys.* 15 (2013) 10367–10375.

[241] T. Jurzinsky, R. Bär, C. Cremers, J. Tübke, P. Elsner, Highly active carbon supported palladium–rhodium PdXRh/C catalysts for methanol electrooxidation in alkaline media and their performance in anion exchange direct methanol fuel cells (AEM-DMFCs), *Electrochim. Acta* 176 (2015) 1191–1201.

[242] W. Zhang, Q. Yao, X. Wu, Y. Fu, K. Deng, X. Wang, Intimately coupled hybrid of graphitic carbon nitride nanoflakelets with reduced graphene oxide for supporting Pd nanoparticles: a stable nanocatalyst with high catalytic activity towards formic acid and methanol electrooxidation, *Electrochim. Acta* 200 (2016) 131–141.

[243] L. Gao, W. Yue, S. Tao, L. Fan, Novel strategy for preparation of graphene-Pd, Pt composite, and its enhanced electrocatalytic activity for alcohol oxidation, *Langmuir* 29 (2013) 957–964.

[244] K. Mishra, V. Kumar Thakur, S. Singh, Siwal, Graphitic carbon nitride based palladium nanoparticles: a homemade anode electrode catalyst for efficient direct methanol fuel cells application, *Mater. Today.: Proc.* 56 (2022) 107–111.

[245] Z. Ou, Z. An, Z. Ma, N. Li, Y. Han, G. Yang, Q. Jiang, Q. Chen, W. Chu, S. Wang, T. Yu, W. Yang, 3D porous graphene-like carbons encaged single-atom-based Pt for ultralow loading and high-performance fuel cells, *ACS Catal.* 13 (2023) 1856–1862.

[246] B. Kaur, R. Srivastava, B. Satpati, Highly efficient CeO₂ decorated nano-ZSM-5 catalyst for electrochemical oxidation of methanol, *ACS Catal.* 6 (2016) 2654–2663.

[247] A. Akinpelu, B. Merzougui, S. Bukola, A.-M. Azad, R.A. Basheer, G.M. Swain, Q. Chang, M. Shao, A. Pt-free, Electrocatalyst based on pyrolyzed vinazene-carbon composite for oxygen reduction reaction, *Electrochim. Acta* 161 (2015) 305–311.

[248] E.M. Miner, S. Gul, N.D. Ricke, E. Pastor, J. Yano, V.K. Yachandra, T. Van Voorhis, M. Dincă, Mechanistic evidence for ligand-centered electrocatalytic oxygen reduction with the conductive MOF Ni3(hexaminotriphenylene)2, *ACS Catal.* 7 (2017) 7726–7731.

[249] J. Li, Q.-L. Zhu, Q. Xu, Pd nanoparticles supported on hierarchically porous carbons derived from assembled nanoparticles of a zeolitic imidazolate framework (ZIF-8) for methanol electrooxidation, *Chem. Commun.* 51 (2015) 10827–10830.

[250] A. Samadi-Maybodi, S. Ghasemi, H. Ghaffari-Rad, Application of nano-sized nanoporous zinc 2-methylimidazole metal-organic framework for electrocatalytic oxidation of methanol in alkaline solution, *J. Power Sources* 303 (2016) 379–387.

[251] Y. Wang, Electrocatalytic oxidation of methanol on nickel doped metal- organic frameworks MIL-110 modified glassy carbon electrode in alkaline medium, *Int. J. Electrochem. Sci.* (2019) 5247–5258.

[252] R. Mehek, N. Iqbal, T. Noor, H. Nasir, Y. Mahmood, S. Ahmed, Novel Co-MOF/ graphene oxide electrocatalyst for methanol oxidation, *Electrochim. Acta* 255 (2017) 195–204.

[253] T. Noor, M. Ahmad, N. Zaman, N. Iqbal, L. Yaqoob, H. Nasir, A highly efficient and stable copper BTC metal organic framework derived electrocatalyst for oxidation of methanol in DMFC application, *Catal. Lett.* 149 (2019) 3312–3327.

[254] T. Noor, N. Zaman, H. Nasir, N. Iqbal, Z. Hussain, Electro catalytic study of NiO-MOF/rGO composites for methanol oxidation reaction, *Electrochim. Acta* 307 (2019) 1–12.

[255] L. Yaqoob, T. Noor, N. Iqbal, H. Nasir, N. Zaman, Development of nickel-BTC-MOF-derived nanocomposites with rGO towards electrocatalytic oxidation of methanol and its product analysis, *Catalysts* (2019).

[256] L. Yaqoob, T. Noor, N. Iqbal, H. Nasir, N. Zaman, L. Rasheed, M. Yousuf, Development of an efficient non-noble metal based anode electrocatalyst to promote methanol oxidation activity in DMFC, *ChemistrySelect* 5 (2020) 6023–6034.

[257] S.J. Hoseini, M. Bahrami, S.M. Nabavizadeh, ZIF-8 nanoparticles thin film at an oil–water interface as an electrocatalyst for the methanol oxidation reaction without the application of noble metals, *N. J. Chem.* 43 (2019) 15811–15822.

[258] Y.-P. Wu, J.-W. Tian, S. Liu, B. Li, J. Zhao, L.-F. Ma, D.-S. Li, Y.-Q. Lan, X. Bu, Bimicroporous metal-organic frameworks with cubane [M4(OH)4] (M=Ni, Co) clusters and pore-space partition for electrocatalytic methanol oxidation reaction, *Angew. Chem. Int. Ed.* 58 (2019) 12185–12189.

[259] Y. Liu, B. Hu, S. Wu, M. Wang, Z. Zhang, B. Cui, L. He, M. Du, Hierarchical nanocomposite electrocatalyst of bimetallic zeolitic imidazolate framework and MoS₂ sheets for non-Pt methanol oxidation and water splitting, *Appl. Catal. B: Environ.* 258 (2019), 117970.

[260] D. Zhu, L. Li, J. Cai, M. Jiang, J. Qi, X. Zhao, Nitrogen-doped porous carbons from bipyridine-based metal-organic frameworks: electrocatalysis for oxygen reduction reaction and Pt-catalyst support for methanol electrooxidation, *Carbon* 79 (2014) 544–553.

[261] A. Vulcu, L. Olenic, G. Blanita, C. Berghian-Grosan, The electrochemical behavior of a Metal-Organic Framework modified gold electrode for methanol oxidation, *Electrochim. Acta* 219 (2016) 630–637.

[262] W. Zhan, L. Ma, M. Gan, J. Ding, S. Han, D. Wei, J. Shen, C. Zhou, MOF-derived N-doped carbon coated CoP/carbon nanotube Pt-based catalyst for efficient methanol oxidation, *Int. J. Hydrol. Energy* 45 (2020) 15630–15641.

[263] Y. Yan, Y. Hou, Z. Yu, L. Tu, S. Qin, D. Lan, S. Chen, J. Sun, S. Wang, B-doped graphene quantum dots implanted into bimetallic organic framework as a highly active and robust cathodic catalyst in the microbial fuel cell, *Chemosphere* 286 (2022), 131908.

[264] R.P. Antony, A.K. Satpati, B.N. Jagatap, Performance of MOF-derived spinel type Ni_xCo_{3-x}O₄-y nanocages in efficient methanol electro-oxidation, *ChemElectroChem* 4 (2017) 2989–2996.

[265] Y. Lv, X. Li, PtCo/N-doped carbon sheets derived from a simple pyrolysis of graphene oxide/ZIF-67/H₂PtCl₆ composites as an efficient catalyst for methanol electro-oxidation, *Int. J. Hydrol. Energy* 45 (2020) 12766–12776.

[266] S. Samarjeet, G. Sarit, N. Debkumar, D. Nishu, K.P. Venkata, B. Rasmita, M. Kaushik, Synergistic effect of graphene oxide on the methanol oxidation for fuel cell application, *Mater. Res. Express* 4 (2017), 095306.

[267] C. Li, H. Bai, G. Shi, Conducting polymer nanomaterials: electrosynthesis and applications, *Chem. Soc. Rev.* 38 (2009) 2397–2409.

[268] X. Lu, W. Zhang, C. Wang, T.-C. Wen, Y. Wei, One-dimensional conducting polymer nanocomposites: Synthesis, properties and applications, *Prog. Polym. Sci.* 36 (2011) 671–712.

[269] S. Ghosh, S. Bera, S. Bysakh, R.N. Basu, Highly active multimetallic palladium nanoalloys embedded in conducting polymer as anode catalyst for electrooxidation of ethanol, *ACS Appl. Mater. Interfaces* 9 (2017) 33775–33790.

[270] S. Xie, L. Deng, H. Huang, J. Yuan, J. Xu, R. Yue, One-pot synthesis of porous Pd-polypyrrole/nitrogen-doped graphene nanocomposite as highly efficient catalyst for electrooxidation of alcohols, *J. Colloid Interface Sci.* 608 (2022) 3130–3140.

[271] Y. Zhao, K. Watanabe, K. Hashimoto, Self-supporting oxygen reduction electrocatalysts made from a nitrogen-rich network polymer, *J. Am. Chem. Soc.* 134 (2012) 19528–19531.

[272] X. Lu, X. Bian, G. Nie, C. Zhang, C. Wang, Y. Wei, Encapsulating conducting polypyrrole into electrospun TiO₂ nanofibers: a new kind of nanoreactor for in situ loading Pd nanocatalysts towards p-nitrophenol hydrogenation, *J. Mater. Chem. B* 22 (2012) 12723–12730.

[273] L. Yang, Z. Zhang, G. Nie, C. Wang, X. Lu, Fabrication of conducting polymer/noble metal composite nanorings and their enhanced catalytic properties, *J. Mater. Chem. A* 3 (2015) 83–86.

[274] M. Choudhary, S. Siwal, K. Mallick, Single step synthesis of a ‘silver-polymer hybrid material’ and its catalytic application, *RSC Adv.* 5 (2015) 58625–58632.

[275] M. Choudhary, S.K. Shukla, R.U. Islam, M.J. Witcomb, C.W. Holzapfel, K. Mallick, Polymerization assisted reduction reaction: a sequential electron–proton transfer reaction catalyzed by gold nanoparticle, *J. Phys. Chem. C* 117 (2013) 23009–23016.

[276] M. Choudhary, S. Siwal, R. Ul Islam, M.J. Witcomb, K. Mallick, Polymer stabilized silver nanoparticle: an efficient catalyst for proton-coupled electron transfer reaction and the electrochemical recognition of biomolecule, *Chem. Phys. Lett.* 608 (2014) 145–151.

[277] H. Han, Y. Noh, Y. Kim, V.S.K. Yadav, S. Park, W. Yoon, S. Lee, W.B. Kim, Electrocatalytic oxidations of formic acid and ethanol over Pd catalysts supported on a doped polypyrrole-carbon composite, *ChemistrySelect* 2 (2017) 6260–6268.

[278] L.A. Fard, R. Ojani, J.B. Raoof, E.N. Zare, M.M. Lakouraj, Poly (pyrrole-co-aniline) hollow nanosphere supported Pd nanoflowers as high-performance catalyst for methanol electrooxidation in alkaline media, *Energy* 127 (2017) 419–427.

[279] H. Liu, C. Song, L. Zhang, J. Zhang, H. Wang, D.P. Wilkinson, A review of anode catalysis in the direct methanol fuel cell, *J. Power Sources* 155 (2006) 95–110.

[280] A. Arico, S. Srinivasan, V. Antonucci, DMFCs: from fundamental aspects to technology development, *Fuel Cells* 1 (2001) 133–161.

[281] A. Lindermeir, G. Rosenthal, U. Kunz, U. Hoffmann, On the question of MEA preparation for DMFCs, *J. Power Sources* 129 (2004) 180–187.

[282] R. Bashyam, P. Zelenay, A class of non-precious metal composite catalysts for fuel cells, *Nature* 443 (2006) 63–66.

[283] Y. Zhang, F. Gao, D. Wang, Z. Li, X. Wang, C. Wang, K. Zhang, Y. Du, Amorphous/Crystalline heterostructure transition-metal-based catalysts for high-performance water splitting, *Coord. Chem. Rev.* 475 (2023), 214916.

[284] S. Gamil, Waleed M.A. El Rouby, M. Antuch, I.T. Zedan, Nano-hybrid layered double hydroxide materials as efficient catalysts for methanol electro-oxidation, *RSC Adv.* 9 (2019) 13503–13514.

[285] S. Wei, L. Qian, D. Jia, Y. Miao, Synthesis of 3D flower-like Ni0.6Zn0.4O microspheres for electrocatalytic oxidation of methanol, *Electrocatalysis* 10 (2019) 540–548.

[286] D. Zhang, L. Zhang, W. Zhang, M. Huo, J. Yin, G. Dang, Z. Ren, Q. Zhang, J. Xie, S. S. Mao, Morphology-dependent electrocatalytic performance of Fe2(MoO4)3 for electro-oxidation of methanol in alkaline medium, *J. Mater.* 3 (2017) 135–143.

[287] M. Li, J. Zhou, Y.-G. Bi, S.-Q. Zhou, C.-H. Mo, Transition metals (Co, Mn, Cu) based composites as catalyst in microbial fuel cells application: the effect of catalyst composition, *Chem. Eng.* 383 (2020), 123152.

[288] L. Chen, Z. Hua, J. Shi, M. He, CuO/Co(OH)2 nanosheets: a novel kind of electrocatalyst for highly efficient electrochemical oxidation of methanol, *ACS Appl. Mater. Interfaces* 10 (2018) 39002–39008.

[289] F. Zhao, B. Zhu, S. Li, X. Kong, Q. Liu, Bismuth-doped cobaltosic oxide as a noble-metal free electrocatalyst for the efficient methanol oxidation reaction, *J. Taiwan Inst. Chem. Eng.* 131 (2022), 104182.

[290] B. Hu, J. Yu, J. Meng, C. Xu, J. Cai, B. Zhang, Y. Liu, D. Yu, X. Zhou, C. Chen, Porous Ni–Cu alloy dendrite anode catalysts with high activity and selectivity for direct borohydride fuel cells, *ACS Appl. Mater. Interfaces* 14 (2022) 3910–3918.

[291] X. Cui, Y. Yang, Y. Li, F. Liu, H. Peng, Y. Zhang, P. Xiao, Electrochemical fabrication of porous Ni0.5Co0.5Alloy film and its enhanced electrocatalytic activity towards methanol oxidation, *J. Electrochem. Soc.* 162 (2015) F1415–F1424.

[292] L. Qian, L. Gu, L. Yang, H. Yuan, D. Xiao, Direct growth of NiCo2O4 nanostructures on conductive substrates with enhanced electrocatalytic activity and stability for methanol oxidation, *Nanoscale* 5 (2013) 7388–7396.

[293] Z.K. Ghouri, N.A.M. Barakat, H.Y. Kim, M. Park, K.A. Khalil, M.H. El-Newehy, S. S. Al-Deyab, Nano-engineered ZnO/CeO2 dots@CNFs for fuel cell application, *Arab. J. Chem.* 9 (2016) 219–228.

[294] P. Pattanayak, N. Pramanik, P. Kumar, P.P. Kundu, Fabrication of cost-effective non-noble metal supported on conducting polymer composite such as copper/polypyrrole graphene oxide (Cu2O/PPy-GO) as an anode catalyst for methanol oxidation in DMFC, *Int. J. Hydrog. Energy* 43 (2018) 11505–11519.

[295] M.M. Shahid, A. Pandikumar, A.M. Golsheikh, N.M. Huang, H.N. Lim, Enhanced electrocatalytic performance of cobalt oxide nanocubes incorporating reduced graphene oxide as a modified platinum electrode for methanol oxidation, *RSC Adv.* 4 (2014) 62793–62801.

[296] I. Danaee, M. Jafarian, F. Forouzandeh, F. Gobal, M.G. Mahjani, Electrocatalytic oxidation of methanol on Ni and NiCu alloy modified glassy carbon electrode, *Int. J. Hydrog. Energy* 33 (2008) 4367–4376.

[297] J. Li, Z. Luo, Y. Zuo, J. Liu, T. Zhang, P. Tang, J. Arbiol, J. Llorca, A. Cabot, NiSn bimetallic nanoparticles as stable electrocatalysts for methanol oxidation reaction, *Appl. Catal. B: Environ.* 234 (2018) 10–18.

[298] M. Asgari, M.G. Maragheh, R. Davarkhah, E. Lohrasbi, A.N. Golikand, Electrocatalytic oxidation of methanol on the nickel–cobalt modified glassy carbon electrode in alkaline medium, *Electrochim. Acta* 59 (2012) 284–289.

[299] J. Feng, F. Lv, W. Zhang, P. Li, K. Wang, C. Yang, B. Wang, Y. Yang, J. Zhou, F. Lin, G.-C. Wang, S. Guo, Iridium-based multimetallic porous hollow nanocrystals for efficient overall-water-splitting catalysis, *Adv. Mater.* 29 (2017), 1703798.

[300] F. Gao, Y. Zhang, Z. Wu, H. You, Y. Du, Universal strategies to multi-dimensional noble-metal-based catalysts for electrocatalysis, *Coord. Chem. Rev.* 436 (2021), 213825.

[301] H. Burhan, K. Arikhan, M.H. Alma, M.S. Nas, H. Karimi-Maleh, F. Sen, F. Karimi, Y. Vasseghian, Highly efficient carbon hybrid supported catalysts using nano-architecture as anode catalysts for direct methanol fuel cells, *Int. J. Hydrog. Energy* 48 (2023) 6657–6665.

[302] X. Cao, R. Song, X. Zhou, X. Wang, X. Dong, N. Yuan, J. Ding, 3D TM-N-C electrocatalysts with dense active sites for the membraneless direct methanol fuel cell and Zn-air batteries, *Langmuir* 38 (2022) 4948–4957.

[303] D. Xie, S. Hu, D. Teng, J. Ma, B. Wang, M. Zhu, Non-noble Si NWs@ZnO core-shell heterojunction anode enables a photo-assisted micro direct methanol fuel cell, *Chem. Eng. J.* 457 (2023), 141310.

[304] X. Tian, X. Zhao, Y.-Q. Su, L. Wang, H. Wang, D. Dang, B. Chi, H. Liu, E.J. M. Hensen, X.W. Lou, B.Y. Xia, Engineering bunched Pt–Ni alloy nanocages for efficient oxygen reduction in practical fuel cells, *Science* 366 (2019) 850–856.

[305] H. Tian, L. Zeng, Y. Huang, Z. Ma, G. Meng, L. Peng, C. Chen, X. Cui, J. Shi, In situ electrochemical Mn(III)/Mn(IV) generation of Mn(II)O electrocatalysts for high-performance oxygen reduction, *Nano-Micro Lett.* 12 (2020) 161.

[306] Y. Nie, L. Li, Z. Wei, Recent advancements in Pt and Pt-free catalysts for oxygen reduction reaction, *Chem. Soc. Rev.* 44 (2015) 2168–2201.

[307] M.K. Debe, Electrocatalyst approaches and challenges for automotive fuel cells, *Nature* 486 (2012) 43–51.

[308] L. Dubau, L. Castanheira, F. Maillard, M. Chatenet, O. Lottin, G. Maranzana, J. Dillet, A. Lambrac, J.-C. Perrin, E. Moukheiber, A. ElKaddouri, G. De Moor, C. Bas, L. Flandin, N. Caqué, A review of PEM fuel cell durability: materials degradation, local heterogeneities of aging and possible mitigation strategies, *WIREs Energy Environ.* 3 (2014) 540–560.

[309] A. Bhargava, C.Y. Chen, K. Dhaka, Y. Yao, A. Nelson, K.D. Finkelstein, C. J. Pollock, M. Caspary Toroker, R.D. Robinson, Mn cations control electronic transport in spinel CoxMn3-xO4 nanoparticles, *Chem. Mater.* 31 (2019) 4228–4233.

[310] C. Xie, D. Yan, H. Li, S. Du, W. Chen, Y. Wang, Y. Zou, R. Chen, S. Wang, Defect chemistry in heterogeneous catalysis: recognition, understanding, and utilization, *ACS Catal.* 10 (2020) 11082–11098.

[311] G.W. Sievers, A.W. Jensen, J. Quinson, A. Zana, F. Bizzotto, M. Oezaslan, A. Dworzak, J.J.K. Kirkensgaard, T.E.L. Smitshuysen, S. Kadkhodazadeh, M. Juelsholz, K.M.Ø. Jensen, K. Anklam, H. Wan, J. Schäfer, K. Cépe, M. Escudero-Escribano, J. Rossmeisl, A. Quade, V. Brüser, M. Arenz, Self-supported Pt–CoO networks combining high specific activity with high surface area for oxygen reduction, *Nat. Mater.* 20 (2021) 208–213.

[312] E. Antolini, E.R. Gonzalez, Tungsten-based materials for fuel cell applications, *Appl. Catal. B: Environ.* 96 (2010) 245–266.

[313] J.E. Benson, H.W. Kohn, M. Boudart, On the reduction of tungsten trioxide accelerated by platinum and water, *J. Catal.* 5 (1966) 307–313.

[314] H. Tian, X. Cui, J. Shi, Emerging electrocatalysts for PEMFCs applications: tungsten oxide as an example, *Chem. Eng. J.* 421 (2021), 129430.

[315] M.B. Kale, R.A. Borse, A. Gomaa Abdelkader Mohamed, Y. Wang, Electrocatalysts by electrodeposition: recent advances, synthesis methods, and applications in energy conversion, *Adv. Funct. Mater.* 31 (2021), 2101313.

[316] S.T. Chang, I.C. Leu, M.H. Hon, Preparation and characterization of nanostructured tin oxide films by electrochemical deposition, *Electrochim. Solid-State Lett.* 5 (2002) C71.

[317] I.M. Dharmadasa, J. Haigh, Strengths and advantages of electrodeposition as a semiconductor growth technique for applications in macroelectronic devices, *J. Electrochem. Soc.* 153 (2006) G47.

[318] X. Zhang, J. Cai, W. Liu, B. Huang, S. Lin, MnO2 coated with graphene by galvanostatic electrodeposition and its enhanced electrocatalysis for oxygen reduction, *J. Appl. Electrochem.* 50 (2020) 713–722.

[319] C. Paoletti, A. Cemmi, L. Giorgi, R. Giorgi, L. Pilloni, E. Serra, M. Pasquali, Electro-deposition on carbon black and carbon nanotubes of Pt nanostructured catalysts for methanol oxidation, *J. Power Sources* 183 (2008) 84–91.

[320] J. Lee, J. Seo, K. Han, H. Kim, Preparation of low Pt loading electrodes on Nafion (Na+)-bonded carbon layer with galvanostatic pulses for PEMFC application, *J. Power Sources* 163 (2006) 349–356.

[321] T.T. Cheng, E.L. Gyenge, Novel catalyst-support interaction for direct formic acid fuel cell anodes: Pt electrodeposition on surface-modified graphite felt, *J. Appl. Electrochem.* 39 (2009) 1925.

[322] F. Gloaguen, J.M. LeGer, C. Lamy, Electrocatalytic oxidation of methanol on platinum nanoparticles electrodeposited onto porous carbon substrates, *J. Appl. Electrochem.* 27 (1997) 1052–1060.

[323] J. Mitzel, F. Arena, H. Natter, T. Walter, M. Batzer, M. Stefen, R. Hempelmann, Electrodeposition of PEM fuel cell catalysts by the use of a hydrogen depolarized anode, *Int. J. Hydrog. Energy* 37 (2012) 6261–6267.

[324] S.H. Ahn, I. Choi, O.J. Kwon, J.J. Kim, One-step co-electrodeposition of Pt–Ru electrocatalysts on carbon paper for direct methanol fuel cell, *Chem. Eng. J.*, 181–182 (2012) 276–280.

[325] S. Lamaison, D. Wakerley, J. Blanchard, D. Montero, G. Rousse, D. Mercier, P. Marcus, D. Taverna, D. Giaume, V. Mougel, M. Fontecave, High-current-density CO2-to-CO electroreduction on Ag-Alloyed Zn dendrites at elevated pressure, *Joule* 4 (2020) 395–406.

[326] L.-K. Wu, J.-M. Hu, A silica co-electrodeposition route to nanoporous Co3O4 film electrode for oxygen evolution reaction, *Electrochim. Acta* 116 (2014) 158–163.

[327] C. Ghiabi, A. Ghaffarinejad, H. Kazemi, R. Salahandish, In situ, one-step and co-electrodeposition of graphene supported dendritic and spherical nano-palladium-silver bimetallic catalyst on carbon cloth for electrooxidation of methanol in alkaline media, *Renew. Energy* 126 (2018) 1085–1092.

[328] P. Dhanasekaran, K. Lokesh, P.K. Ojha, A.K. Sahu, S.D. Bhat, D. Kalpana, Electrochemical deposition of three-dimensional platinum nanoflowers for high-performance polymer electrolyte fuel cells, *J. Colloid Interface Sci.* 572 (2020) 198–206.

[329] H. Firouzi-Nerbin, F. Nasirpouri, E. Moslehifard, Pulse electrodeposition and corrosion properties of nanocrystalline nickel-chromium alloy coatings on copper substrate, *J. Alloy. Compd.* 822 (2020), 153712.

[330] S. Imanian Ghazanlou, A.H.S. Farhood, S. Ahmadiyeh, E. Ziayei, A. Rasooli, S. Hosseinpour, Characterization of pulse and direct current methods for electrodeposition of Ni–Co composite coatings reinforced with nano and micro ZnO particles, *Metall. Mater. Trans. A* 50 (2019) 1922–1935.

[331] M. Yao, N. Wang, W. Hu, S. Komarneni, Novel hydrothermal electrodeposition to fabricate mesoporous film of Ni0.8Fe0.2 nanosheets for high performance oxygen evolution reaction, *Appl. Catal. B: Environ.* 233 (2018) 226–233.

[332] P. Zhao, N. Wang, M. Yao, H. Ren, W. Hu, Hydrothermal electrodeposition incorporated with CVD-polymerisation to tune PPy@MnO2 interlinked core-shell nanowires on carbon fabric for flexible solid-state asymmetric supercapacitors, *Chem. Eng. J.* 380 (2020), 122488.

[333] U. Kumar Sur, F. Marken, R.G. Compton, B.A. Coles, Microwave effects on the electrochemical deposition of copper, *N. J. Chem.* 28 (2004) 1544–1549.

[334] S.S. Sankar, K. Karthick, K. Sangeetha, A. Karmakar, R. Madhu, S. Kundu, Current perspectives on 3D ZIFs incorporated with 1D carbon matrices as fibers via electrospinning processes towards electrocatalytic water splitting: a review, *J. Mater. Chem. A* 9 (2021) 11961–12002.

[335] H. Chen, X. Huang, L.-J. Zhou, G.-D. Li, M. Fan, X. Zou, Electrospinning synthesis of bimetallic nickel–iron oxide/carbon composite nanofibers for efficient water oxidation electrocatalysis, *ChemCatChem* 8 (2016) 992–1000.

[336] K. Waldrop, R. Wycisk, P.N. Pintauro, Application of electrospinning for the fabrication of proton-exchange membrane fuel cell electrodes, *Current Opinion in Electrochemistry* 21 (2020) 257–264.

[337] S. Hong, M. Hou, H. Zhang, Y. Jiang, Z. Shao, B. Yi, A high-performance PEM fuel cell with ultralow platinum electrode via electrospinning and underpotential deposition, *Electrochim. Acta* 245 (2017) 403–409.

[338] A. Sokka, M. Mooste, M. Käärik, V. Gudkova, J. Kozlova, A. Kikas, V. Kisand, A. Treshchalov, A. Tamm, P. Paisite, J. Aruväli, J. Leis, A. Krumme, S. Holdcroft, S. Cavaliere, F. Jaouen, K. Tammeveski, Iron and cobalt containing electrospun carbon nanofibre-based cathode catalysts for anion exchange membrane fuel cell, *Int. J. Hydrol. Energy* 46 (2021) 31275–31287.

[339] A.M. Al-Enizi, A.A. Elzatahy, A.-R.I. Soliman, S.S. Al-Theyab, Electrospinning synthesis and electrocatalytic performance of cobalt oxide/carbon nanofibers nanocomposite based PVA for fuel cell applications, *Int. J. Electrochem. Sci.* 7 (2012) 12646–12655.

[340] A.V. Nikam, B.L.V. Prasad, A.A. Kulkarni, Wet chemical synthesis of metal oxide nanoparticles: a review, *CrystEngComm* 20 (2018) 5091–5107.

[341] A.S. Ethiraj, D.J. Kang, Synthesis and characterization of CuO nanowires by a simple wet chemical method, *Nanoscale Res. Lett.* 7 (2012) 70.

[342] M. Daka, M. Ferrara, M. Bevilacqua, P. Pengo, P. Rajak, R. Cianci, T. Montini, L. Pasquato, P. Fornasiero, Wet-chemical synthesis of porous multifaceted platinum nanoparticles for oxygen reduction and methanol oxidation reactions, *ACS Appl. Nano Mater.* 5 (2022) 4710–4720.

[343] S. Ganguli, S. Ghosh, G. Tudu, H.V.S.R.M. Koppisetti, V. Mahalingam, Design principle of monoclinic NiCo₂Se₄ and Co₃Se₄ nanoparticles with opposing intrinsic and geometric electrocatalytic activity toward the OER, *Inorg. Chem.* 60 (2021) 9542–9551.

[344] M.M. Rahman, M.M. Alam, A.M. Asiri, M.A. Chowdhury, J. Uddin, Electrocatalysis of 2,6-dinitrophenol based on wet-chemically synthesized PbO-ZnO microstructures, *Catalysts* 12 (2022).

[345] D.-J. Chen, Q.-L. Zhang, J.-X. Feng, K.-J. Ju, A.-J. Wang, J. Wei, J.-J. Feng, One-pot wet-chemical co-reduction synthesis of bimetallic gold–platinum nanochains supported on reduced graphene oxide with enhanced electrocatalytic activity, *J. Power Sources* 287 (2015) 363–369.

[346] L. Sun, G. Yuan, L. Gao, J. Yang, M. Chhowalla, M.H. Gharahcheshmeh, K. K. Gleason, Y.S. Choi, B.H. Hong, Z. Liu, Chemical vapour deposition, *Nat. Rev. Methods Prim.* 1 (2021) 5.

[347] P. Duverneuil, F. Maury, N. Pebere, F. Senocq, H. Vergnes, Chemical vapor deposition of SnO₂ coatings on Ti plates for the preparation of electrocatalytic anodes, *Surf. Coat. Technol.*, 151 152 (2002) 9–13.

[348] M.A. García-Contreras, S.M. Fernández-Valverde, J.R. Vargas-García, Pt, PtNi and PtCoNi film electrocatalysts prepared by chemical vapor deposition for the oxygen reduction reaction in 0.5M KOH, *J. Alloy. Compd.* 504 (2010) S425–S428.

[349] X. Qin, X. Wang, H. Xiang, J. Xie, J. Li, Y. Zhou, Mechanism for hydrothermal synthesis of LiFePO₄ platelets as cathode material for lithium-ion batteries, *J. Phys. Chem. C* 114 (2010) 16806–16812.

[350] J. Lai, W. Niu, R. Luque, G. Xu, Solvothermal synthesis of metal nanocrystals and their applications, *Nano Today* 10 (2015) 240–267.

[351] A.H. Mamaghani, F. Haghigheh, C.-S. Lee, Hydrothermal/solvothermal synthesis and treatment of TiO₂ for photocatalytic degradation of air pollutants: preparation, characterization, properties, and performance, *Chemosphere* 219 (2019) 804–825.

[352] N. Ye, T. Yan, Z. Jiang, W. Wu, T. Fang, A review: conventional and supercritical hydro/solvothermal synthesis of ultrafine particles as cathode in lithium battery, *Ceram. Int.* 44 (2018) 4521–4537.

[353] Y. Huo, S. Xiu, L.-Y. Meng, B. Quan, Solvothermal synthesis and applications of micro/nano carbons: a review, *Chem. Eng. J.* 451 (2023), 138572.

[354] R. Ghasemi, B.K. Moghadas, I. Mohammadi, Solvothermal synthesis of Pd10–Ni45–Co45/rGO composites as novel electrocatalysts for enhancement of the performance of DBFC, *Int. J. Hydrol. Energy* 45 (2020) 21808–21815.

[355] R. Jana, S. Dhiman, S.C.J.M.R.E. Peter, Facile solvothermal synthesis of highly active and robust Pd1.87Cu0.11Sn electrocatalyst towards direct ethanol fuel cell applications, *Mater. Res. Express* 3 (2016), 084001.

[356] I. Das, M.T. Noori, M. Shaikh, M.M. Ghangrekar, R. Ananthakrishnan, Synthesis and application of zirconium metal–organic framework in microbial fuel cells as a cost-effective oxygen reduction catalyst with competitive performance, *ACS Appl. Energy Mater.* 3 (2020) 3512–3520.

[357] K. Kakaeei, M. Rahnavardi, Synthesis of nitrogen-doped reduced graphene oxide and its decoration with high efficiency palladium nanoparticles for direct ethanol fuel cell, *Renew. Energy* 163 (2021) 1277–1286.

[358] M. Mukherjee, M. Samanta, U.K. Ghorai, S. Murmu, G.P. Das, K. Chattopadhyay, One pot solvothermal synthesis of ZnPc nanotube and its composite with RGO: a high performance ORR catalyst in alkaline medium, *Appl. Surf. Sci.* 449 (2018) 144–151.

[359] T.M.D. Dang, T.T.T. Le, E. Fribourg-Blanc, M.C. Dang, Synthesis and optical properties of copper nanoparticles prepared by a chemical reduction method, *Adv. Nat. Sci. Nanosci. Nanotechnol.* 2 (2011), 015009.

[360] A. Khan, A. Rashid, R. Younas, R. Chong, A chemical reduction approach to the synthesis of copper nanoparticles, *Int. Nano Lett.* 6 (2016) 21–26.

[361] M.F.R. Hanifah, J. Jaafar, M.H.D. Othman, A.F. Ismail, M.A. Rahman, N. Yusof, F. Aziz, N.A.A. Rahman, One-pot synthesis of efficient reduced graphene oxide supported binary Pt-Pd alloy nanoparticles as superior electro-catalyst and its electro-catalytic performance toward methanol electro-oxidation reaction in direct methanol fuel cell, *J. Alloy. Compd.* 793 (2019) 232–246.

[362] H. Yang, L. Geng, Y. Zhang, G. Chang, Z. Zhang, X. Liu, M. Lei, Y. He, Graphene-templated synthesis of palladium nanoplates as novel electrocatalyst for direct methanol fuel cell, *Appl. Surf. Sci.* 466 (2019) 385–392.

[363] Z.-B. Wang, G.-P. Yin, Y.-G. Lin, Synthesis and characterization of PtRuMo/C nanoparticle electrocatalyst for direct ethanol fuel cell, *J. Power Sources* 170 (2007) 242–250.

[364] M. Blosi, S. Albionetti, M. Dondi, C. Martelli, G. Baldi, Microwave-assisted polyol synthesis of Cu nanoparticles, *J. Nanopart. Res.* 13 (2011) 127–138.

[365] Z. Zhou, S. Wang, W. Zhou, G. Wang, L. Jiang, W. Li, S. Song, J. Liu, G. Sun, Q. Xin, Novel synthesis of highly active Pt/C cathode electrocatalyst for direct methanol fuel cell, *Chem. Commun.* (2003) 394–395.

[366] T. Jiang, L. Yan, Y. Meng, M. Xiao, Z. Wu, P. Tsikaras, S. Song, Glucose electrooxidation in alkaline medium: performance enhancement of PdAu/C synthesized by NH₃ modified pulse microwave assisted polyol method, *Appl. Catal. B: Environ.* 162 (2015) 275–281.

[367] M. Sakthivel, A. Schlange, U. Kunz, T. Turek, Microwave assisted synthesis of surfactant stabilized platinum/carbon nanotube electrocatalysts for direct methanol fuel cell applications, *J. Power Sources* 195 (2010) 7083–7089.

[368] P. Nekooi, M. Akbari, M.K. Amini, CoSe nanoparticles prepared by the microwave-assisted polyol method as an alcohol and formic acid tolerant oxygen reduction catalyst, *Int. J. Hydrol. Energy* 35 (2010) 6392–6398.

[369] A. Bharti, G. Cheruvally, S. Mulianteekuzhi, Microwave assisted, facile synthesis of Pt/CNT catalyst for proton exchange membrane fuel cell application, *Int. J. Hydrol. Energy* 42 (2017) 11622–11631.

[370] Z. Liu, L.M. Gan, L. Hong, W. Chen, J.Y. Lee, Carbon-supported Pt nanoparticles as catalysts for proton exchange membrane fuel cells, *J. Power Sources* 139 (2005) 73–78.

[371] C.T. Hsieh, J.-L. Gu, Y.-C. Chen, D.-Y. Tzou, Pulse microwave synthesis of palladium catalysts on graphene electrodes for proton exchange membrane fuel cells, *Electrochim. Acta* 98 (2013) 39–47.

[372] Y.B. Pottathara, Y. Grohens, V. Kokol, N. Kalarikkal, S. Thomas, Chapter 1 - synthesis and processing of emerging two-dimensional nanomaterials, in: Y. Beeren Pottathara, S. Thomas, N. Kalarikkal, Y. Grohens, V. Kokol (Eds.), *Nanomaterials Synthesis*, Elsevier, 2019, pp. 1–25.

[373] J.-O. Carlsson, P.M. Martin, Chapter 7 - chemical vapor deposition, in: P. M. Martin (Ed.), *Handbook of Deposition Technologies for Films and Coatings*, Third edition., William Andrew Publishing, Boston, 2010, pp. 314–363.

[374] Y. Zhu, T. Mei, Y. Wang, Y. Qian, Formation and morphology control of nanoparticles via solution routes in an autoclave, *J. Mater. Chem. B* 21 (2011) 11457–11463.

[375] D.C. Onwudire, Microwave-assisted synthesis of PbS nanostructures, *Heliyon* 5 (2019), e01413.

[376] L. DeRita, J. Resasco, S. Dai, A. Boubnov, H.V. Thang, A.S. Hoffman, I. Ro, G. W. Graham, S.R. Bare, G. Pacchioni, X. Pan, P. Christopher, Structural evolution of atomically dispersed Pt catalysts dictates reactivity, *Nat. Mater.* 18 (2019) 746–751.

[377] W.C. Elias, K.N. Heck, S. Guo, S. Yazdi, C. Ayala-Orozco, S. Grossweiler, J. B. Domingos, E. Ringe, M.S. Wong, Indium-decorated Pd nanocubes degrade nitrate anions rapidly, *Appl. Catal. B: Environ.* 276 (2020), 119048.

[378] H. Zhou, X. Yang, L. Li, X. Liu, Y. Huang, X. Pan, A. Wang, J. Li, T. Zhang, PdZn intermetallic nanostructure with Pd–Zn–Pd ensembles for highly active and chemoselective semi-hydrogenation of acetylene, *ACS Catal.* 6 (2016) 1054–1061.

[379] K. Epping Martin, J.P. Kopasz, K.W. McMurphy, Status of fuel cells and the challenges facing fuel cell technology today, fuel cell chemistry and operation, *Am. Chem. Soc.* (2010) 1–13.

[380] D.A. Cullen, K.C. Neyerlin, R.K. Ahluwalia, R. Mukundan, K.L. More, R.L. Borup, A.Z. Weber, D.J. Myers, A. Kusoglu, New roads and challenges for fuel cells in heavy-duty transportation, *Nat. Energy* 6 (2021) 462–474.

[381] M. Singh, D. Zappa, E. Comini, Solid oxide fuel cell: Decade of progress, future perspectives and challenges, *Int. J. Hydrol. Energy* 46 (2021) 27643–27674.